REPORT

- Degree in aerospace vehicles engineering
- Final work title:
  - Study of supercritical airfoils by means of computational fluid dynamics
- Done by:
  - Miguel García Cepeda
- Director of the study:
  - David del Campo Sud
- Delivered on January 9, 2015 (Autumn session, 2014)
- ETSEIAT (UPC)

Escola Tècnica Superior d'Enginyeries
Industrial i Aeronàutica de Terrassa
UNIVERSITAT POLITÈCNICA DE CATALUNYA

Contents

List of Tables

List of Figures

1 Abbreviations

- Supercritical airfoil/airfoils: SCA
- Angle/angles of attack: AoA
- Shockwave/Shockwaves: SW
- Boundary layer: BL

Part I

OBJECTIVE, TASKS AND SPECIFICATIONS

The aim of this study is to analyze a supercritical airfoil (NASA sc(2)-0714) specially at the condition for which it was designed, the transonic regime (a regime between the subsonic and the supersonic), but also at off design conditions: high angles of attack and low Mach numbers. The transonic regime (in which most of the jetliners fly) is difficult to study analytically (the reasons will be explained soon), so even at the first stages of the design of an airfoil intended to fly at these speeds, Computational Fluid Dynamics (CFD) must be used.

To do so, the main characteristics of the transonic flow (shockwave, boundary layer interaction...) will be explained based on Mach fields obtained using Fluent (commercial software), as well as the characteristic speeds of the airfoil will be found. In order to achieve this, four meshes will be implemented (using ICEM, a commercial software), to test 5 angles of attack and 10 transonic Mach numbers, necessary to accurately find the required results. Then, at least two angles of attack will be tested at a low Mach number to study the low speed behavior. Perhaps, the most important part of the study is the analysis of the results, so the theory learned in the following sections will be compared with the results.

The specifications constrain the different results of a same test to be within a 5% of difference; otherwise a result will not be considered valid.

Part II

INTRODUCTION

2 Introduction to the transonic regime and supercritical airfoils

As an introduction, the aim of supercritical airfoils is to reduce the flow acceleration in the upper surface when it is flying at speeds near Mach 1, so the SW that will appear is not strong enough to detach the BL (or to thicken it too much). This way, the drag will not increase dramatically, while lift will remain constant. This is achieved by its shape. As SCA are designed specifically for the transonic regime, a brief introduction to this type of flow is mandatory.

2.1 Transonic regime

The transonic regime appears over a body moving at Mach numbers near unity. A mixed region of subsonic and supersonic flow develops not only in the boundary layer, but also in the inviscid part of the field. One of the main differences from other types of regimes is the propagation of the pressure waves. In the subsonic flow, the perturbations are propagated in all directions, while in supersonic one they follow the characteristic lines. Consequently, in the transonic flow there will be two types of propagation of the perturbation originated in a certain point, depending on the position of the point (in the supersonic or the subsonic zone). Another important aspect is the drag over the airfoil: the types of drag encountered in transonic flow (over an airfoil) are the same as the ones in the supersonic flow: pressure (due to wave drag, due to the BL thickening and due to the possible detachment of the flow after the SW) and friction. The wave drag appears when supersonic fluid exists, and is caused by local compression of the fluid. The BL thickening and possible detachment affect the pressure distribution, increasing the drag. By far, the most important difference is the interaction between viscous and inviscid phenomena, with a high dependence in the transonic flow (the BL downstream the SW is affected, thickening).

When the free stream velocity reaches the critical Mach number, a point of the velocity field (on the nearby of the airfoil) is supersonic: we are entering the transonic regime. Above this speed, a supersonic zone appears, and it usually ends in a SW, after which the BL thickens, increasing a little bit the drag. If increasing the Mach number, this supersonic zone gets larger and the shock wave appearance is delayed towards the trailing edge of the airfoil. Its intensity increases, and if the increase in pressure across the SW is high enough, the BL is detached somewhere behind the SW, increasing more the drag. After the detachment of the BL, reattachment may occur. With higher Mach numbers, a SW in the pressure side of the airfoil may also appear, being less intense than the suction side one. If the BL is not detached just

after the SW, it might detach if an adverse pressure gradient exists in that zone of the airfoil. A recirculation bubble may appear; However, this will not be shown in Fluent, as Direct Numerical Simulation would be needed.

2.1.1 Critical Mach number

For every AoA, the airfoil has a critical Mach number, a drag divergence Mach number and a lift divergence Mach number.

The critical Mach number is one of the two Mach borders of the transonic regime. When the free stream velocity reaches the critical Mach number, a point of the velocity field (on the nearby of the airfoil) is supersonic: we are entering the transonic regime. It depends on the AoA, and is a conservative border to consider: although above this speed the supersonic zone increases, there are not problems of strong SW or other transonic phenomena just above this speed. The main advantage of this number is its ease to calculate analytically, taken into account that no SW appear just at the critical Mach number and the BL is thin. Knowing the minimum pressure coefficient (obviously, it depends on the AoA) for incompressible flow, the next equation can be used to find this number:

$$\frac{2}{\gamma \cdot M_{crit}^2}\left[\left(\frac{1+\frac{\gamma-1}{2}\cdot M_{crit}^2}{\frac{\gamma+1}{2}}\right)^{\frac{\gamma}{\gamma-1}}-1\right]=\frac{Cp_{imin}}{\sqrt{1-M_{crit}^2}+\frac{Cp_{imin}}{2}\cdot\frac{M_{crit}^2}{1+\sqrt{1-M_{crit}^2}}} \quad (1)$$

As just below the critical Mach number the regime is subsonic, if we consider that the superposition of solutions is valid (it is valid cause for the incompressible flow it is valid and we are doing only Karman-Tsien), we can split the resultant pressure distribution over the chord in the effect of the thickness and camber of the airfoil, and then in the effect of the AoA. Depending on the value of the AoA, the importance of the suction (low pressure) of the leading edge will be different: the higher the AoA, the higher the importance of this suction. The higher the AoA, the more important is the variation of the Cpmin , so the higher is the variation of the critical Mach number. At first, with low AoA, this leading edge suction is not important, so the critical Mach number is almost constant. As the AoA increases, the suction peak of the leading edge is higher, so the Cpmin gets lower, the speed in this point increasing. So, the critical Mach number decreases (the free stream needs less velocity in order a point over the airfoil to be supersonic). To sum up, in the zone of low AoA, the variation of critical Mach number with the variation of AoA is low, while with greater AoA this variation is higher.

2.1.2 Drag divergence Mach number

Although the Mach number is slightly higher than the critical Mach number and a SW exists, the increase in drag caused by the BL thickening is extremely small (~$(M_1 - 1)^3$ with M_1 the local Mach number in front of the SW). But when the SW is intense enough to strongly modify the characteristics of the BL (detaching it) and as the wave drag increases with the Mach number, the drag will increase with a high variation (divergence of the drag). The divergence of drag appears in the majority of the airfoils (not in SCA) when the SW surpasses the crest of the airfoil[1]. The cause of this divergence is that (with the SW after the crest) the already supersonic flow increases its velocity downstream the crest (due to the shape of the normal airfoils) so the intensity of the SW rapidly increases. In SCA, due to its flatter upper surface, this acceleration of the fluid after the crest is minimized, being the SW well downstream the crest. Different criterions exists to consider if the flow has reached the drag divergence Mach number. The criterion that was used by Douglas will be used, which states that in the drag divergence Mach number [1]:

$$\frac{\partial C_d}{\partial M} > 0.1 \tag{2}$$

A representation can be seen in figure 1.

[1] The crest of the airfoil is the highest point of the airfoil, and it varies with the AoA.

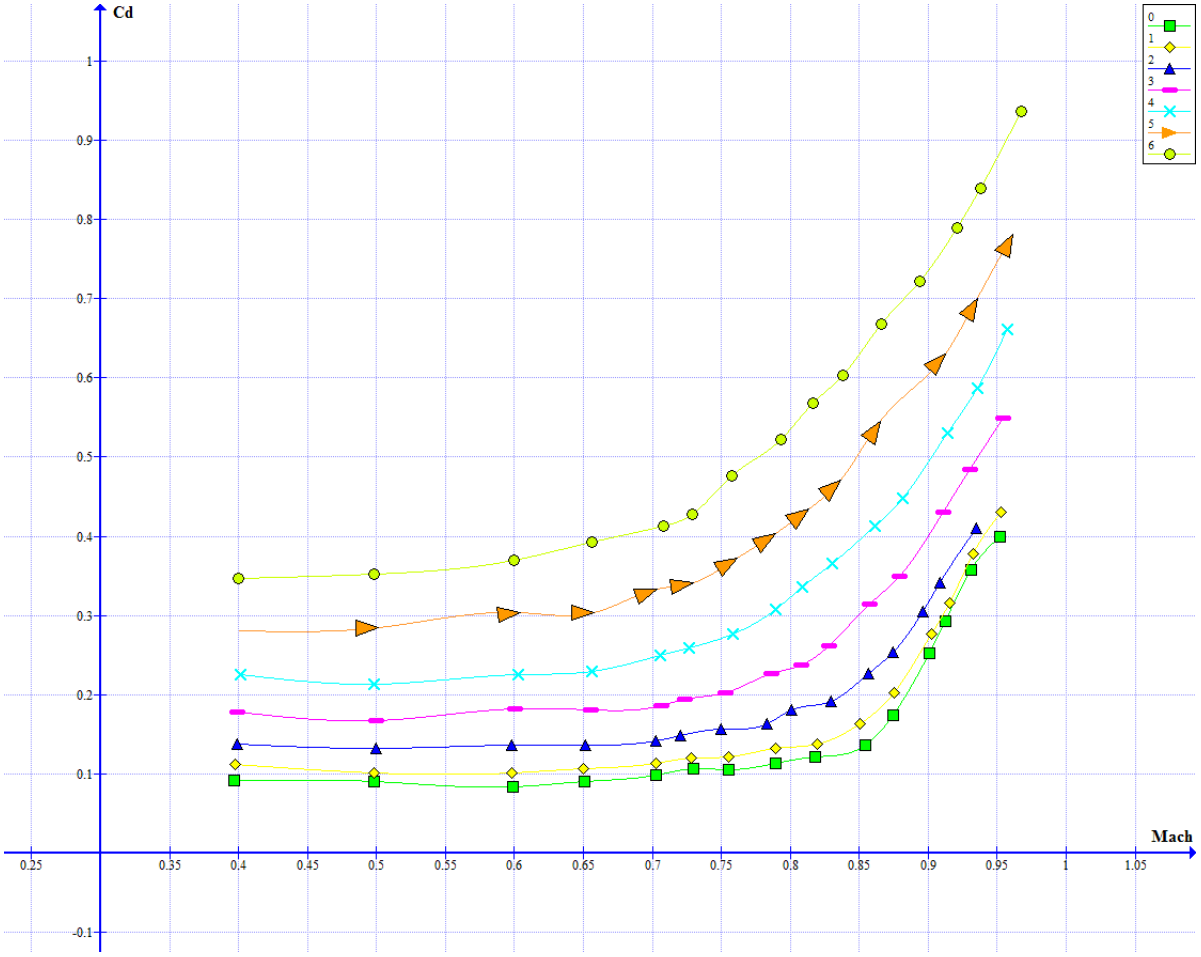

Figure 1: Cd versus Mach at various angles of attack (different lines); From Meseguer [2]

2.1.3 Lift divergence Mach number

Surpassing the drag divergence Mach number, the SW travels towards the trailing edge and is stronger if the Mach number increases. The BL can detach, but we have to take into account the possible re-adhesion bubble, so a divergence of the lift also appears at another Mach number, the lift divergence Mach number. The bubble can become larger traveling to the trailing edge, but when it reaches the trailing edge, the lift starts to decrease. This speed is the lift divergence Mach number. A representation can be seen in figure 2:

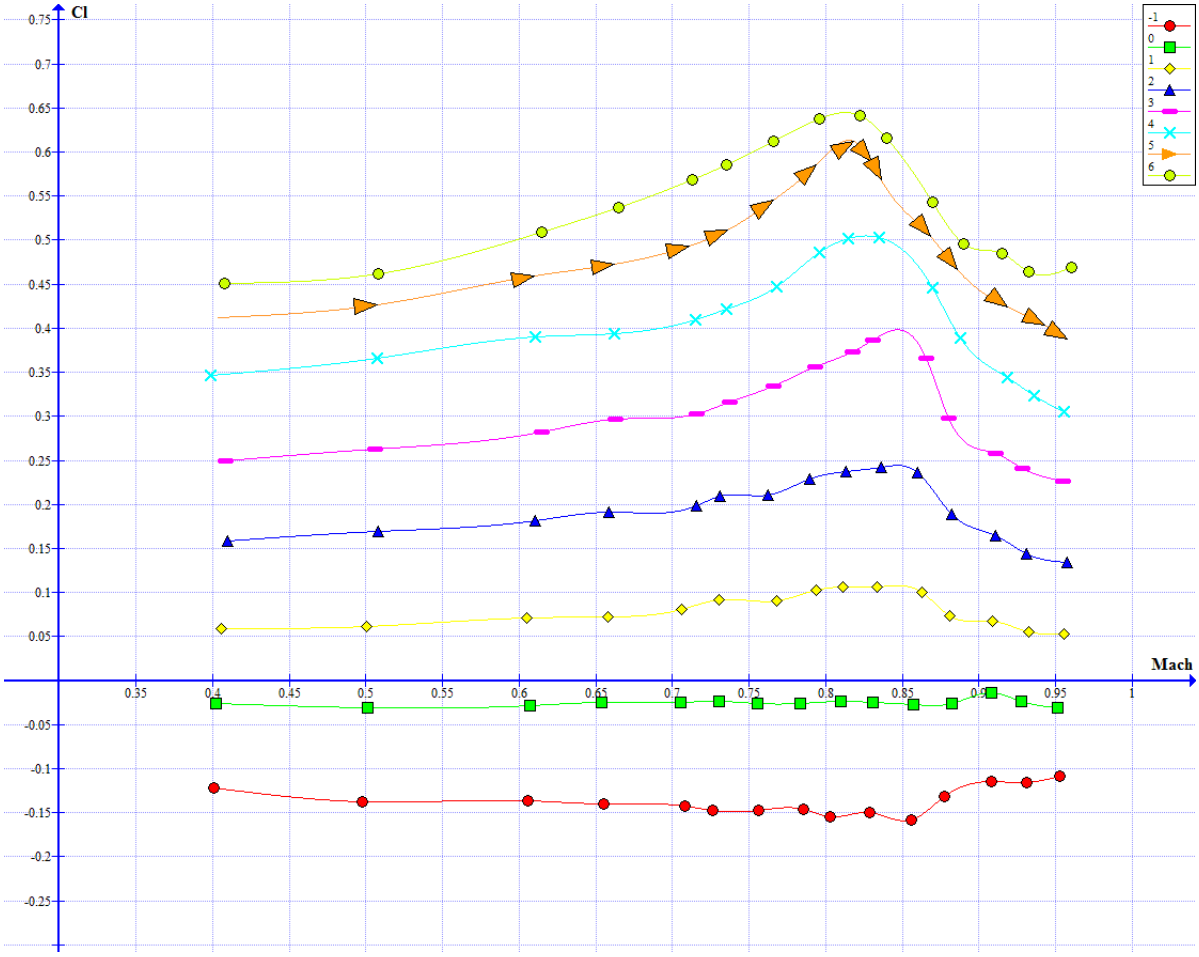

Figure 2: Cl versus Mach at various angles of attack (different lines); From Meseguer [2]

The variation of the critical Mach numbers with the Cl (AoA) can be seen in figure 3, where C is the critical Mach number, D is the drag divergence Mach number and L the lift divergence Mach number:

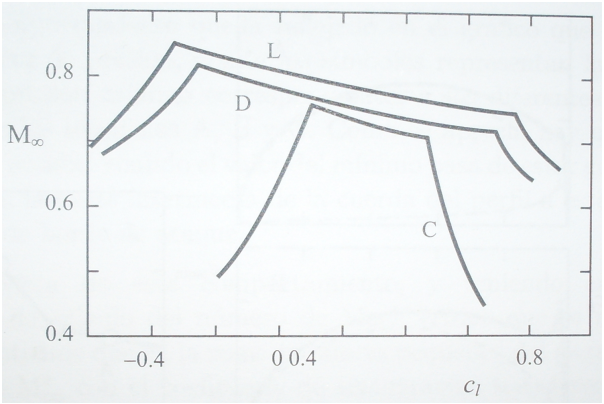

Figure 3: Variation of the Mach numbers with Cl; From Meseguer [2]

2.1.4 What about the momentum?

Concerning the momentum respect the aerodynamic center, it is difficult to explain what happens. The transonic flow can be translated as a huge tendency of the airfoil to dive (negative momentum), due to the relatively elevated pressure in the afterward part of the pressure side. With higher Mach numbers, the value of the pressure of the minimum of pressure in the upper side of the airfoil (usually just upstream the SW) gets lower, and this point gets closer to the trailing edge (as the SW also travels backwards).

2.2 Supercritical airfoils

This type of airfoil is designed to be efficient even though it is flying faster than the critical Mach number (so zones of the flow field will be at supersonic speeds). The predecessor sonic rooftop airfoil was designed to avoid the fluid to accelerate much more than Mach 1, but SCA are thought to cope with SW. The aim in fact is to avoid the formation of a strong SW, but weak SW are admitted. They are used in current aircraft such as the Boeing 777. By using SCA in a wing, less sweep angle is required to fly at the same free stream Mach number, so the drawbacks of a highly sweep wing, such as the decrease in maximum lift coefficient or the worse stall characteristics, starting from the wingtip, can be avoided. However, the combination of SCA, sweep back and area rulling can led to high subsonic aircraft such as the Convair Coronado, a retired civil aircraft that, equipped with different SCA from root to tip, 39° of sweep back and antishock bodies over the wing was capable of M=0.84 cruise speed at 35000 feet (Proctor, J. [3]).

Figure 4: Convair coronado; From Proctor [3]

Unlike the SCA, the normal ones generate a strong SW behind the crest just after crossing their critical Mach number, so these airfoils are unsuitable for transonic

flight, as the drag would increase dramatically, and lift would decrease.

The most important conclusion of H. H. Pearcey, an aerodynamicist of the middle of the twentieth century, is that the most interesting airfoils for transonic flight are the ones that in subcritical regime have a suction peak near the leading edge with a localized minimum of pressure (peaky distribution). When this type of airfoil enters the transonic regime, but near the subcritical regime, the pressure distribution still maintains a peak near the leading edge but the rest of the distribution over the suction side is reasonably uniform (so the fluid does not accelerate so much and the SW, if exists, is not strong). It must be said that this peaky distributed airfoil might have a lower critical Mach number when comparing to non-uniform pressure distributed airfoils, but the drag divergence Mach number will be higher and the drag coefficient lower. A comparison between a normal airfoil and a SCA can be seen in figure 5 and figure 6 (to directly go to the photo, click the number).

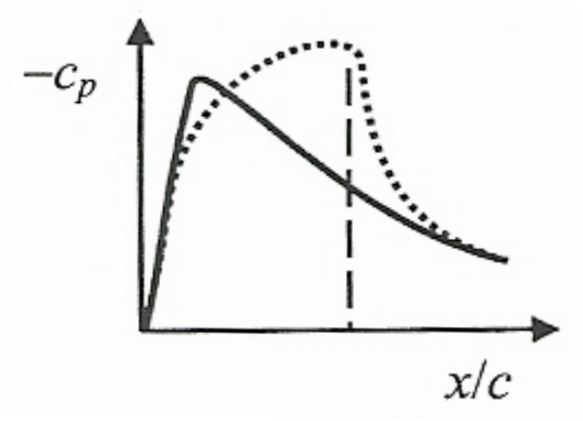

Figure 5: Normal airfoil pressure distribution, foreward suction side, in subsonic and transonic conditions (striped line); From Meseguer [2]

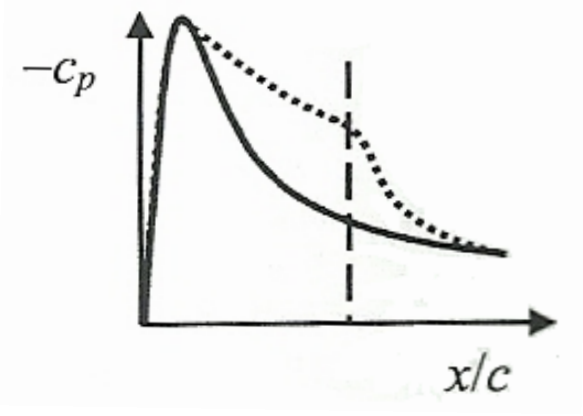

Figure 6: Supercritical airfoil pressure distribution, foreward suction side, in subsonic and transonic conditions (striped line); From Meseguer [2]

Increasing the free stream Mach number, another important aspect to take into

account is the deceleration of the fluid through the supersonic section: the SW will move backwards, and we do not want the fluid to decelerate just through the SW, because this would be a strong one. A gradual deceleration in the supersonic zone is desired. This way the SW will be weak.

The main drawback of the weevil pressure distributed airfoil (the ones with a notably peak in the leading edge) is its bad low speed behavior. That is why the firsts SCA were only used in high speed propeller blades. As there is a suction peak in the leading edge (greater at subsonic speeds), when reducing the speed of the aircraft and higher AoA are needed, the adverse pressure gradient just downstream the peak becomes higher, increasing the probabilities of a stalled airfoil. This low speed behavior will be studied in section 13.4.1.

2.2.1 The shape

Actual SCA (that combine the effect of rearward loading, peaky distribution and flat pressure distribution over upper side) have a relatively high leading edge radius (this allows reductions of the curvature of midchord regions of both upper and lower surfaces, followed by a reduction of the induced velocities) with a flat suction side (substantially reduced curvature of the middle region of the upper surface), so the supercritical pressure distribution at transonic speeds has a moderate suction peak near the leading edge, followed by a flat or slightly increasing pressure distribution, so the fluid can be gradually decelerated before the SW, so this is weak. However, the extent of this flat zone of the upper surface is restricted to avoid flow separation due to the steepness of the afterward pressure rise, that can be alleviated with the low included angle at the trailing edge (Bocci, A. [4]). Another characteristic is the large amount of camber near the trailing edge. The trailing edge is thick not only for structural purposes, but also to improve the high speed aerodynamic characteristics, with the drawback of a very little increase in the drag when subsonic regime (Sethunathan, P. [5]). This airfoil must have these characteristics in the supercritical regime; obviously in other regimes it will have another distribution. Each type of airfoil is conceived for a certain regime and designed for a desired performance: it would be unthinkable to design a STOL aircraft with a SCA, mainly due to the low speeds bad behavior. A comparison between an airfoil and a SCA, at transonic regimes, can be seen in figure 8.

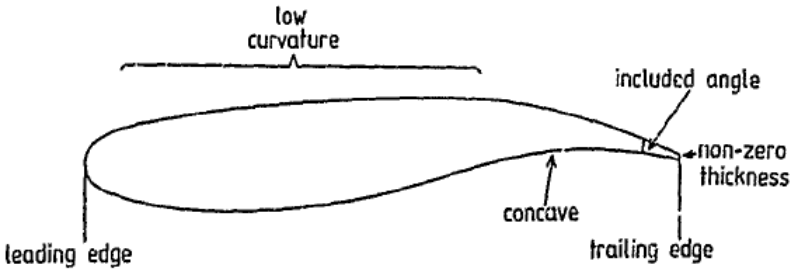

Figure 7: Supercritical airfoil shape; From Bocci [4]

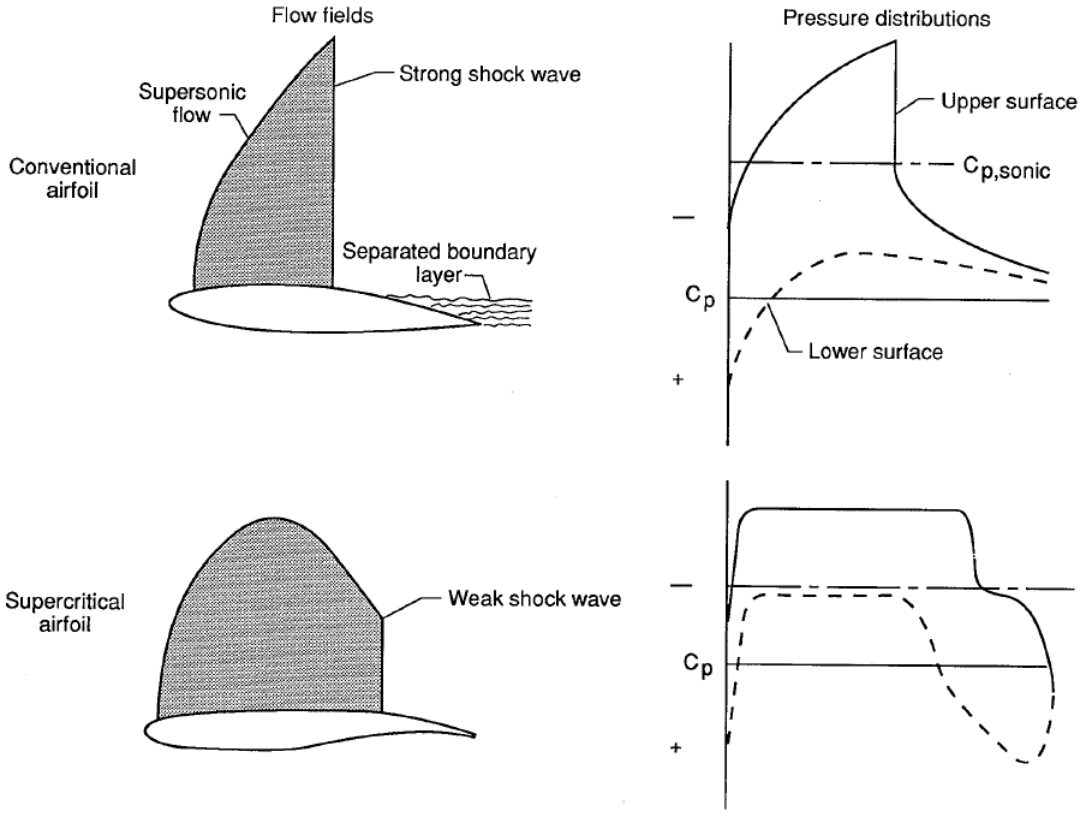

Figure 8: Comparison between airfoils in transonic regime; From Meseguer [2]

In the normal airfoil, the SW appears at the middle of the chord, being more intense (as the fluid accelerates downstream the crest, the SW is more intense). Downstream the SW, as there is also an adverse pressure gradient, the BL detaches, increasing drag.

In the SCA, though, the SW can be formed well behind the middle point of the chord without BL detachment, and as the pressure distribution in front of the shock is flatter due to the reduced curvature in this region, the fluid has been progressively decelerated or maintained at a uniform supersonic speed, being the SW weaker. So the local Mach number in front of the SW is relatively low. A uniform pressure

distribution rearward of the SW allows the BL to be reenergized by the external flow before the final adverse pressure gradient near the trailing edge. As a result, the BL can move through a greater pressure rise without separating. The positive pressure on the rear part of the lower surface, associated with the surface concavity of this region, allows a significant reduction in the required negative pressure coefficients on the upper surface to achieve a certain lift, and it is related with the diving moment of the airfoil. However, BL separation may occur in this zone of the lower surface. To avoid this, a solution is to make the trailing edge pressure and suction side parallels, so the trailing edge has some thickness.

2.2.2 Supercritical airfoil at various Mach numbers

In figure 9 a representation of the pressure distribution of a SCA at different conditions can be examined.

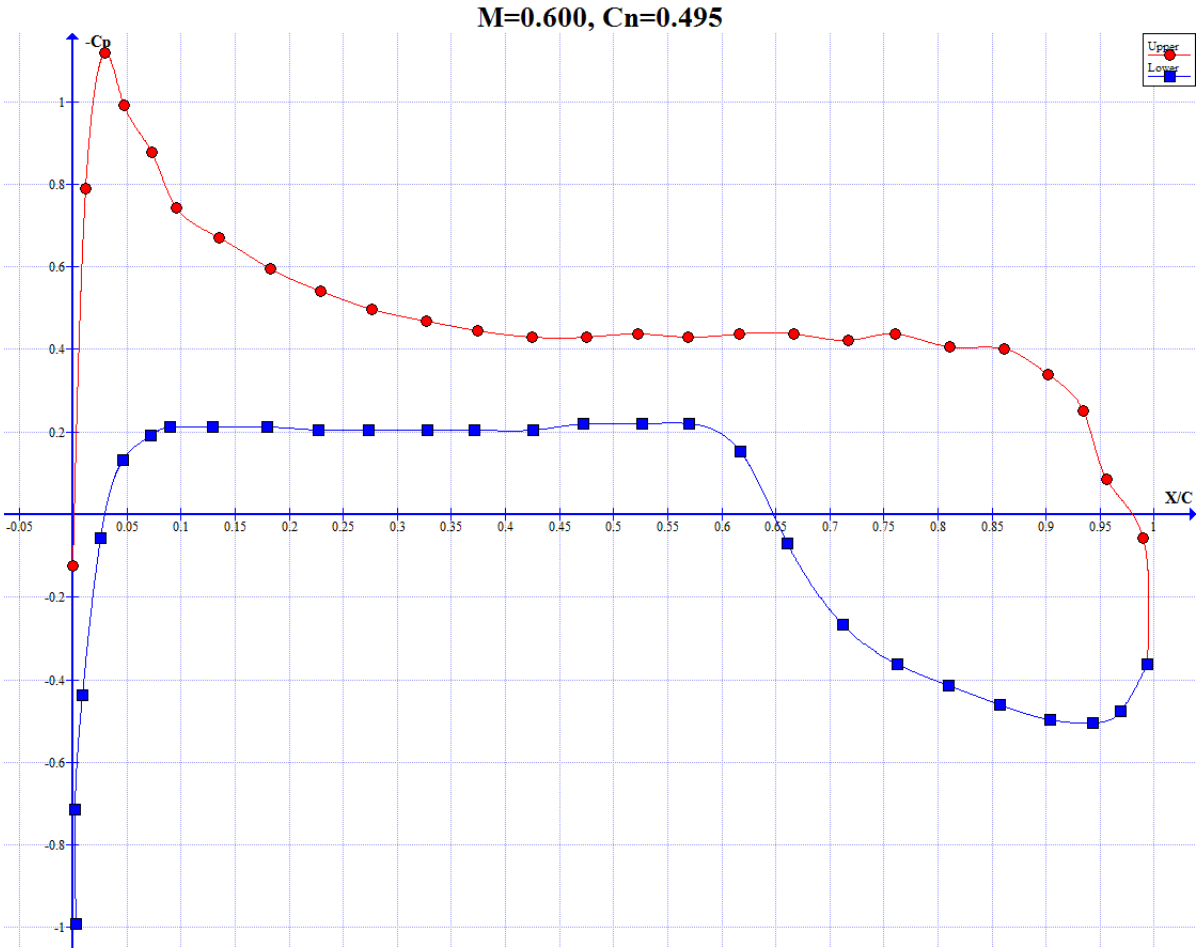

Figure 9: Supercritical airfoil pressure distribution at M=0.600 and Cn=0.495. The upper surface pressure coefficient is in red, while the lower is in blue; From Harris [6]

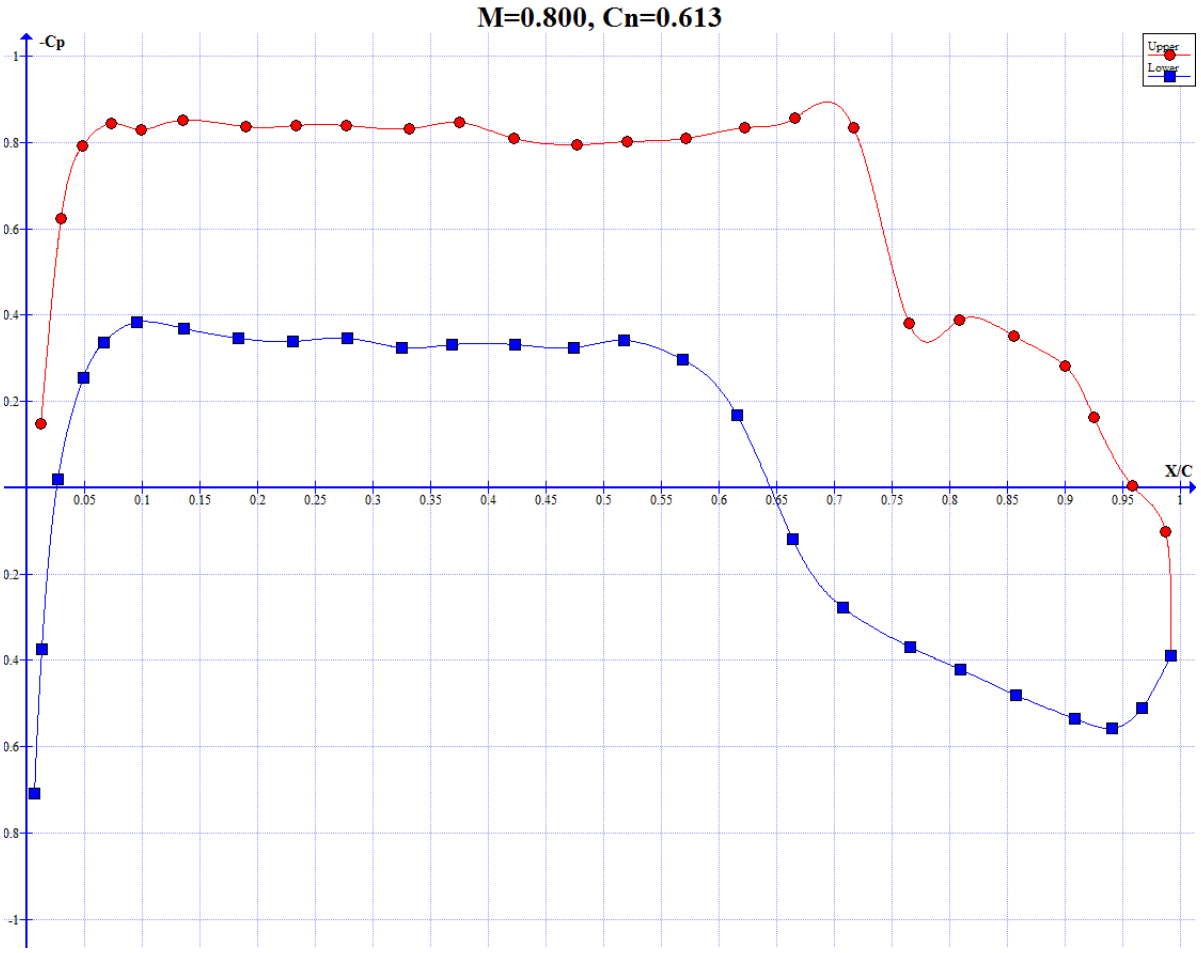

Figure 10: Supercritical airfoil pressure distribution at M=0.800 and Cn=0.613. The upper surface pressure coefficient is in red, while the lower is in blue; From Harris [6]

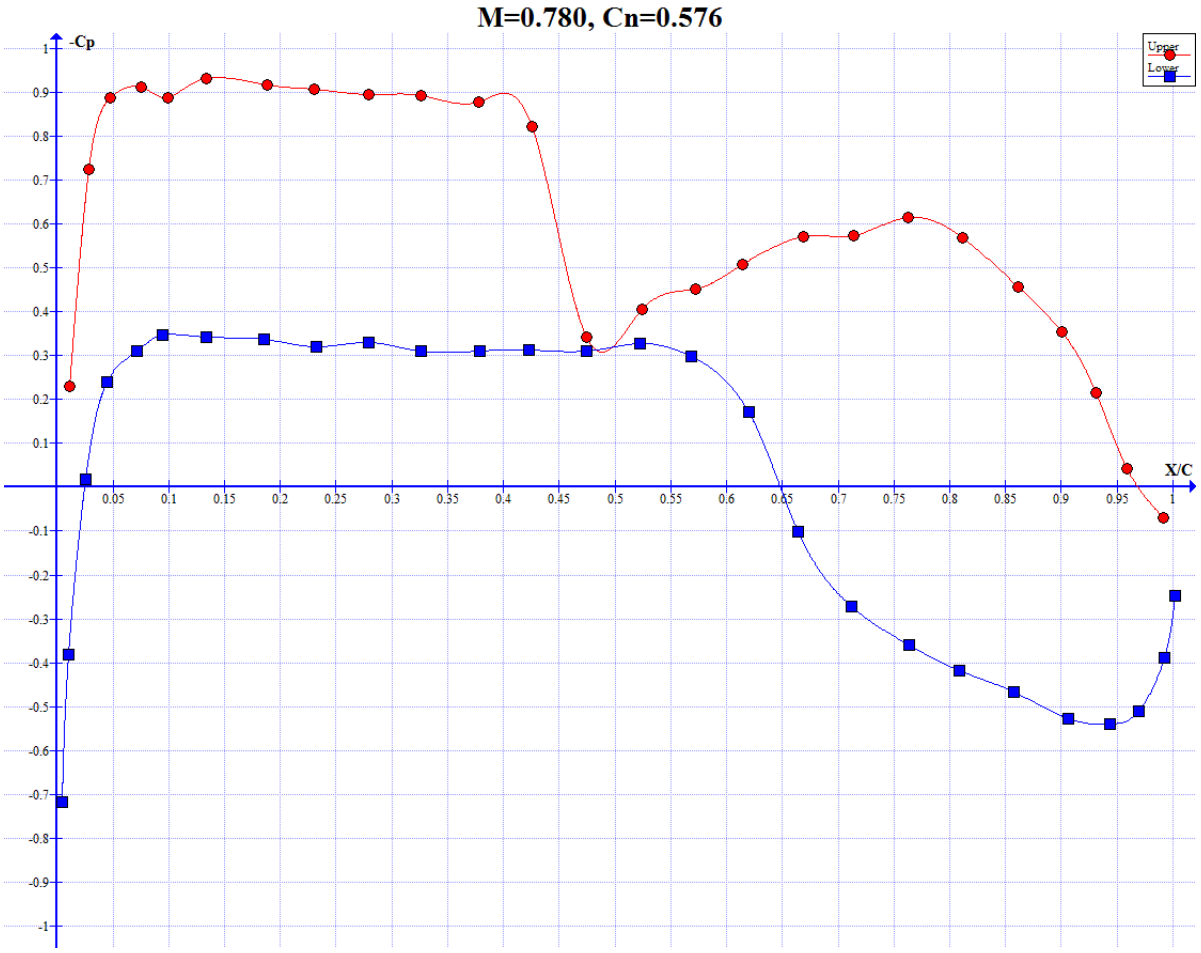

Figure 11: Supercritical airfoil pressure distribution at M=0.780 and Cn=0.576. The upper surface pressure coefficient is in red, while the lower is in blue; From Harris [6]

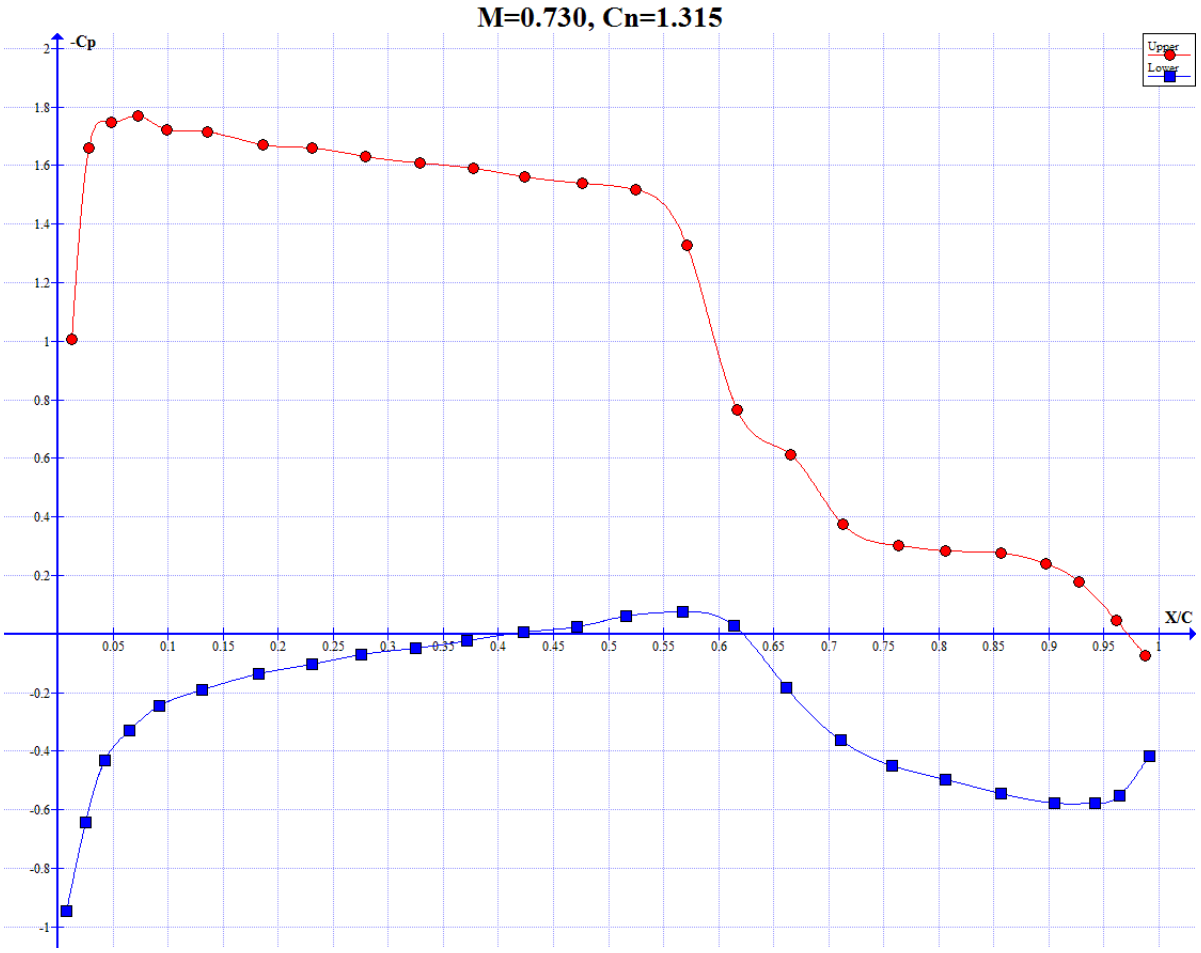

Figure 12: Supercritical airfoil pressure distribution at M=0.730 and Cn=1.315. The upper surface pressure coefficient is in red, while the lower is in blue; From Harris [6]

In figure 9, corresponding to subcritical and slightly supercritical regime (above the critical Mach number), we can observe a suction peak in the leading edge (that results in a small drag increment for subcritical and slightly supercritical conditions) followed by a smooth adverse pressure gradient and just at the trailing edge a higher adverse pressure gradient, so the BL is not likely to detach. The pressure distribution in the pressure side of the airfoil is almost the same as the one in the supercritical flow (if the angle of attack is the same), as in the pressure side of the airfoil the flow is subsonic, so there are not SW.

In figure 10, the airfoil is at a speed slightly higher than the optimum one. We can observe that the SW is a little bit behind the optimum position, as before the SW (that develops in the curved afterward part of the upper side of the airfoil) there is an acceleration, observed as the Cp gets more negative just before the SW (if in this zone the fluid were subsonic, the velocity here would decrease and the pressure would rise). But the SW is still weak, and downstream it there is not a high adverse

pressure gradient (it could be considered a constant pressure coefficient) until the trailing edge, so the BL is not detached. This constant pressure coefficient zone downstream the SW helps to stabilize the BL. As the BL is thickened and weakened when it cross through the SW, if the pressure distribution after the SW had a high adverse pressure gradient, it would probably detach. So, by using a flatter pressure distribution (achieved by a flat upper surface) after the SW instead of an adverse pressure gradient, the BL can be energized by the mixing with the potential zone, so the BL arrives to the trailing edge without detaching. In the lower surface there is a high adverse pressure gradient, and the BL thickens. The rapid pressure decrease in the trailing edge of the lower surface causes a pronounced thinning in the BL (figure 13, from own results of following numerical calculations). These effects in the lower surface contribute to a substantial reduction in the effective camber in the afterward part of the airfoil.

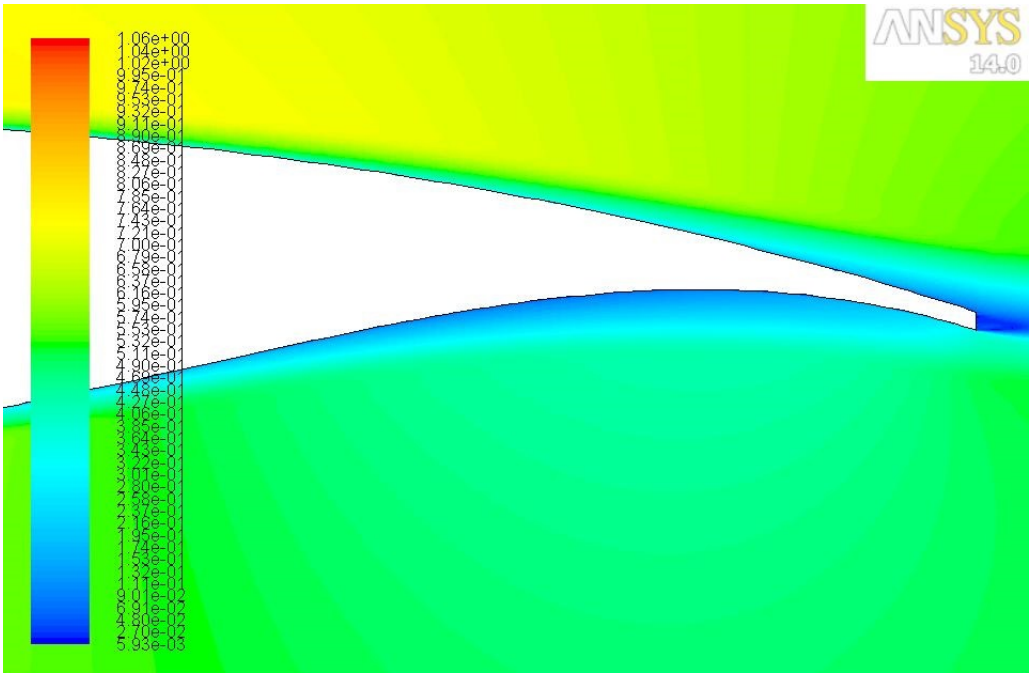

Figure 13: Lower surface BL thickening and narrowing; From own results

In the third case, figure 11, the airfoil is at a speed just below the design value. The SW is significantly forward than for the design condition, and the subsonic flow downstream it suffers another reacceleration, observable in the Cp, that after the SW gets more negative, with another supersonic suction peak near the last fourth of the airfoil (thus a maximum in velocity). Then, a second SW can appear, or a high adverse pressure gradient might exist near the trailing edge, and the BL might detach.

To sum up, depending on the position of the SW, the supersonic flow in front

of the SW or the subsonic flow downstream it will accelerate or not, affecting the pressure gradient, and consequently the possible separation of the BL followed by the increase of drag.

Note that the distribution in the lower surface is almost constant with the Mach number, as in this side there is no SW formation at these Mach numbers (Meseguer, J. [2]) (Bocci, A. [4]) (Harris, C.D. [6]) (Whitcomb, R. T. [7]).

3 Basics of numerical resolution

The equations over the fluid (it does not matter if subsonic or supersonic regime) are the differential conservation equations of mass, momentum and energy. Also, the ideal gas state equation will be considered, so we will have four unknowns (density, velocity, pressure and temperature) and four equations (well, the velocity will be a vector with two components, and a momentum conservation equation for each component). As for this study the fluid must be treated as compressible (the density will vary), the energy equation must be solved not only to find the temperature, but also the rest of the variables of the flow, as nearly in the four equations all the unknowns are present. The ideal gas state equation must also be solved. The equations are the following:

$$\frac{\partial \rho}{\partial t} + \vec{\nabla}\cdot(\rho\vec{v}) = 0 \tag{3}$$

$$\rho\frac{\partial \vec{v}}{\partial t} + \rho(\vec{v}\cdot\vec{\nabla})\vec{v} = \rho\vec{g} - \vec{\nabla}p + \mu[\triangle\vec{v} + \frac{1}{3}\vec{\nabla}(\vec{\nabla}\cdot\vec{v})] \tag{4}$$

$$\rho\frac{Du}{Dt} + \rho\frac{Dk}{Dt} = -\vec{\nabla}\vec{q} - \vec{\nabla}(p\vec{v}) + \vec{\nabla}(\vec{v}\cdot\vec{\tau}) + \rho\vec{v}g \tag{5}$$

$$P = \rho\cdot R\cdot T \tag{6}$$

Being k the kinetic energy. As these equations cannot be solved analytically, its discretization is compulsory. This can be thought as applying the integral conservation equations to tiny control volumes (the mesh) but approximating them as if they were differential control volumes, so properties will be considered constant through their surfaces, for example. Obviously, as this is an approximation, the smaller the control volumes in which we divide the fluid field, the more accurate will be the solution. When discretizing, the infinitesimal variations of the members of the equations are now finite variations, so the differential equations are now a set of four algebraic equations to solve for every control volume. There is a specific section dedicated to the mesh, section 8. Summarizing, the process followed is the next:

1. Division of the domain into discrete control volumes (meshing).
2. Integration of the differential equations over the individual control volumes, so algebraic equations are obtained for the four unknowns.

When discretizing the differential equations, several approaches can be made for each member of the equation; there is a balance between the accuracy of the approach and the stability of the resolution and the convergence of the results (as it will be an iterative process). The discretized equation is as follows (this is not still the equation solved by the software, as values in the faces must be approximated, and here comes the problem, as there are several ways to find them):

$$\frac{(\rho\theta)^{n+1}-(\rho\theta)^{n}}{\triangle t}V_c+\sum_f(\rho_f\vec{v}_f\theta_f)^{n+1}\cdot\vec{A}_f=\sum_f(\Gamma_f\nabla\theta_f)^{n+1}\cdot\vec{A}_f+S^{n+1}\cdot V_c \qquad (7)$$

where f refers to the values at the cell faces.

Although the case of study is steady, we will use a pseudo transient resolution, so time will not be eliminated from the equation.

The cell values are the values for the control volume, exactly at the centroid of it. They are the values calculated with the equations. The nodal values are the values on each of the vertices of the control volume, and as the solver calculates the cell values, to find the nodal values it uses a weighted average using the surrounding cell values. The cell-face values, or face values, are the values of each of the faces that comprises the control volume.

3.1 Numerical schemes

As Fluent uses a cell-centered formulation, it calculates all values for the center of the control volume, so the values of the faces, as said before, must be interpolated, using different numerical schemes depending on the solver used.

- Low order: they used only up to two nodal values to calculate the value at the face. They provide enough accuracy if the flow is aligned with the mesh (for example, a rectangular mesh in a straight duct with laminar flow). If not, it might introduce diffusion, so the accuracy will be worse. For more complex flows, it is better to use second order schemes. The low order schemes are:

  - Central difference scheme
  - Upwind difference scheme

  - Hybrid difference scheme
  - Exponential difference scheme
  - Powerlaw difference scheme

- High order: they use more than two nodal values, so the accuracy is improved. However, one of the problems of accurate numerical schemes is the instability. This problem is solved if they are bounded; it means that the value in the face is between nearest nodal grid points values. A high order numerical scheme that is tailor made is the SMART.

  - Upwind difference scheme of second order
  - QUICK
  - MUSCL

MUSCL or QUICK do not provide a significant improvement in accuracy compared with second order schemes, so they are not likely to be used.

We will calculate a high Mach number flow; if the supposed initial values for start the calculation are expected to be so different from the final results, it is advisable to start the first iterations with a low order scheme, to assure the convergence, and once some realistic results are obtained, use higher order schemes.

3.2 Evaluation of the gradients

Gradient evaluation at the cell centers is required for the discretization of convective and diffusive terms, to pass from the differential equations to the integral ones (not to confuse with, for example, the gradient of temperatures calculated in the energy equation to calculate the conduction heat).

- Green-Gauss cell-based gradient evaluation: the value of the face is the average of the neighboring cell values.
- Green-Gauss node-based gradient evaluation: the value of the face is the average of the nodal values of that face. This method is usually more accurate than the cell-based one, although it takes more time to compute.

- Least squares cell-based gradient evaluation: on skewed and distorted unstructured meshes, the accuracy of this method is comparable with that of the node-based method, but less expensive to compute.

These different numerical schemes will be used according to the type of solver used.

3.3 Flow solvers: pressure or density based solvers

In both methods the velocity is obtained from the momentum equation, and the temperature from the energy equation. In the density based method, the density is obtained from the continuity equation, while the pressure is obtained from the state equation. By contrast, using the pressure based method, by manipulating continuity and momentum equations, the pressure is obtained. For both types of solver, their models are presented.

3.3.1 Pressure based solver

The pressure equation is derived from the continuity and momentum equations. Depending on the type of pressure-velocity coupling, we can use a segregated or a coupled algorithm.

The segregated algorithm solves each of the four equations one after another, sequentially, and then, after solving the four equations, it iterates another time until the convergence is achieved. Some algorithms include the SIMPLE, SIMPLEC and PISO. The first two are recommended for steady state calculations, while the last is recommended for transient situations. The difference between SIMPLE and SIMPLEC is that when turbulence exists in the flow, as in our study, if the coupling of pressure and velocity is the unique factor that affects the convergence, the SIMPLEC method improves the convergence. If more factors affect the convergence, both methods give similar convergence rates. PISO with skewness correction is recommended for steady state calculations if the mesh is highly distorted.

In the coupled algorithm, momentum and pressure-based continuity equations are solved in a coupled manner. It is faster than the segregated but requires twice the memory needed by the first. It is also more robust for steady state equations. The pressure based coupled algorithm performs well in applications involving high speed aerodynamics with shocks, as this case.

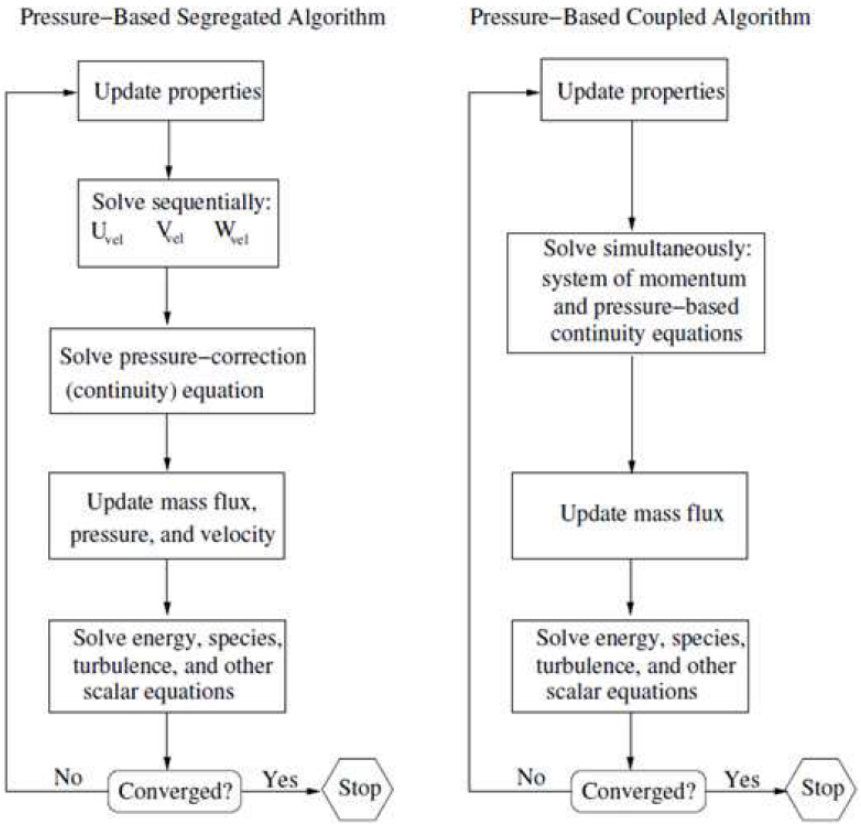

Figure 14: Pressure based segregated vs. coupled; From [8]

Pressure based generalities and some decisions: for the momentum equation, as we will calculate values at the center of the cell, an interpolation is needed to find velocity values in the cell´s faces. This is the concept of pressure interpolation scheme. By default, Fluent interpolates the pressure value at the faces using the momentum equation coefficients. This will work well while the pressure variation between cells is smooth. However, as in this case of transonic flow there are SW (that is, huge gradients of pressure in a small area), this is not valid if actions are not taken.

To solve this, a finer mesh could be used comprising the SW. Another way to solve this problem, the ideal one, is to use a discretization scheme, such as the second order upwind (more accurate than the standard method, but stability problems if bad mesh), recommended for compressible flows, as in this case. The third method is the body-force-weighted scheme, recommended for flows with large body forces, and the fourth is the PRESTO!, recommended for flows in strongly curved domains.

For the continuity equation, velocity values in the faces must be interpolated. If linear interpolation of cell centered velocities is used, non physical solutions for the pressure will be obtained. So, a momentum weighted average is used, just to know the values of the velocities in the faces. This drives to realistic results.

To find the density in the cell faces, a first order upwind scheme could be used. It is stable, but is not the best choice when considering SW. The second order upwind scheme is more accurate when SW exists. Choosing the QUICK scheme for all variables is also suitable for quadrilateral or hybrid meshes with SW. The MUSCL scheme is applicable to all type of meshes.

3.3.2 Density based solver

It solves in each iteration momentum, continuity and energy equations simultaneously, and then the state equation, until convergence is reached. This method may be more accurate for high speed compressible flows.

3.4 Under-relaxation factors

To control the change of the variable from one iteration to another, we can use under-relaxation factors. It can help to achieve convergence, and to make it simple this process consists on giving a certain importance to the variation of the variable: $\Phi = \Phi_{old} + \alpha \cdot \Delta\Phi$, where α is the under-relaxation factor. Under-relaxation of equations is also possible. It is highly recommended to start with the default values of these factors, but if the residuals continue to increase after the first five iterations, decreasing the value of the factors should be considered. An increase in the under-relaxation factors usually drives to an increase in the residuals, but as calculation progresses, these residuals should become lower. If unstable or divergent behavior is observed, values of the factors for pressure and momentum should firstly be changed to 0.2 and 0.5, respectively.

3.5 Turbulence models

Turbulence is the unsteady and random motion of the fluid at elevated Reynolds number. It can be solved within the Navier-Stokes equation, but Direct Numerical Simulation would need a lot of computational resources, so averaging procedures for the time and space are used.

Fluent solves the Reynolds Averaged Navier Stokes equations (the Navier-Stokes equations, but averaged in time), by contrast with the the Direct Numerical Simulation or the Large Eddy Simulation. To find the RANS equations, the variables are decomposed into mean and fluctuating values. This is done for the velocity components and other scalars such as the pressure or the energy. This decomposition is substituted on each of the equations and then they are averaged. However,

when averaging the Navier-Stokes equations with the variables splitted into mean and fluctuating value to find the RANS equations, new unknowns appear. These unknowns can be found using different conditions, which drives to the different turbulence models, like differential Reynolds stress models, algebraic Reynolds stress models or the eddy viscosity models. Some of these conditions are experimental based, so depending on the case being studied one model or another should be selected.

Several viscous models can be chosen for the solver. Some of them will automatically be discarded, such as the inviscid and laminar model. As in the transonic regime there is a strong interaction between the SW and the BL, the latter is likely to detach, altering the whole fluid field. In several cases we will have BL detachment, so an inviscid model would be unthinkable, as the results would be inaccurate. At the Reynolds number at which the airfoil will be moving ($4 \cdot 10^6$), the flow is turbulent, so the laminar model will not be used. Depending on the turbulent model used, slight disparity in the SW location may exist.

To select the turbulence model several factors must be taken into account, such as the accuracy, the available computational resources and the time.

- Spalart-Allmaras: it is a one equation model. It was developed for use in the aerospace industry, being accurate for attached wall-bounded flows and flows with mild separation and recirculation. The model is not thought to be used in massively separated flows. It is suitable to simulate the shock induced separation (Xu, X. [9]).

- k-ε: it consists in two transport equations. Although it is robust and accurate in many industrial cases, it is insensitive to adverse pressure gradients and BL detachment in smooth geometries, such as an airfoil, giving optimistic results of the separation size. As a consequence, this model is not widely used in external aerodynamics.

- k-ω: also a two equations model, it is far better when considering adverse pressure gradient and BL detachment compared with the k-ε model. The most important drawback is its high sensitivity to the free flow values of k and ω, so the solutions can be extremely different.

- SST k-ω: it is designed to avoid the free flow sensitivity of the standard k-ω model and to enhance the calculations of the flow separation from smooth surfaces. This way, it is widely used for aerodynamic flows. Compared with the Spalart-Allmaras model, the SST k-ω is more accurate in predicting the

characteristics of the BL. It uses a k-ω formulation for the inner parts of the BL, and switches to a k-ε in the free stream.

- Reynolds stress: it is ideal for flows with strong swirl.

A recommendation is to use the standard k-ε model for the first 100 iterations and first order upwind scheme. For further information about the turbulence models, see [10] or the Fluent theory guide [11] (Bakker, A. [12]).

3.6 Convergence

In this section, some tips and criterions to assure and verify the convergence of a certain calculation are presented. The convergence of the calculation is monitored using the unscaled residuals and the integrated values, such as the drag coefficient.

3.6.1 Tips

- Starting the calculation with small under-relaxation factors avoids the solution to diverge at the firsts iterations.
- For the turbulent quantities, if the initial values are poor, their respective residuals (shown in the monitors) will start low but will increase. As calculation progresses, it will eventually decrease. To verify that the solution is converged, their residuals should decrease or remain low for several iterations.
- Set a surface monitor, for example a velocity of a point of the BL, and control its variation.

3.6.2 Criterions

The default criterions for the scaled residuals are that all values, except energy, drop below 10^{-3}(10^{-6} for energy). However, this is not a rule, as it depends on the case. For this case, and based on the different observations of the monitors in the validation process, the calculation will be considered as converged when the continuity residual drops below 10^{-4}, k below $10^{-5}$and the rest of variables (ω,

energy and $v_x$and v_y) below 10^{-6}. Also when the Cl, Cd and Cm monitors are stabilized (besides the other condition) the result will have converged. To improve accuracy, several gradient adaptions will be done to the mesh, explained in the solver configuration section, section 9.

3.7 Transient calculation

Although the boundary conditions are steady, it is expected that with strong SW (with Mach numbers higher than the lift divergence Mach number) the solution become time dependant. This is due to the turbulent flow. Besides of this, buffeting may appear, so a constant solution is not assured. If the numerical simulation seem not to converge or has oscillations, the problem will be solved in a transient way.

For a transient calculation, the key parameter is the Courant number. It is defined as

$$C = \frac{V \cdot \triangle t}{\triangle x} \tag{8}$$

where $\triangle t$ is the time step and $\triangle x$ the cell size. In order the calculation to be stable, it must be in the order of 3 to 7 (the lower, the better, but more time to calculate) (Xiao, Q. [13]).

For each time step, it is not necessary to achieve the convergence, so the number of iterations per time step can be lower.

Part III

STATE OF THE ART

Too much studies about the use of CFD for the study of SCA have been carried out. Most of them, like "Numerical Simulation of Transonic Buffet over a Supercritical Airfoil" of Sébastien Deck, have taken profit of the computational resources to solve time dependant problems such as the buffeting effect. Other studies focused on the comparison between CFD and experimental results, to improve the corrections used for the experimental results, that must be corrected due to 3D effects (Xu, X. [9]). For this work, several examples of CFD solutions for SCA have been compared to better select the flow parameters.

The current state of the art focuses in devices that allow lower drag coefficients at higher Mach numbers, used in existing SCA.

4 Contour bumps for transonic drag reduction

The main concern on commercial aviation since the last decade has been the reduction in drag to lower the fuel consumption, rather than achieving higher or even supersonic speeds. In this field of investigation, numerical optimization of existing airfoils has been carried out. Is the case of Andreas Sommerer, Thorsten Lutz and Siegfried Wagner. In their numerical studies, they found that fixed and variable bumps in the upper surface of the SCA could be used to reduce the drag by 12-15 %, at design and off-design conditions (out of the transonic regime), by reducing the SW strength. Its height would be of the order of 0.005 C, with the crest of the bump at 1-2 % C downstream of the normal SW.

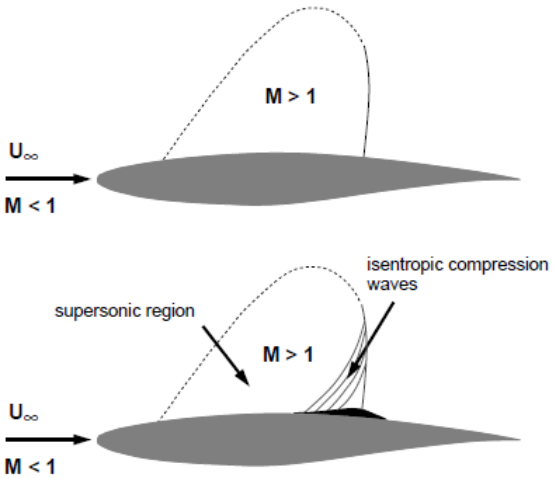

Figure 15: Comparison between a supercritical with and without a bump; From Sommerer [14]

As we can observe in figure 15, these bumps transforms the larger and stronger

SW into smaller and weaker compression waves plus a weak SW. A comparison of the pressure distribution with and without the bump is shown in figure 16. As can be clearly observed, the SW is converted into compression waves and a weaker SW, so the BL is less likely to detach.

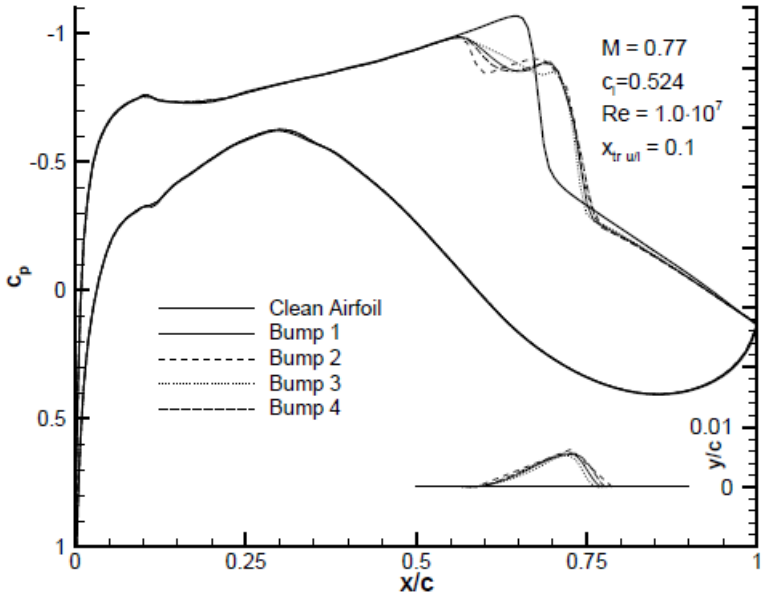

Figure 16: Comparison of pressure distribution with and without bump; From Sommerer [14]

However, some problems might arise: with lower lift coefficients (i.e., lower AoA) a fixed bump creates more drag. This occurs because the shock wave on the airfoil upper surface moves forward of the contour bump. The flow re-accelerates over the bump, and a second normal shock wave forms aft of the contour bump. In addition, the resulting double shock wave pattern separates the BL, further increasing the drag coefficient. The conclusion is that an active bump, capable of varying its shape, should be considered. Also, a possible adverse pressure gradient created by the shape of the bump should be taken into account to avoid flow detachment (Sommerer, A. [14]).

4.1 Boundary layer suction

Another approach to reduce the drag is by using laminar airfoil technology and the use of venting and BL suction close to the upper surface shock to reduce wave drag[2]. Results generally suggested that it was possible to achieve wave drag reduction through passive control, but the overall drag was not reduced because of

[2]Wave drag is not caused by flow separation after the SW, it appears due to the existence of the SW.

the increased viscous drag associated with the surface porosity under the shock wave (Sommerer, A. [14]) (Owens, R. [15]).

5 Laminar supercritical airfoils

Converting the turbulent part of the BL into a laminar one helps reducing the viscous drag. Through modifying the shape of an existing airfoil, natural laminar BL can be obtained (that is, with any kind of devices that alter the BL). As shown in figure 19, a total Cd (the addition of viscous and pressure drag coefficient) reduction is achieved, specially at Mach numbers below the drag divergence Mach number. Viscous drag is always lower for the laminar BL, as shown in figure 18. The increase in pressure drag coefficient experienced in some of the variations of the airfoil with respect to the base airfoil (NASA0412) could be explained due to the laminar boundary detachment (Zhao, K. [16]).

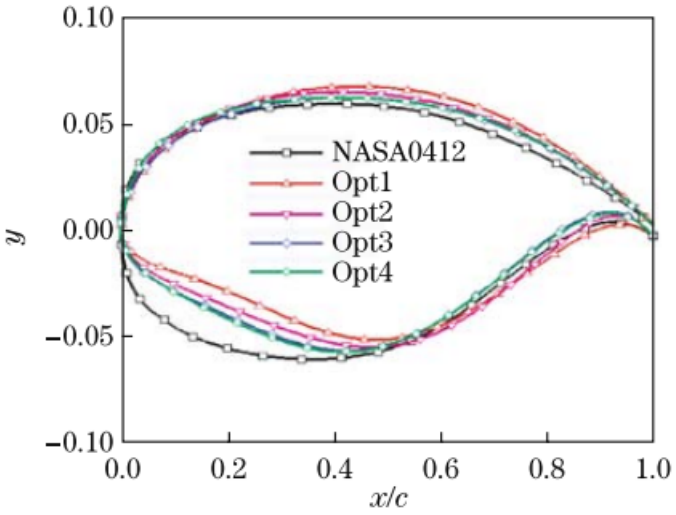

Figure 17: Airfoil modification for laminar BL; From Zhao [16]

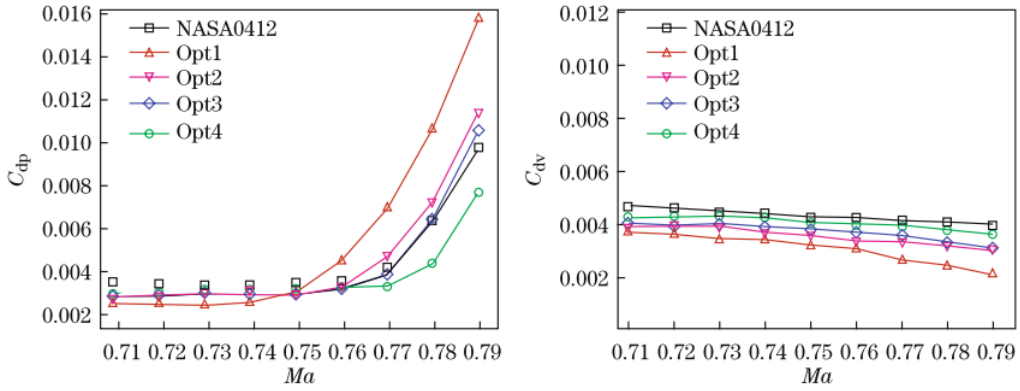

Figure 18: Pressure and viscous drag coefficient for laminar supercritical airfoil; From Zhao [16]

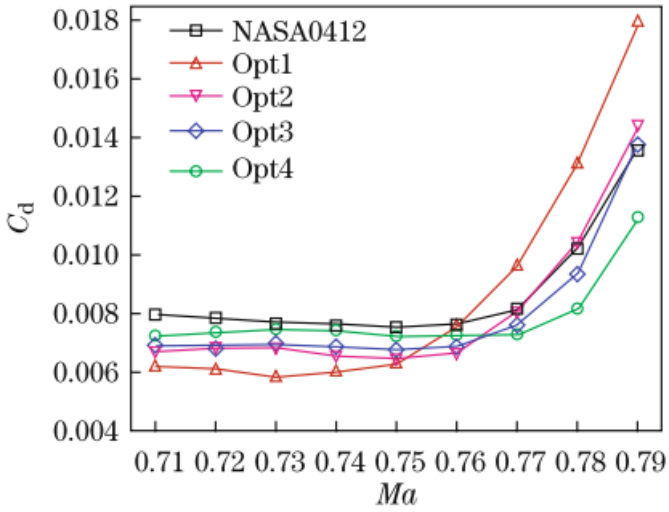

Figure 19: Drag coefficient for laminar supercritical airfoil; From Zhao [16]

6 Buffet control

Buffeting affects both aerodynamic and structural behavior of the wing, affecting strongly the maneuverability. The origin of the buffet phenomenon is the flow separation without control between the SW and the trailing edge. Mechanical and fluidic vortex generators are known to suppress this effect. This is obviously a 3D study, but as it involves transonic flow over a wing of SCA, we will consider them. The objective of these devices is to decrease the separation size. As the mechanical vortex generators increase drag in normal cruise conditions, the need for a device that could be turned off arose: that is the origin of the fluidic vortex generators. The mass flow through the fluidic VG can be regulated, so optimal results are obtained,

with the jet exiting the fluidic VG at Mach 2 (Dandois, J. [17]) (Xiao, Z. [18]).

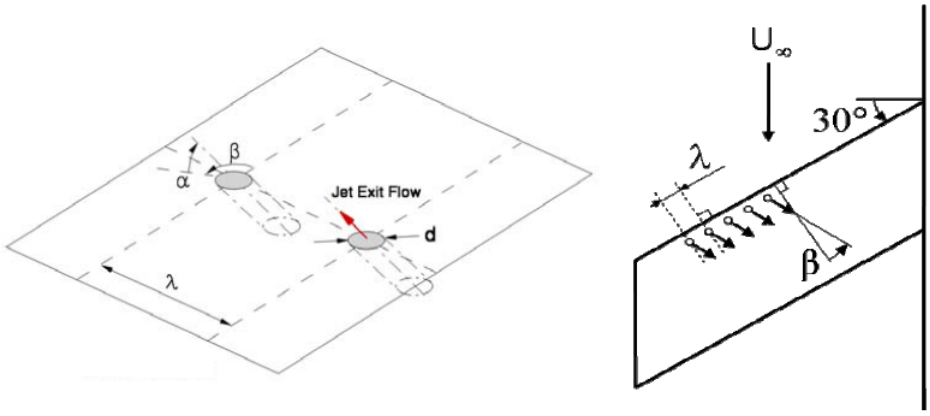

Figure 20: Different parameters of fluidic vortex generators; From Dandois [17]

7 Boundary layer separation control with plasma

As SCA usually have a medium relative thickness, their stall at low speeds starts in the leading edge. One method (and the most common) to avoid the BL separation at high AoA or facilitate the readhesion is the use of passive high lift devices. While passive devices such as leading edge flaps or slats are mechanically complex (increasing weight and manufacturing cost), active devices only require a relatively low power to work and are entirely surface-mounted.

Some active high lift devices are based on applying cyclic velocity perturbations injecting mass to the BL, but and electromechanic driver is used to create the oscillatory flow. To provide large amplitude oscillations, the driver is operated at resonance, so mechanical failure often occurs. Taking all this into account, plasma control (an active high lift device) seems to be a suitable solution for the leading edge stall, and it would be the ideal solution for the more-electric aircraft philosophy.

The flow control with plasma actuation can be divided considering the form of the electric current applied. If alternate current is used, the device is useful with freestream velocities up to 30 m/s. The charged species of the plasma interacts with the neutral air and a near wall jet forms with a velocity of 10 m/s with respect to the airfoil, energizing this way the BL. The main drawback using alternate current is the restricted freestream velocity, too low for a normal civil aircraft. However, using nanopulses (pulses during nanoseconds), the free stream velocity increases to M=0.740. They are not based in the interaction between charged and neutral particles (as in alternate current), and the underlying flow physics remain unanswered. The nanopulse produce very low velocity to the neutral species, but it is believed

that Joule heating generates a local compression wave, and the device is useful, as said before, for higher freestream velocities. However, a deeper analysis should be carried out to verify the electromagnetic compatibility, to assure that the device does not interfere with the electronic equipment (Little, J. [19]) (Huang, X. [20]).

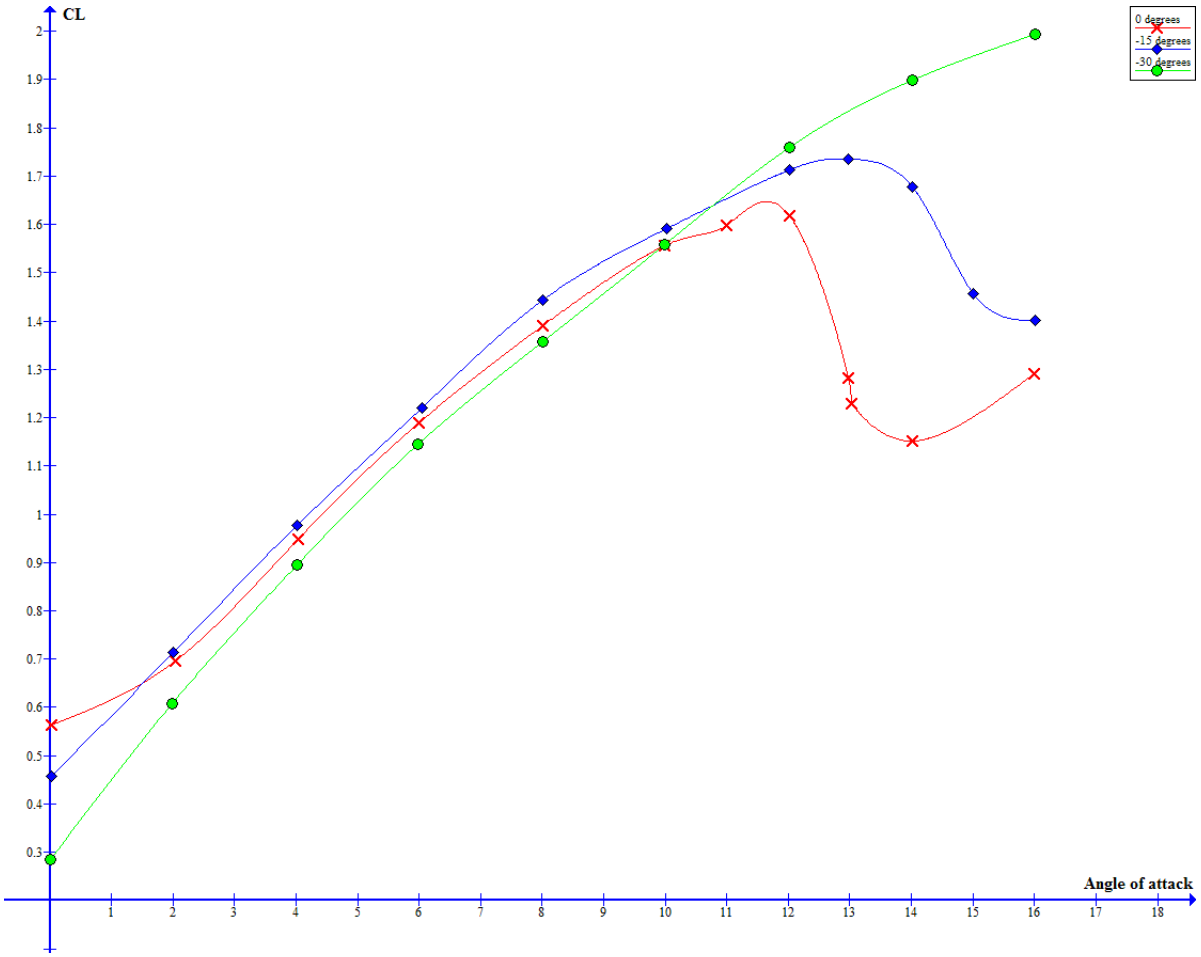

Figure 21: Leading edge slat at different deflections, $Re = 0.75 \cdot 10^{10}$; Adapted from Little [19]

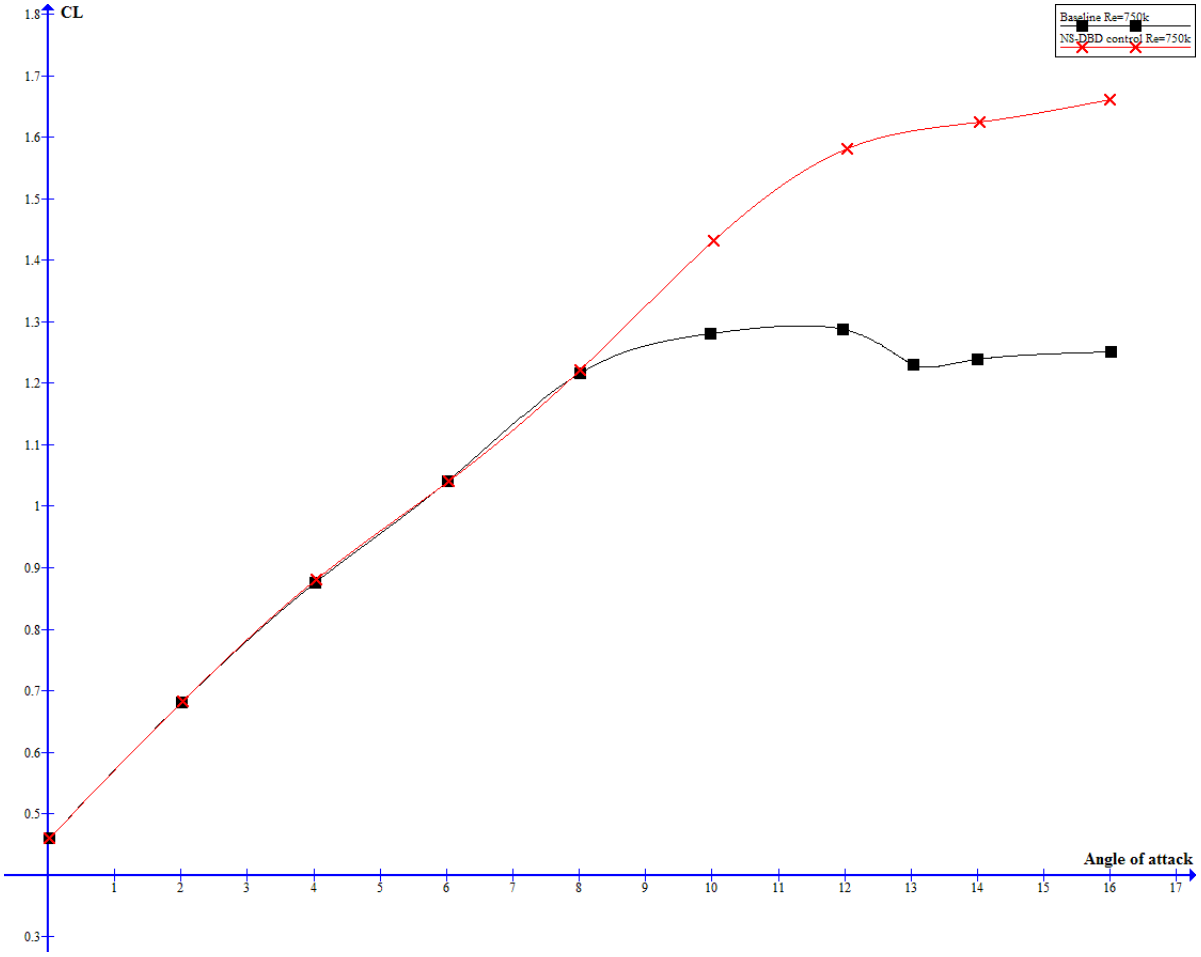

Figure 22: Same supercritical airfoil with the nanopulse plasma device installed; Adapted from Little [19]

Higher lift coefficients can be achieved using plasma control, as shown in figure 21. The vertical red bars are possible values of the lift coefficient.

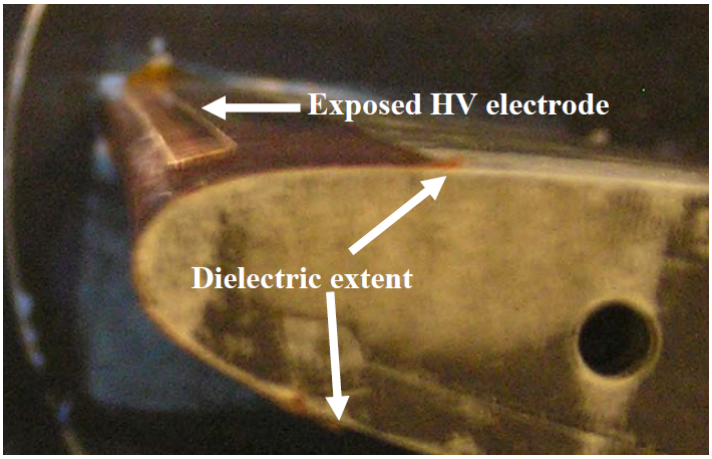

Figure 23: BL control using plasma; From Little [19]

Part IV

RESOLUTION

8 Mesh

Several meshes must be made in order to assure that the solution found is independent of the refinement of the mesh: this is the so-called mesh sensitivity process. Each mesh will be done using ICEM, a commercial software designed for meshing. After the mesh is done, it must be validated with the turbulence model included. After this process, the mesh is suitable for the required numerical calculations.

For further information of each mesh, please refer to the mesh attachment.

8.1 ICEM

The basic principle of ICEM is the creation of blocks. The block can be thought as a quadrangle. Each of the edges of the block can be splitted in several parts, and with the desired distribution of space (more divisions can be concentrated where required). These divisions will constitute, together with the other edges, the mesh. The blocks can be divided or even merged. The edges can vary its shape, so there will be edges with the shape of the airfoil and, consequently, the block that form the edges related to the airfoil will be deleted, as there is no fluid inside. For example, a block could be created and later refined for the analysis of the SW, as elevated gradients in this area require a finer mesh. Although this could be done by estimating the SW location with a coarser mesh in Fluent and then remeshing with ICEM the SW location, this will not be made as several iterations should be done just to find the SW location. The gradient adapt function of Fluent will be used instead: zones with high gradients (of the desired magnitude) can be graphically observed and then cells with the gradient higher than a certain value will be automatically splitted into finer cells.

From the user´s point of view, the main advantage of this software is the total control over the entire mesh and the easiness to see what each command is actually doing. However, this can be also a drawback, as sufficient practice is required to generate a good enough mesh.

Later, as parts have been created, such as the far field or the airfoil, when converting the mesh into a ".msh" file readable by Fluent, boundary conditions can be selected for the different parts.

8.2 Generation

The key for a good mesh is the distribution of the cells: more cells are needed were sections with high gradients might exist. In the leading edge there is expected a huge gradient of pressures, from the stagnation point to the end of the leading edge. Also, in the BL, the gradient of velocity (in the direction perpendicular to the surface) must be found in order the drag results to be accurate. Finally, in the concave zone in the afterward of the lower surface, adverse pressure gradients are likely to appear, so more cells are concentrated there. As said before, no special treatment is considered for the SW, as it is easier to refine it with the gradient adapt function.

For the different meshes that will be used for the mesh sensitivity process, the same BL meshing will be used, as for the turbulence model to be accurate, a parameter called y+ must be equal to a certain value depending on the model.

A coarser mesh will be implemented (mesh 1) and then with the refinement tool the number of cells will be incremented. It has to be noted that if the selected refinement for a block is level 2, the number of cells for that block will be multiplied by four, so a careful study of the zones to refine must be carried on (there is a computational limitation of nearly 200.000 cells).

8.2.1 Why using a structured mesh?

To resume the main advantages or drawbacks of structured and unstructured meshes, table 1 is shown [21].

Mesh	Advantages	Disadvantages
Structured	Easier to write if implementing the solver Faster grid regeneration if geometry is slightly modified More accurate results for airfoils Less time of convergence, due to more efficient algorithms	Concentration of cells in not required zones (fig. 24) Worse with difficult flows
Unstructured	Easier to adapt to difficult shapes (fig. 25) For complex flows, adaptivity may allow more accuracy	Requires storage of cell to cell pointers, so slower execution of code

Table 1: Comparison between structured & unstructured mesh

With all these ideas in mind, a structured mesh is selected, as the the SCA is not a relatively difficult shape and the structured mesh works well for airfoils. Also, the transonic flow is not considered a complex flow, and the convergence time is

lower for the structured mesh.

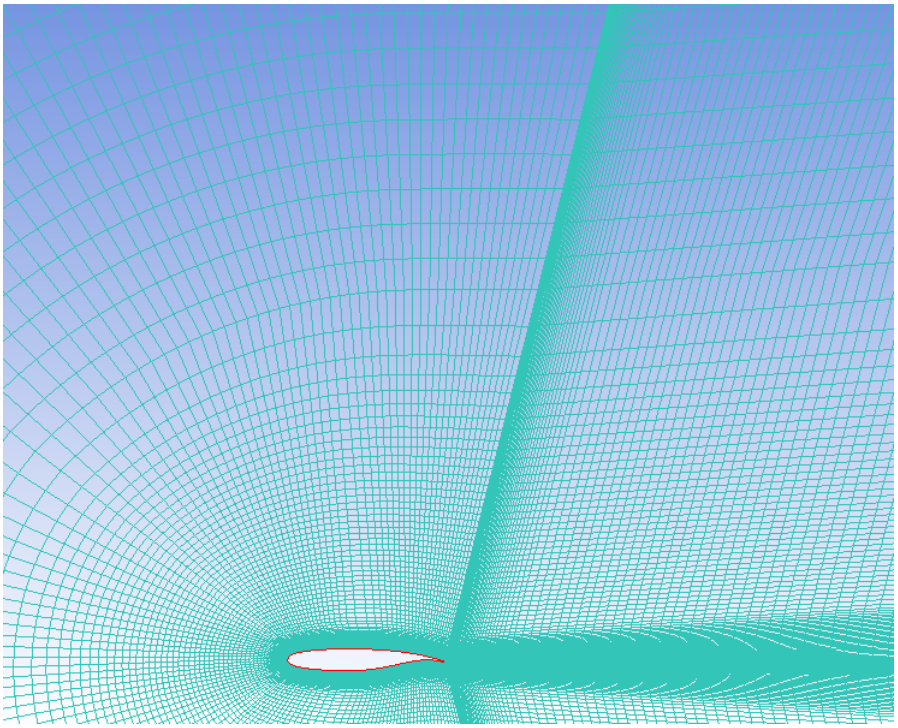

Figure 24: Structured mesh

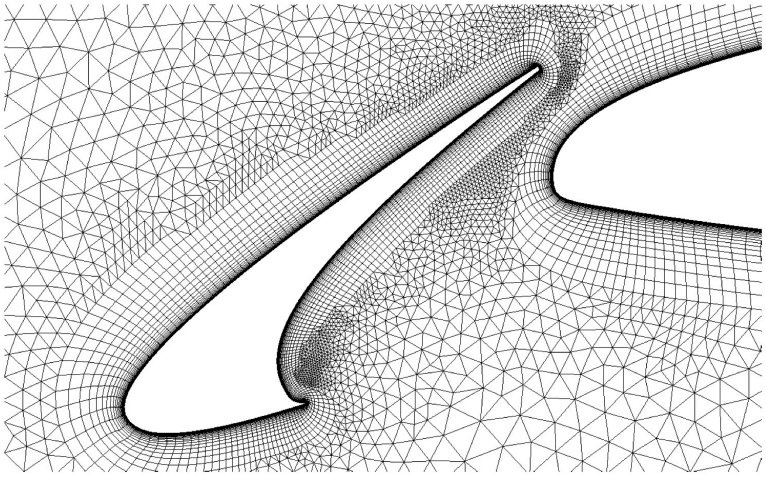

Figure 25: Untructured mesh, difficult shape as a slat

8.2.2 Select the first cell height

To select this important parameter, viscosity must be taken into account, and empirical results must be considered.

$$\triangle y_1 = \frac{y+ \cdot \mu}{\rho \cdot U_\tau} \tag{9}$$

A calculator for y_1 can be found in [22] knowing the Reynolds number and the y+. As the Re used for all calculations will be fixed at $4 \cdot 10^6$, the value of y+ is 5 for the k-ω SST turbulence model[3], this value of the height, for a chord of 1 meter, will be $3.28 \cdot 10^{-5}$ m. With this value, the turbulence model can apply a velocity profile for the laminar sub-BL, being accurate enough. Just to ensure, the values obtained of y+ should be verified in the calculations.

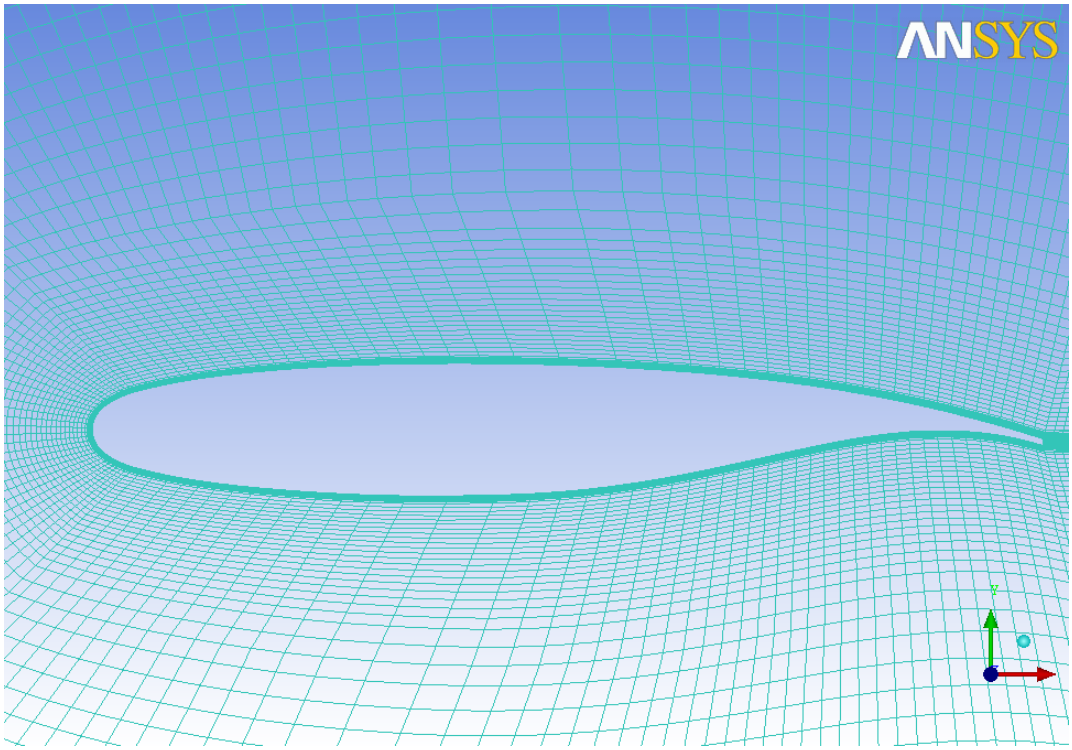

Figure 26: Cells distribution, first mesh

With the refinement function, each cell is divided, so the distribution will remain constant.

8.3 Quality

To check the mesh quality, four different forms to measure it will be considered,

[3]The justification of the election of this turbulence model will be made in section 9.

for each one of the cells:

- Determinant 3X3: it computes the deformation of the cells. A value of 1 is a perfect square, while a value of 0 would be a negative volume. The minimum acceptable value for Fluent is 0.3. For the first mesh, the minimum value is 0.73.
- Angle: if the elements are distorted and the internal angles are small, the accuracy of the solution will decrease. It must be greater than 18°, but at 9° it might be accurate in Fluent. For the first mesh, the minimum value is 50.4°.
- Volume: to check whether a negative volume exists, this tool is useful.
- Quality: it must be greater than 0.3 in order the mesh to be acceptable. For the first mesh, the minimum value is 0.73.

Not only the values have to be taken into account, but also the location where these values take place (it would be worst if the critical points are those in the nearby of the airfoil). In this case, cells in contact with the airfoil have a quality of more than 0.9.

8.4 Validation

For the validation, 6 tests will be carried on for each mesh, at a Reynolds number of $4{\cdot}10^6$ (as the BL meshing is suitable up to this Re number). The validation consists on the comparison of numerical results with experimental ones (to compare them, they must have the same Re number and Mach number). The ideal result to compare is the pressure distribution over the airfoil, to verify whether there are parts that require refinement or not, such as the leading edge. The experimental data is extracted from (Jenkins, R. V. [23]). If experimental data of the selected airfoil did not exist, other SCA should be considered for the validation, with the same distribution of cells in the mesh. Then, after validating the mesh and the turbulence model, we could continue with the calculations of the selected airfoil. An important point to consider during the validation is that the different numerical schemes that are likely to be used during the later calculations should be used in this point of the project, so a clear idea of the different numerical schemes is mandatory. As an example, one of the validations is shown below. More validations can be observed in the Mesh attachment.

8.4.1 Example of the first mesh

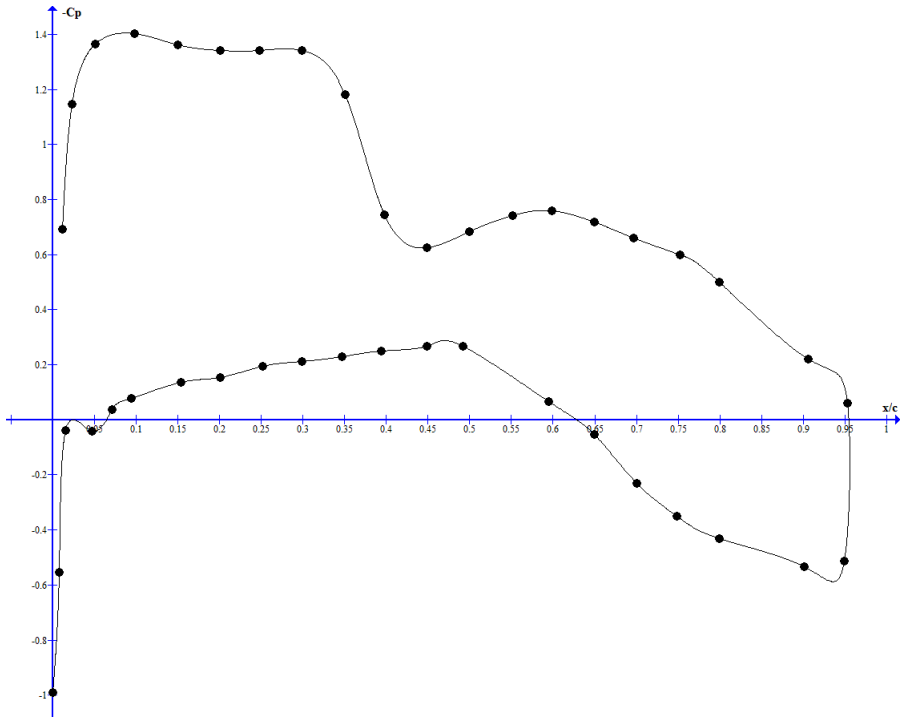

Figure 27: Experimental data at M=0.710 and α=2.00°; From Jenkins [23]

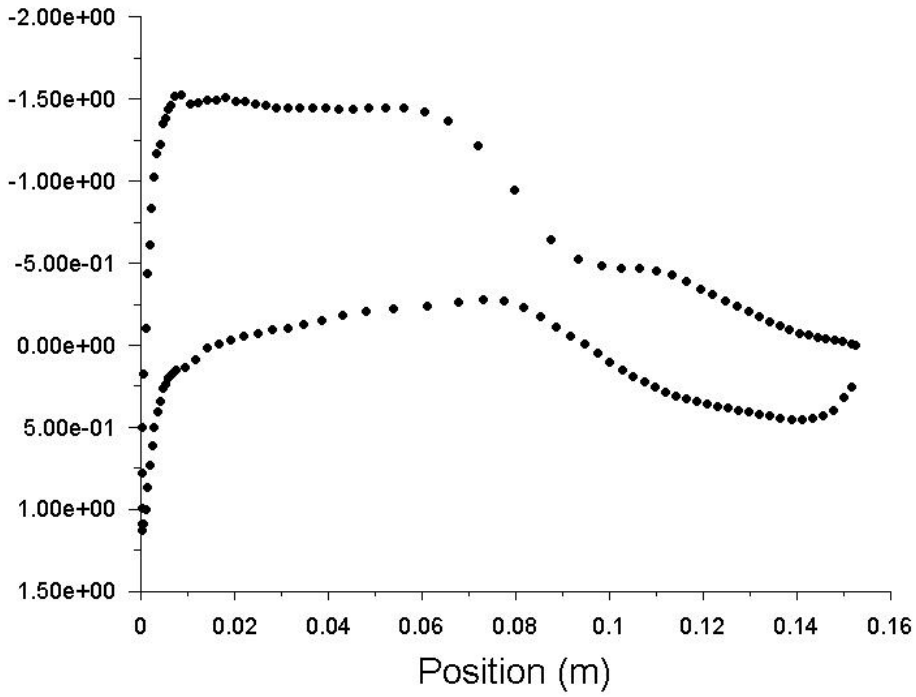

Figure 28: Mesh 1 at M=0.710 and α=2.00°

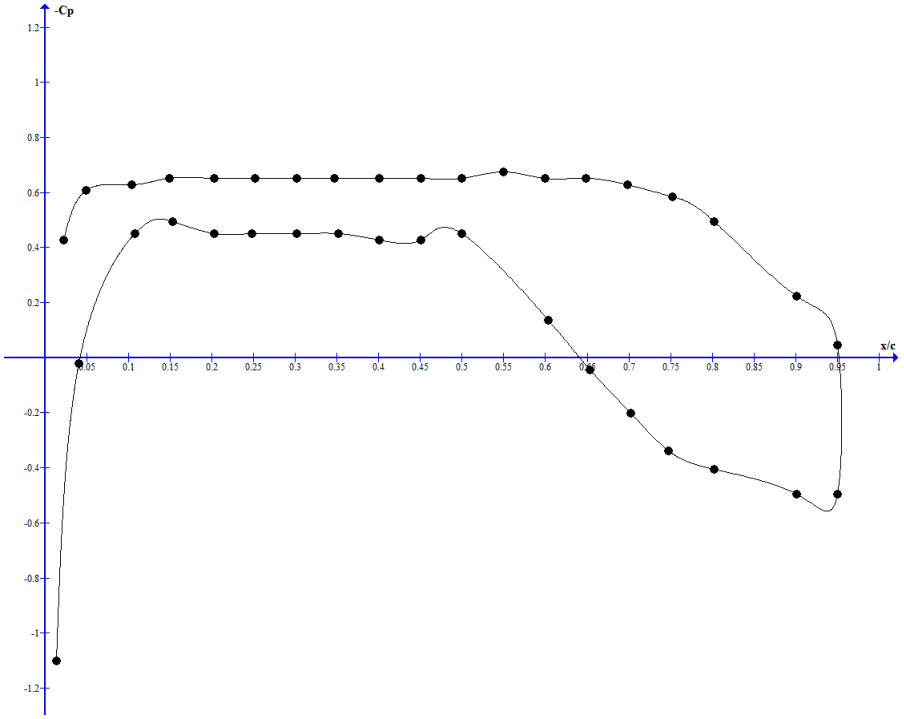

Figure 29: Experimental data at M=0.720 and α=-1.00°; From Jenkins [23]

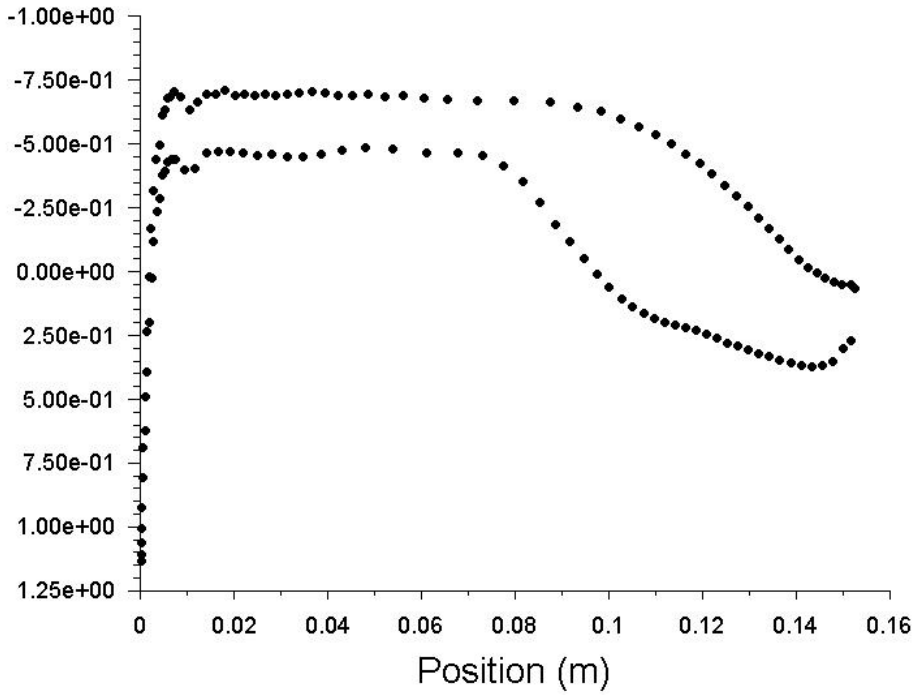

Figure 30: Mesh 1 at M=0.720 and α=-1.00°

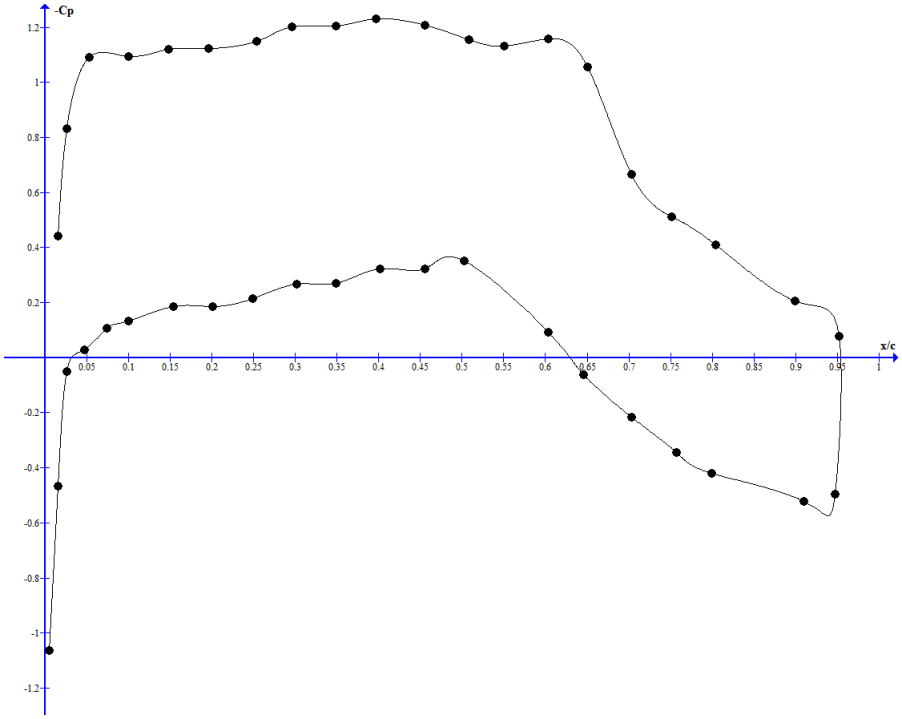

Figure 31: Experimental data at M=0.750 and α=1.51°; From Jenkins [23]

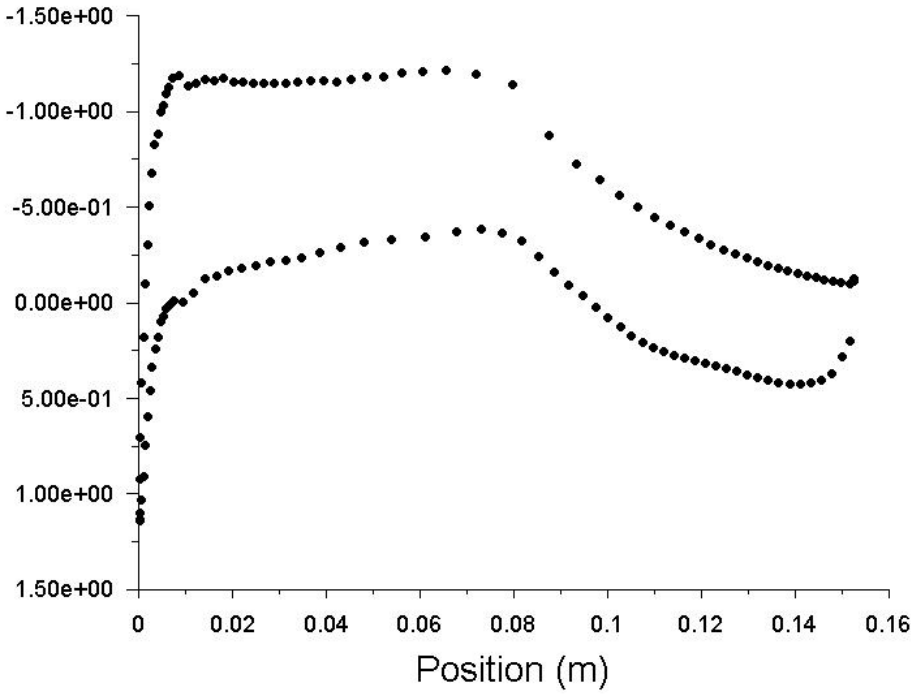

Figure 32: Mesh 1 at M=0.750 and α=1.51°

As it can be observed, the mesh performs well in both upper and lower surfaces. A slight difference in the SW location can be due to the low mesh refinement in the upper surface; this will be compensated through the refinement in the next meshes,

but this mesh is validated and it will be useful for the mesh sensitivity process.

9 Solver configuration

In this section the main parameters that have been selected for the calculations are shown, based on the theory developed in section 3.

9.1 Problem setup

9.1.1 Solver type

The pressure based solver is selected, as with certain numerical schemes it will be accurate when compressible flow and SW exist.

9.1.2 Models

The energy equation must be enabled as for a compressible flow calculation it is needed to find not only the temperature, but also the rest of variables (speed, pressure...).

For the viscous model, the k-ω (2 equations) SST model is selected (Spalart-Allmaras has also been considered). Both are suitable for detached flows, but the first one is more accurate when calculating the BL characteristics. Then, the compressibility effects and the viscous heating must be taken into account.

In the materials section, air is selected as the fluid. The ideal gas model for the density can be applied as in the simulation the pressure is relatively low and the temperatures are high. For the specific heat, although a temperature dependant function could be used (as it would be more accurate), the temperature field is not expected to have a wide range, so for the air the specific heat would barely change. The thermal conductivity is as well considered constant. For the viscosity, the Sutherland model is the right choice for high speed compressible flows [11].

9.1.3 Boundary conditions

The airfoil will be considered adiabatic, so the heat flux is fixed to zero. Only the temperature field would change appreciably in the thermal BL if a heat flux distinct to zero were used. The shear condition over the airfoil is "no slip". For the far field boundary conditions, as this boundary is further than 20 chords from the airfoil, the

angle of the flow is the desired AoA, the Mach number in this boundary is the desired free stream Mach number and the pressure is constant, equal to that ambient pressure. Pressure and temperature will be fixed so the Reynolds number is $4{\cdot}10^6$.

9.1.4 Reference values

These values, from which the coefficients will take their reference, will be set to the free stream values, in the far field.

9.2 Solution

9.2.1 Angles of attack and Mach numbers to calculate

As the SCA are intended to operate at high speeds, the encountered AoA will not be relatively high, so the AoA will be 1º, 2º, 3º, 4º and 5º. For the selection of the Mach numbers, typical values for SCA such as 0.7 to 0.75 should be taken for the first cases. Then, when some cases have been solved, for example five, these rough results can be plotted in a work sheet to visually verify if the Cd is increasing with the Mach number or also the behavior of Cl. This way, the next Mach numbers can be selected to find the critical Mach number (if, for example, for the calculated cases transonic flow exists) and the divergence and the lift coefficient. This way, if unnecessary tests have been done with the first mesh because they do not provide useful information, these tests will not be done to the other meshes to save time.

When enough values are obtained, if the Cd-Mach number plot has a certain positive slope, a polynomial approximation to the points could be made to derive it and find the approximate drag divergence Mach number (as explained in the equation 2), and if the Mach is in the range of the tested points, that will be taken as the solution for the drag divergence Mach number.

9.2.2 Solution methods

For the pressure-velocity coupling, the coupled scheme is chosen (with the pseudo-transient option enabled). It is faster and more robust than the segregated algorithm and performs well in applications involving high speed aerodynamics with shocks. However, if problems with convergence exist, the SIMPLEC method is suitable for flows with SW, and it might also be selected.

In order the solution to converge, for the first mesh (the coarsest one), density,

momentum, turbulent kinetic energy, specific dissipation rate and energy are set at first order upwind (and under-relaxation factors of 0.5). Then, for the first mesh, the solution will be initialized using the hybrid initialization, and then the full multigrid initialization. After 300 iterations with the first order upwind scheme, more or less realistic values are obtained. However, as this is not accurate (due to the numerical diffusion effects), the SW will not even be present, so no gradient adaption can be made at this point. Now, the numerical scheme is changed to second order upwind, and the monitors switched on (if they were switched on for the first iterations, less resolution will be available in the axes, so the convergence would be difficult to verify with the naked eye). 3000 iterations will be made, with a gradient adapt made every 750 iterations (enough to assure stability in every re-mesh) to refine the SW zone (if exists), with the under-relaxation factors set at 0.3. If the gradient adapt were made every 20, for example, the solution would probably diverge as in each re-mesh the stability would not be achieved.

For the rest of the meshes, the solution will not be initialized the way it was for the first one. The interpolation from the first mesh will be used instead. First, 375 iterations will be done. Then, 3000 iterations will be performed, with a gradient adapt made every 750 iterations (enough to assure stability in every re-mesh) to refine the SW zone (if exists), and the monitors switched on.

10 Mesh sensitivity

After each mesh is used in the calculation, and it is considered that it is converged, the results of Cl, Cd and Cm will be compared with the later mesh (coarser). If all three results are within 5% of difference (in absolute value), the mesh sensitivity process will be finished for that calculation and that will be the final results (note that the meshes to compare must have a considerable difference in the number of cells; if not, a low difference in the results would not mean anything). If not, the next finer mesh will be used. If high differences exist, the Mach field and the pressure coefficient diagram will be compared to check whether one of the two meshes has a problem. As an example, the calculation at M=0.725 and $\alpha = 1^{\circ}$ is shown:

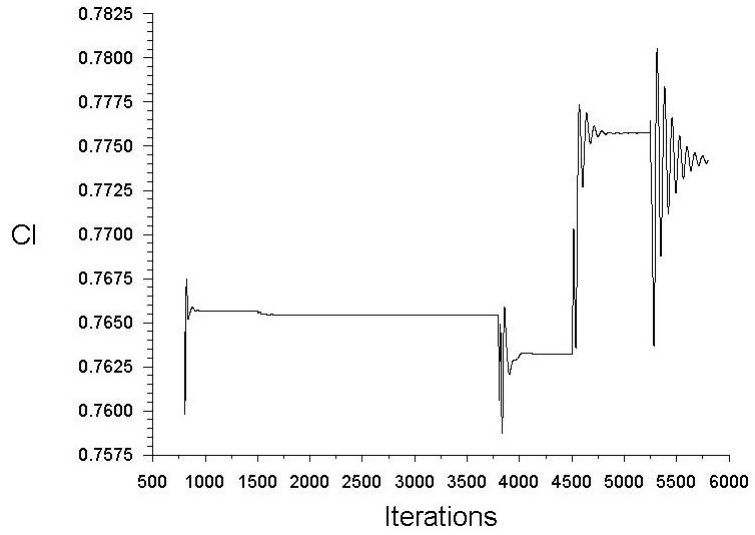

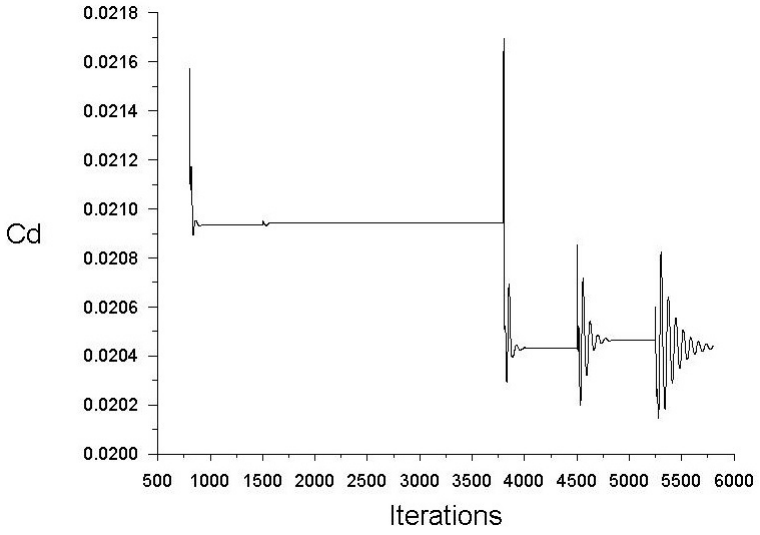

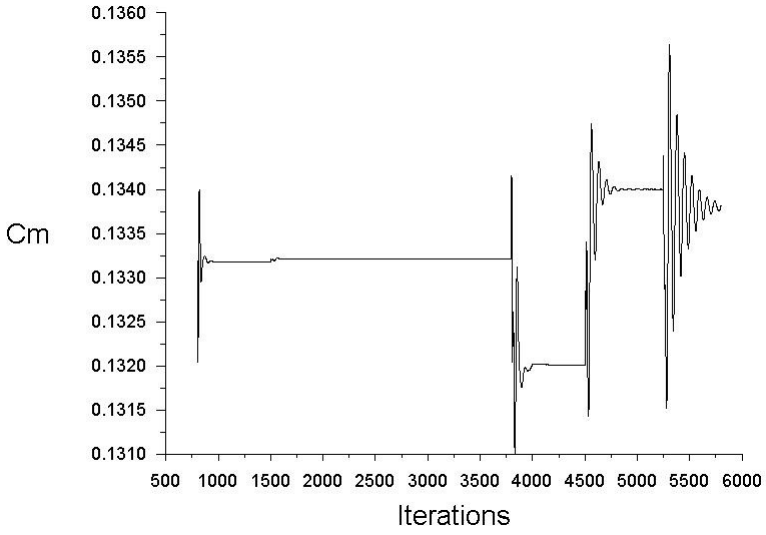

Figure 33: Mesh 1 results for α=1º and M=0.725

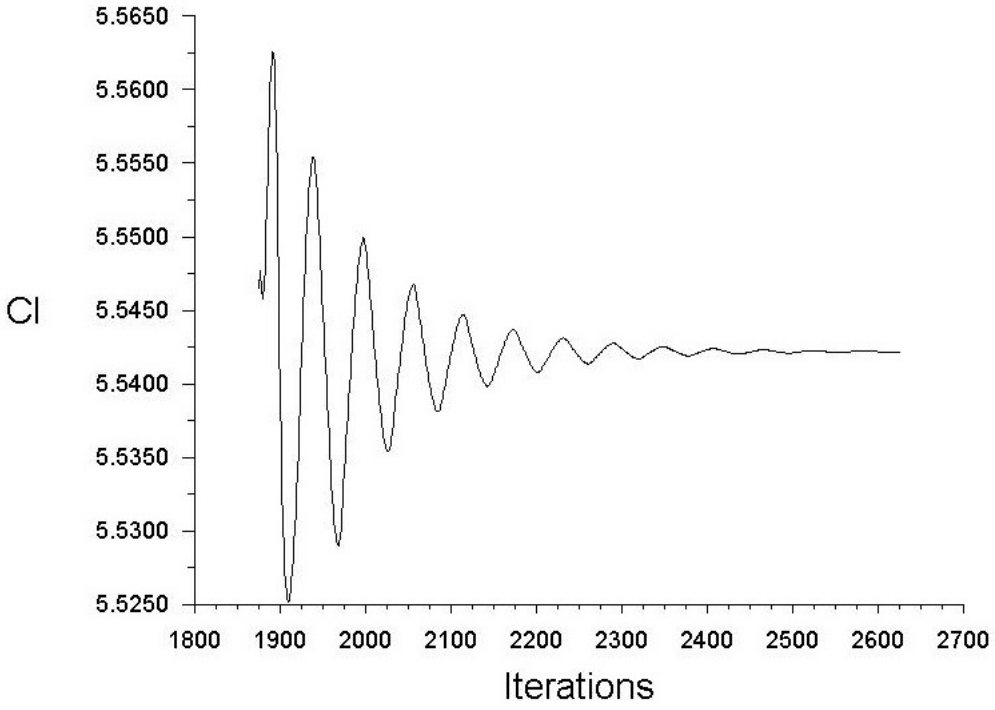

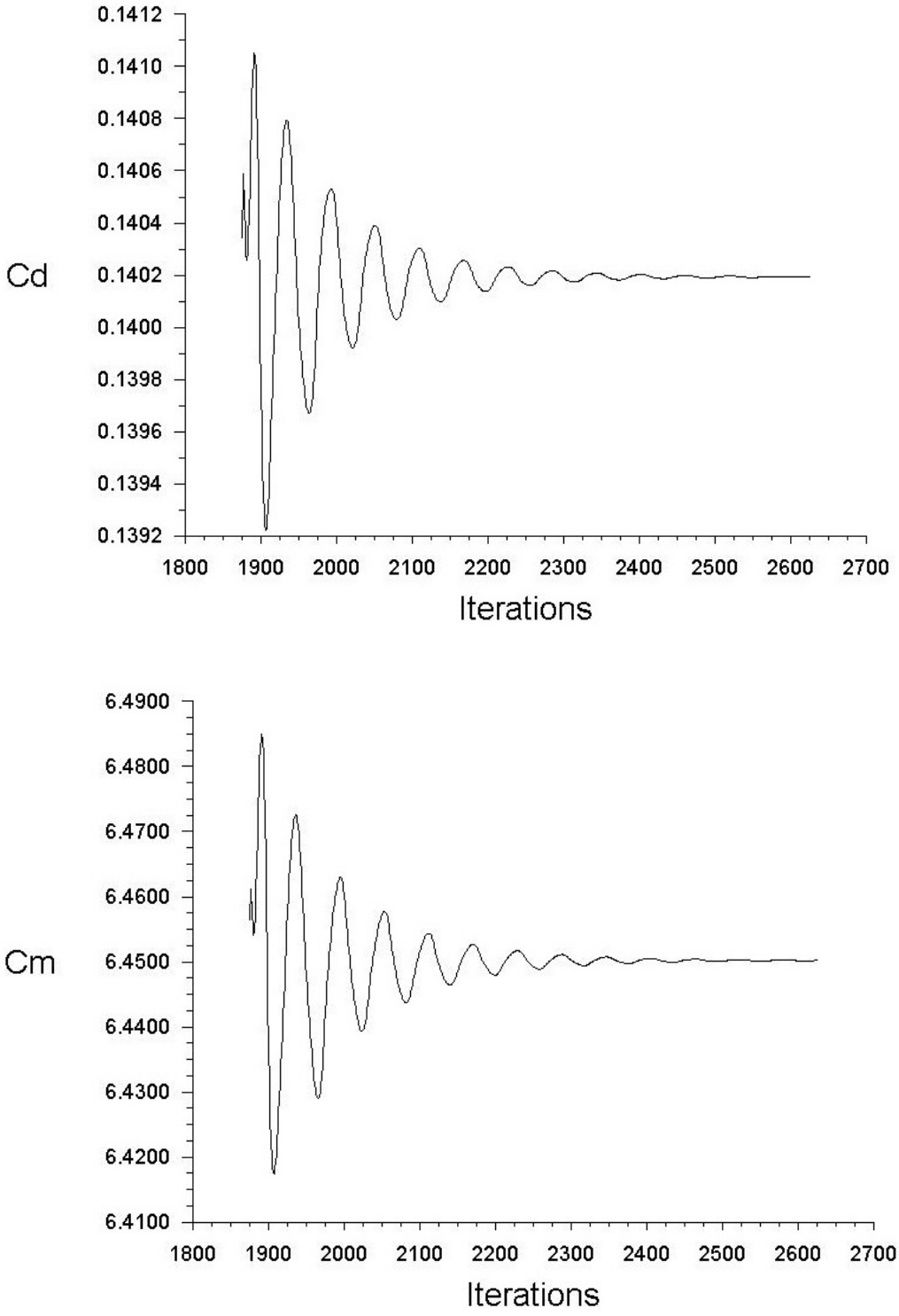

Figure 34: Mesh 2 results for α=1º and M=0.725

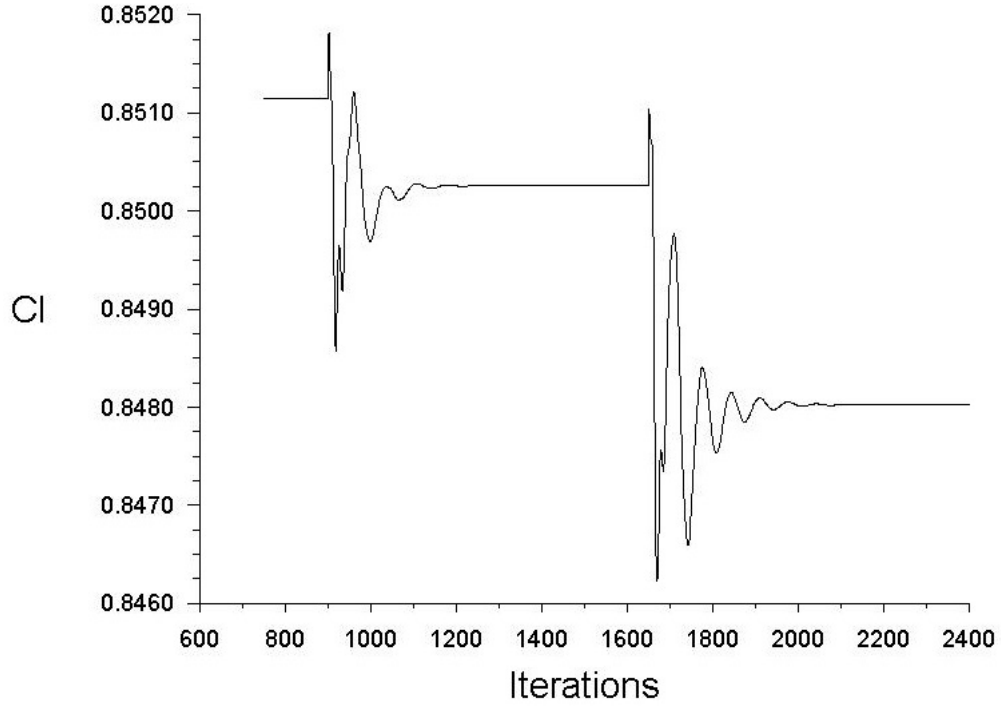
Cl
0.8520
0.8510
0.8500
0.8490
0.8480
0.8470
0.8460
600
800
1000
1200
1400
1600
1800
2000
2200
2400
Iterations

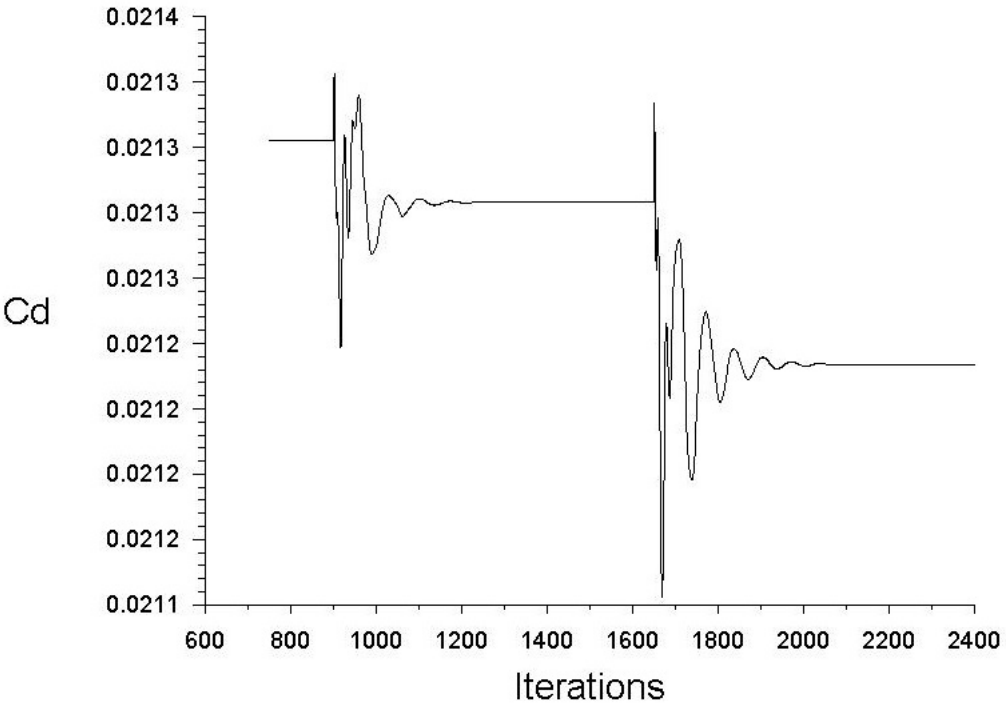
Cd
0.0214
0.0213
0.0213
0.0213
0.0213
0.0212
0.0212
0.0212
0.0212
0.0211
600
800
1000
1200
1400
1600
1800
2000
2200
2400
Iterations

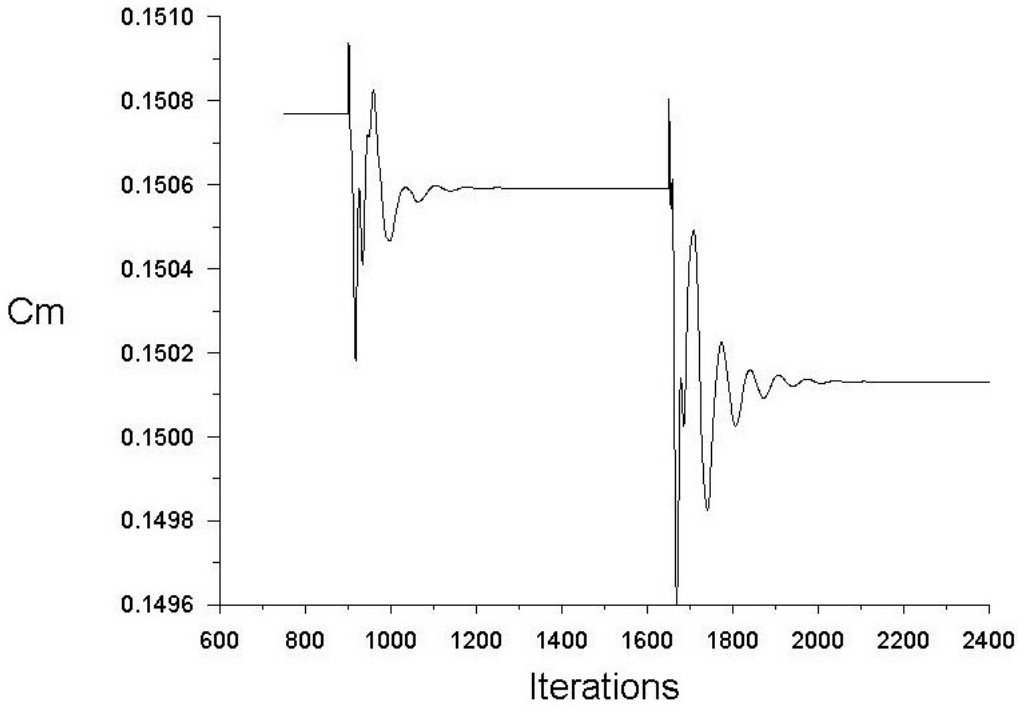

Figure 35: Mesh 4 results for α=1º and M=0.725

The differences between the mesh 1 and 2 are not acceptable: there is a difference of 8.99%, 4.75% and 11.79% in Cl, Cd and Cm values, respectively. However, the difference between mesh 2 and 4 (mesh 3 has not been used as it is mesh 2 but with refinement in not so required zones) are 0.39%, -0.80% and 0.2%, with a ratio of difference of number of cells of 1.76, located in the nearby of the airfoil, so results of mesh 4 are taken as the final results for this problem.

11 Example of transient calculation

Depending on the mesh that is being used, to maintain the Courant number below 7, the time step will be different. As an example, at $\alpha = 2$º and M=0.73, convergence is not achieved; for mesh 2, applying equation 8, a time step of 0.0001 seconds, velocity of 206 m/s and a cell size of 3 milimeter gives a Courant number of 6.87.

The selected cell size is the distance tangent to the airfoil near the BL, as the flow main direction there will be tangent to the airfoil (it is an approximation).

10 iterations per time step are used, and no problems of convergence are observed.

Part V

ANALYSIS OF RESULTS

For each of the five AoA, ten different Mach numbers have been tested. For each of the test, a mesh sensitivity process has been carried on. Although the drag results were virtually the same for all meshes in a same test, both lift and moment coefficient results were so different that required the use of three meshes to verify the mesh sensitivity. As an example, α=2º is shown in figure 36.

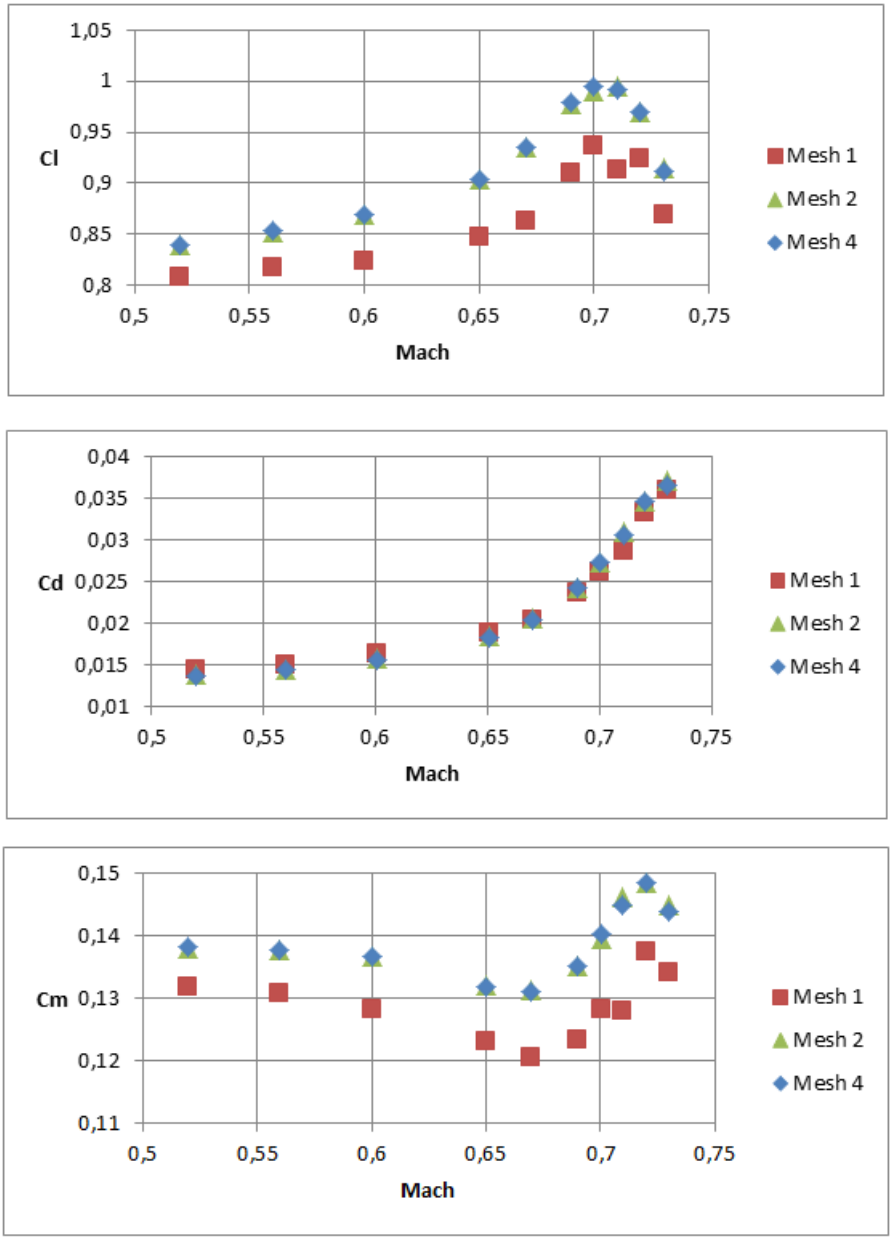

Figure 36: Mesh sensitivity at α=2º

Note that the divergence Mach numbers are the same for all three meshes. As the difference in each test between mesh 2 and 4 is within the 5%, the mesh sensitivity is checked.

12 Results

12.1 $\alpha = 1°$

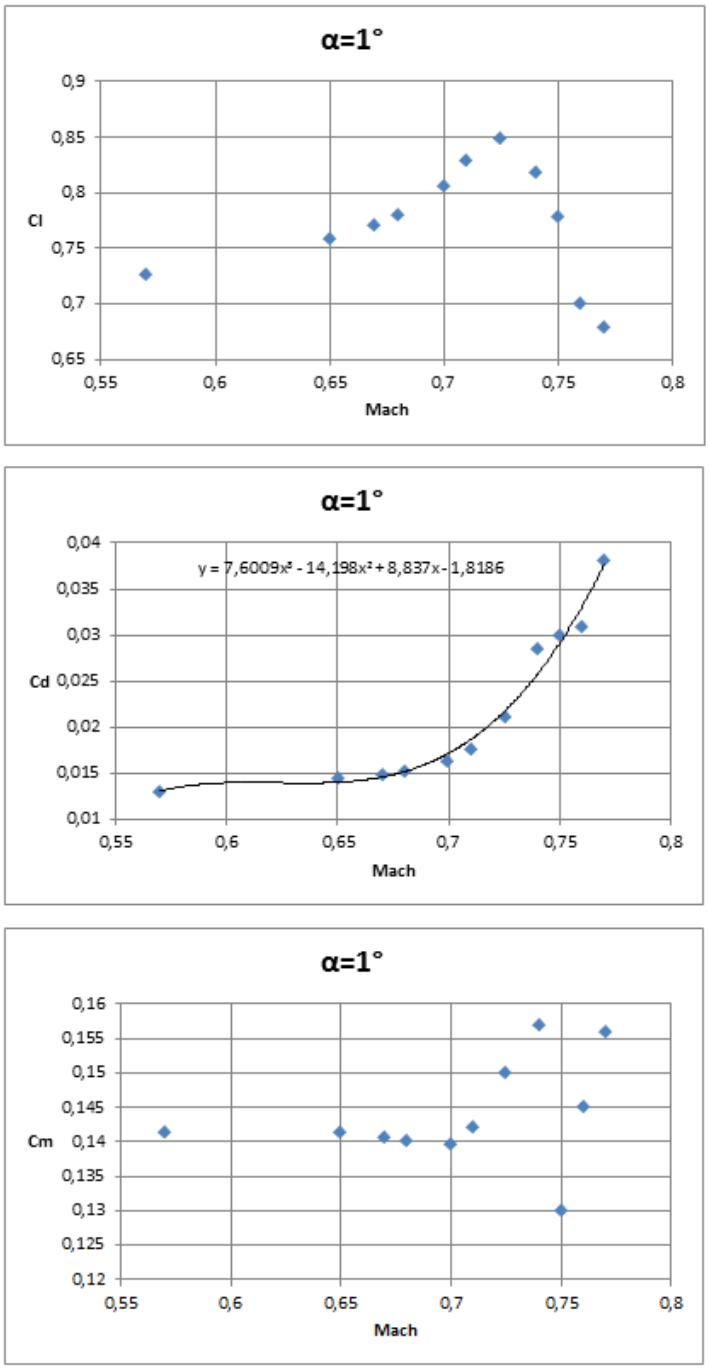

Figure 37: Results at $\alpha = 1°$

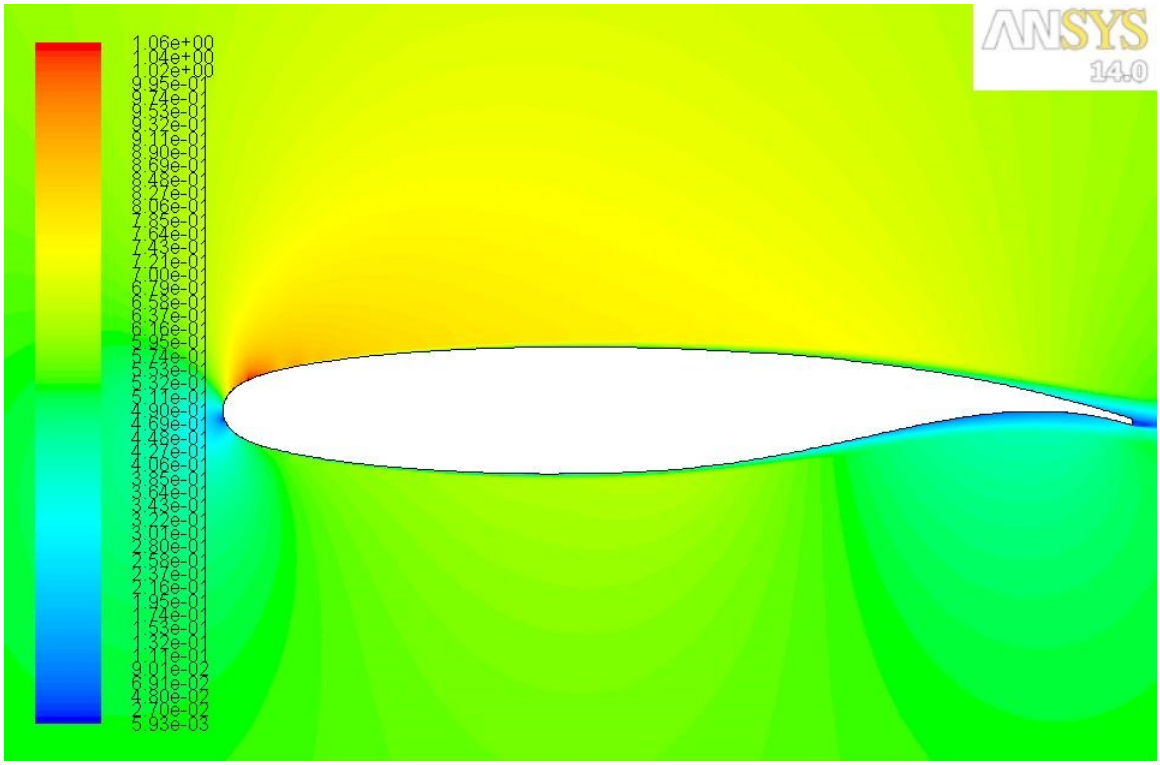

Figure 38: Mach field at $\alpha = 1°$, M=0.570

The critical Mach number is 0.570, as shown in figure 38. The drag divergence Mach number is, using the Douglas criterion (equation 2), 0.690, while the lift divergence Mach number, as can be observed in the first of the graphics in figure 37, is 0.725. The results at Mach number higher than the lift divergence one are not as accurate as the other results: a large detached flow zone exists after the SW and, instead of trying to use SIMPLEC, transient calculation should be performed. Considering the momentum coefficient[4], values seem to follow a certain shape until the lift divergence Mach number, where values disperse. A deeper analysis of the momentum coefficient will be done in the following AoA.

M_{Crit}	0.570
M_{DD}	0.690
M_{LD}	0.725

Table 2: $\alpha = 1°$ Mach numbers

[4]A positive value means a diving moment.

12.2 $\alpha = 2°$

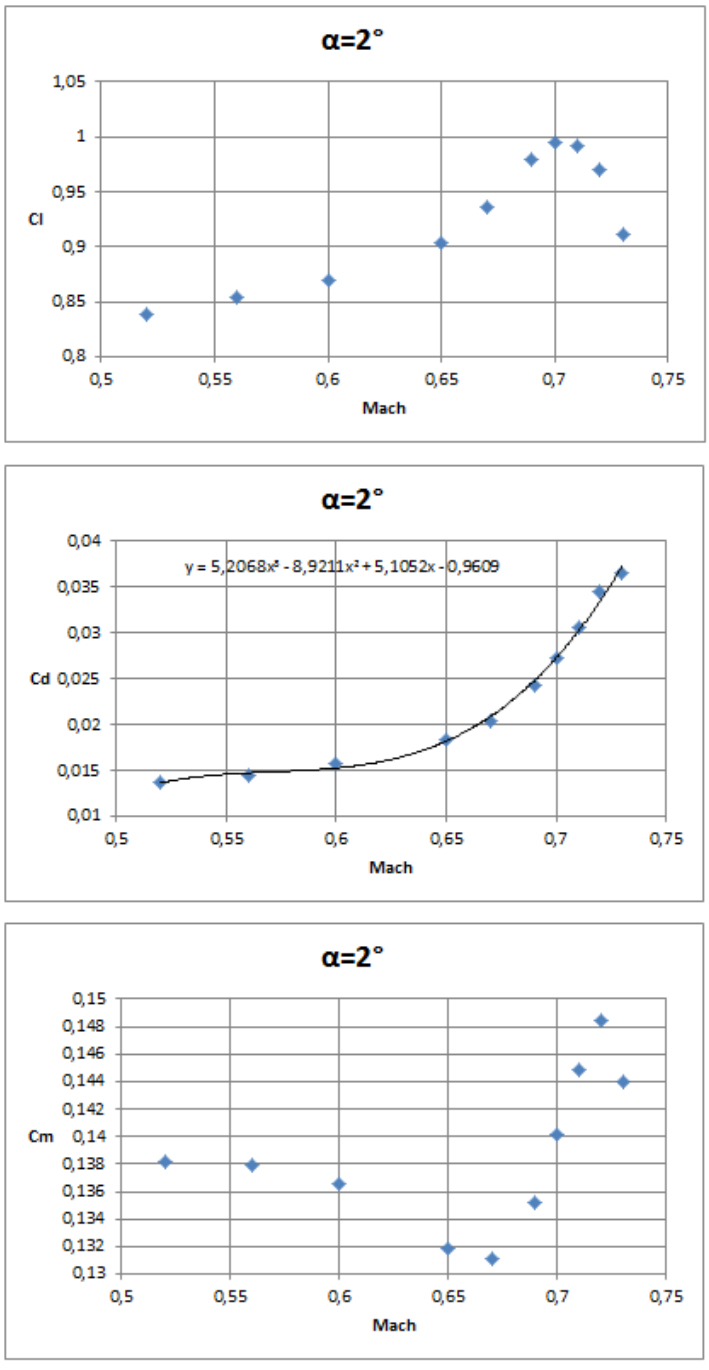

Figure 39: Results at $\alpha = 2°$

In practically any of the simulations BL detachment has been observed in the rearward part of the upper surface, so the drag coefficient increment is caused by the BL thickening. The conclusion is that, for SCA, the drag divergence is caused by the BL thickening, rather than detachment, and also the increment of wave drag.

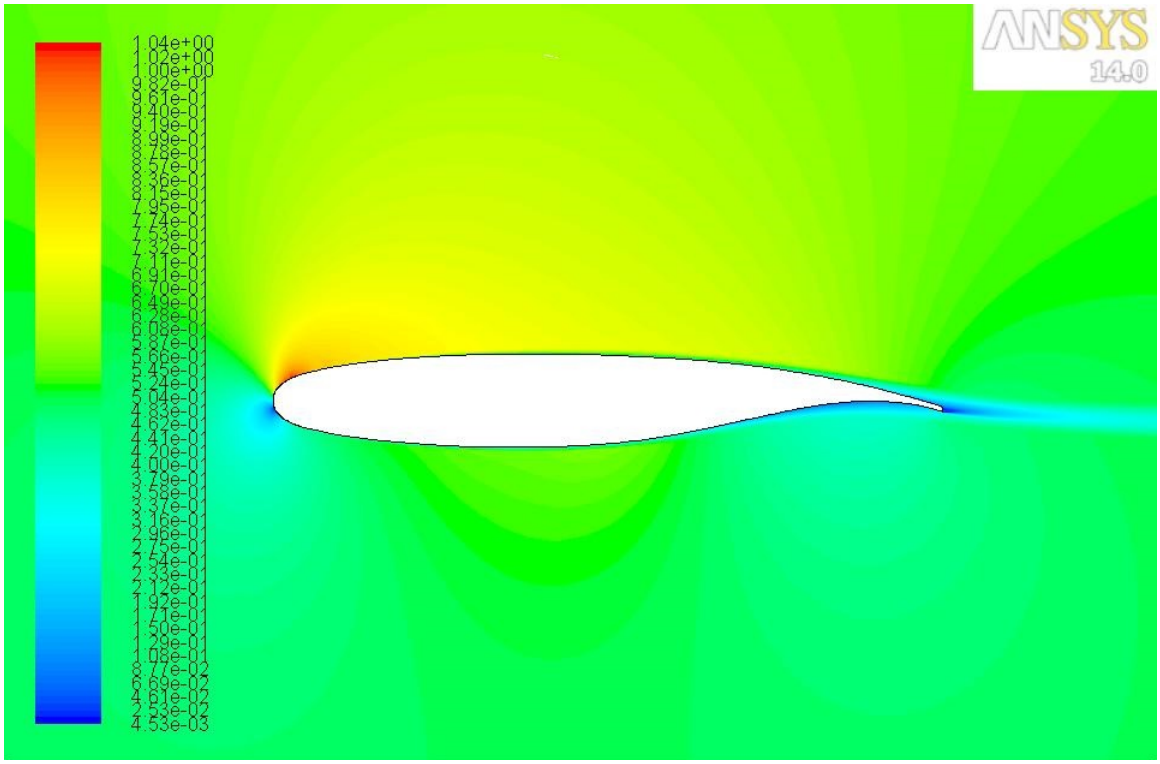

Figure 40: Mach field at $\alpha = 2°$, M=0.520

M_{Crit}	0.520
M_{DD}	0.647
M_{LD}	0.700

Table 3: $\alpha = 2°$ Mach numbers

12.3 $\alpha = 3°$

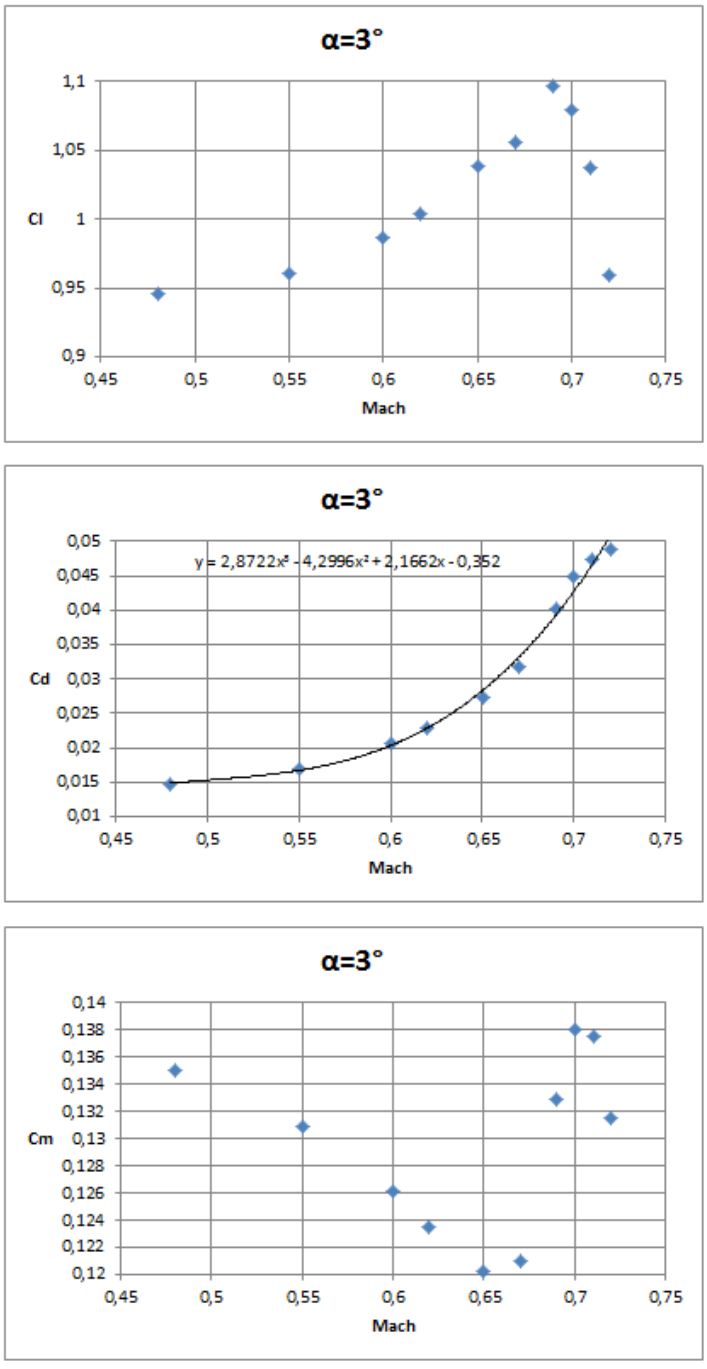

Figure 41: Results at $\alpha = 3°$

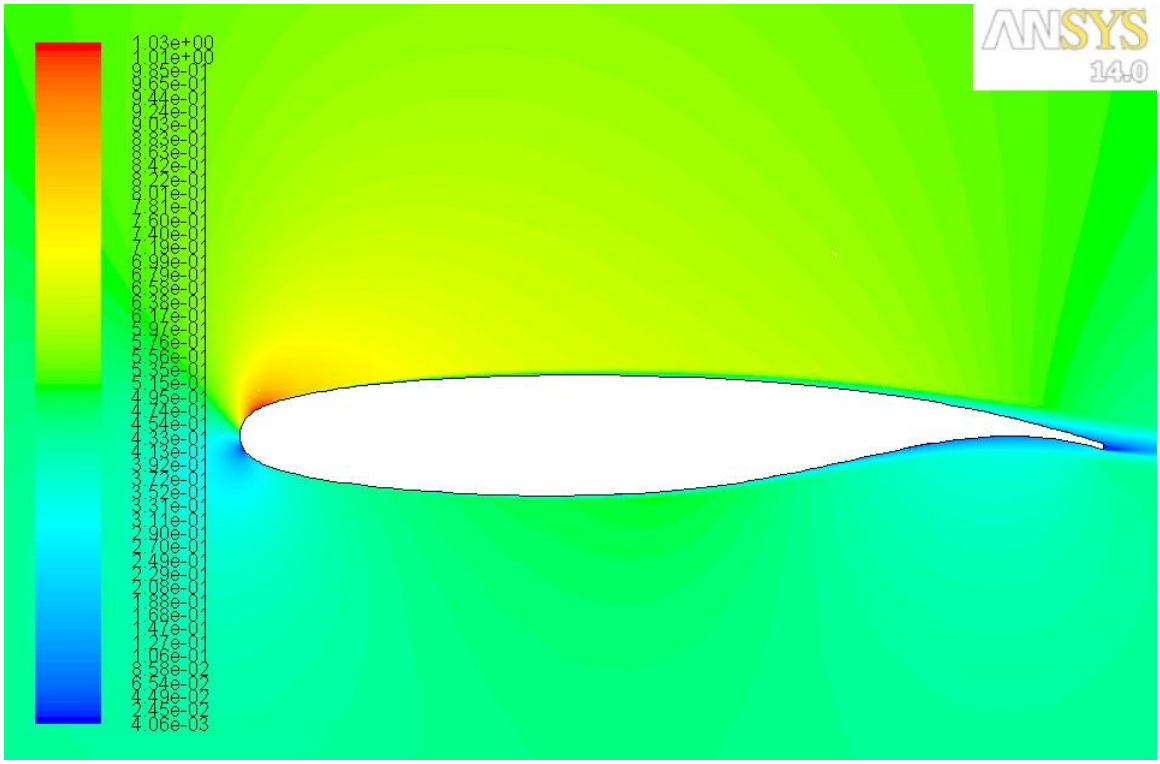

Figure 42: Mach field at $\alpha = 3°$, M=0.480

M_{Crit}	0.480
M_{DD}	0.595
M_{LD}	0.690

Table 4: $\alpha = 3°$ Mach numbers

For this AoA, transient calculation has been used for the highest Mach numbers, to avoid convergence and instability problems. A pattern can now be observed concerning the momentum coefficient: it starts descending from an elevated diving moment (figure 43), at M=0.480, where only a suction peak upstream x=0.25 develops, and the difference between upper and lower surface pressure coefficient (an approximation of the local lift coefficient) concentrates backwards. A minimum value is achieved (in this AoA, M=0.650), where a strong SW develops, near the aerodynamic center x position (x=0.25), figure 44. From this point on, as the SW develops further downstream with increasing Mach numbers, more local lift exists after the aerodynamic center, increasing the momentum respect x=0.25, until M=0.700, figure 45.

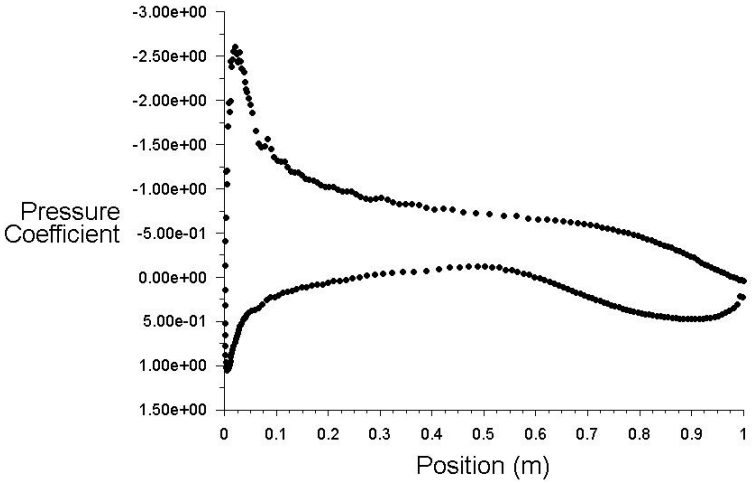

Figure 43: Cp for $\alpha = 3°$and M=0.480

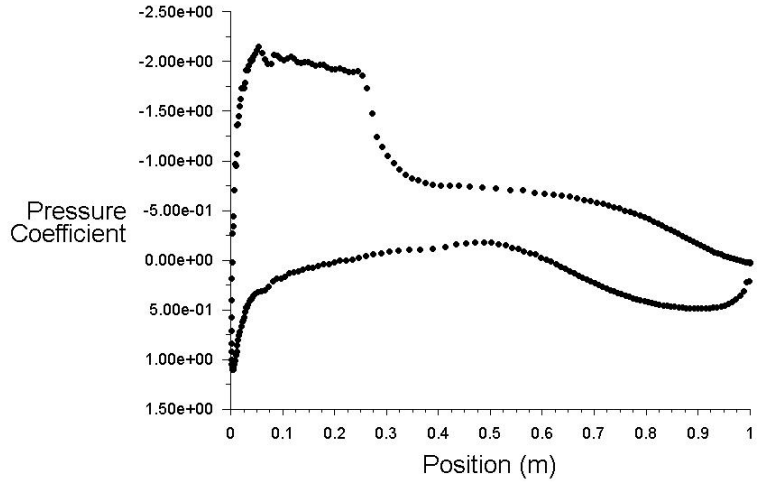

Figure 44: Cp for $\alpha = 3°$and M=0.650

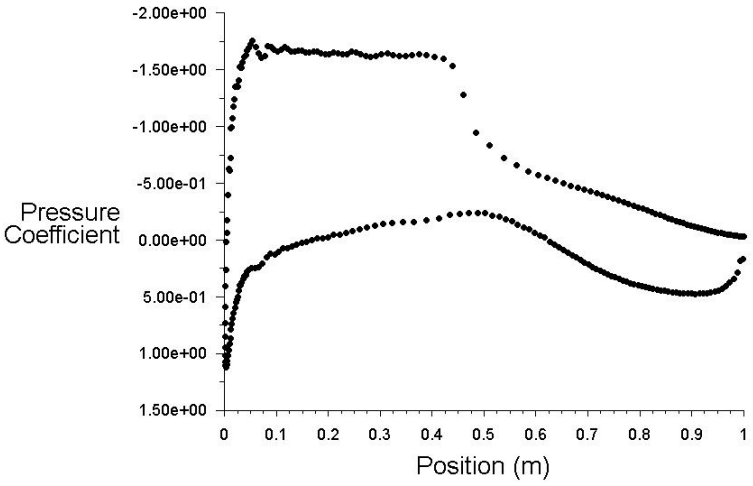

Figure 45: Cp for $\alpha = 3°$and M=0.700

12.4 $\alpha = 4°$

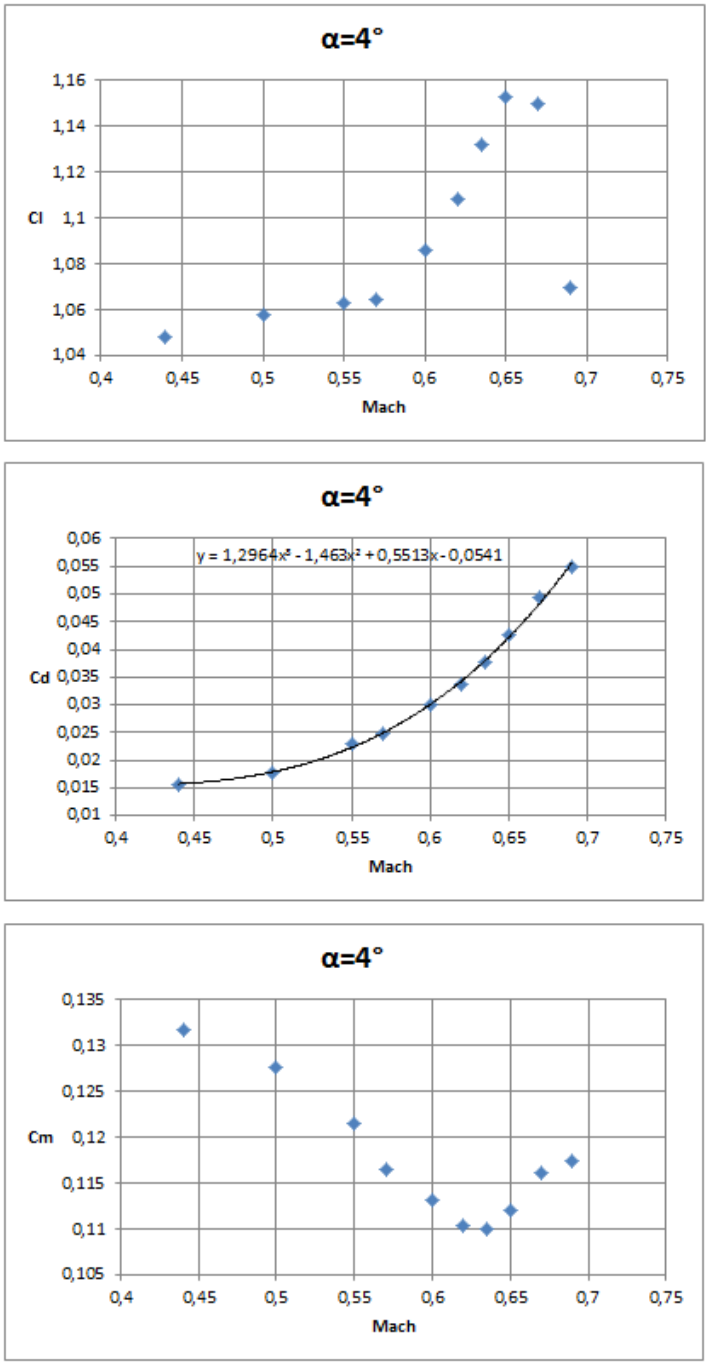

Figure 46: Results at $\alpha = 4°$

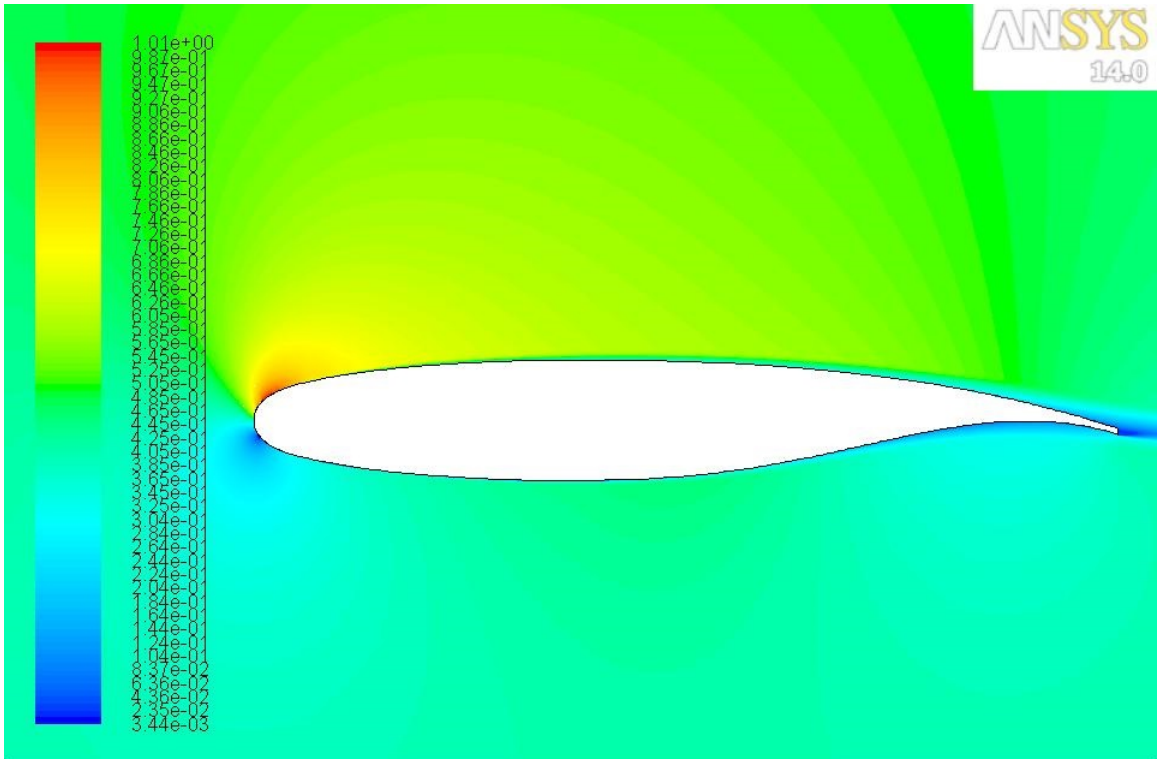

Figure 47: Mach field at $\alpha = 4°$, M=0.440

M_{Crit}	0.440
M_{DD}	0.536
M_{LD}	0.650

Table 5: $\alpha = 4°$ Mach numbers

The drag divergence is caused by the increase in wave drag and also by the BL thickening, caused by the SW (which increases its strength with the Mach number).

12.5 $\alpha = 5°$

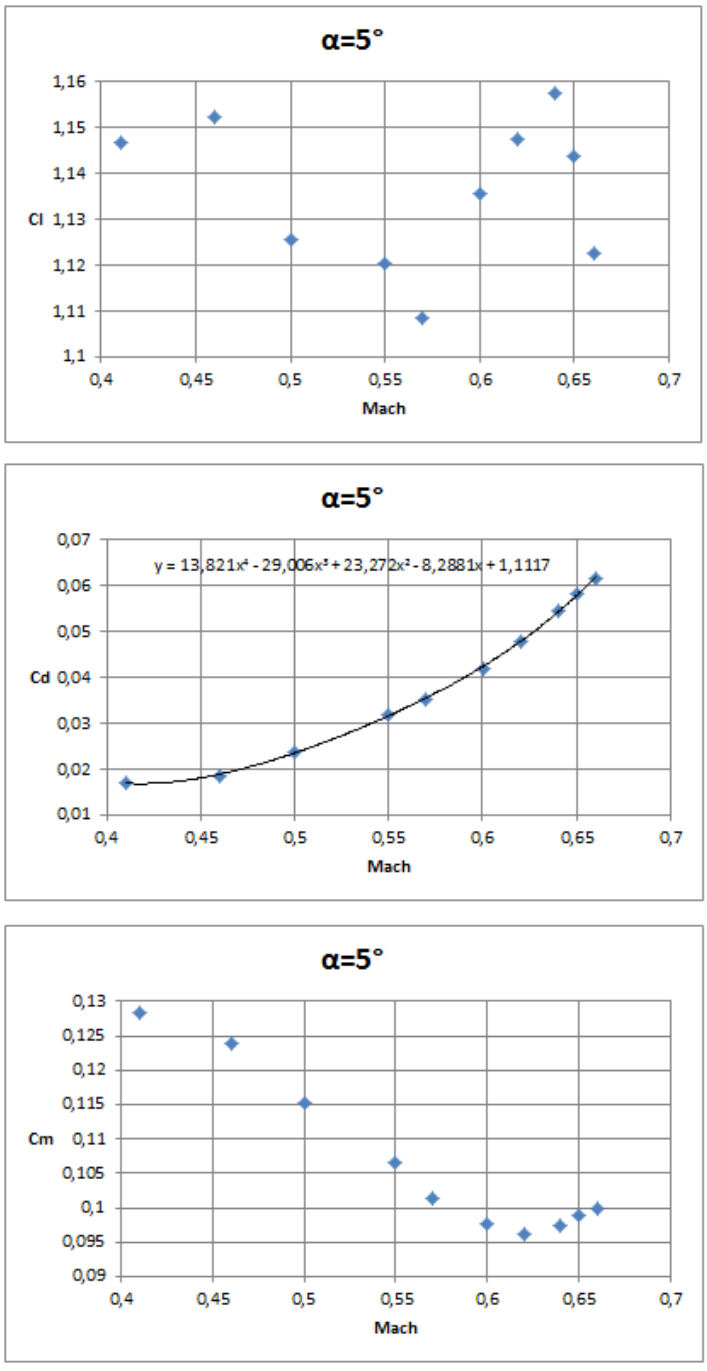

Figure 48: Results at $\alpha = 5°$

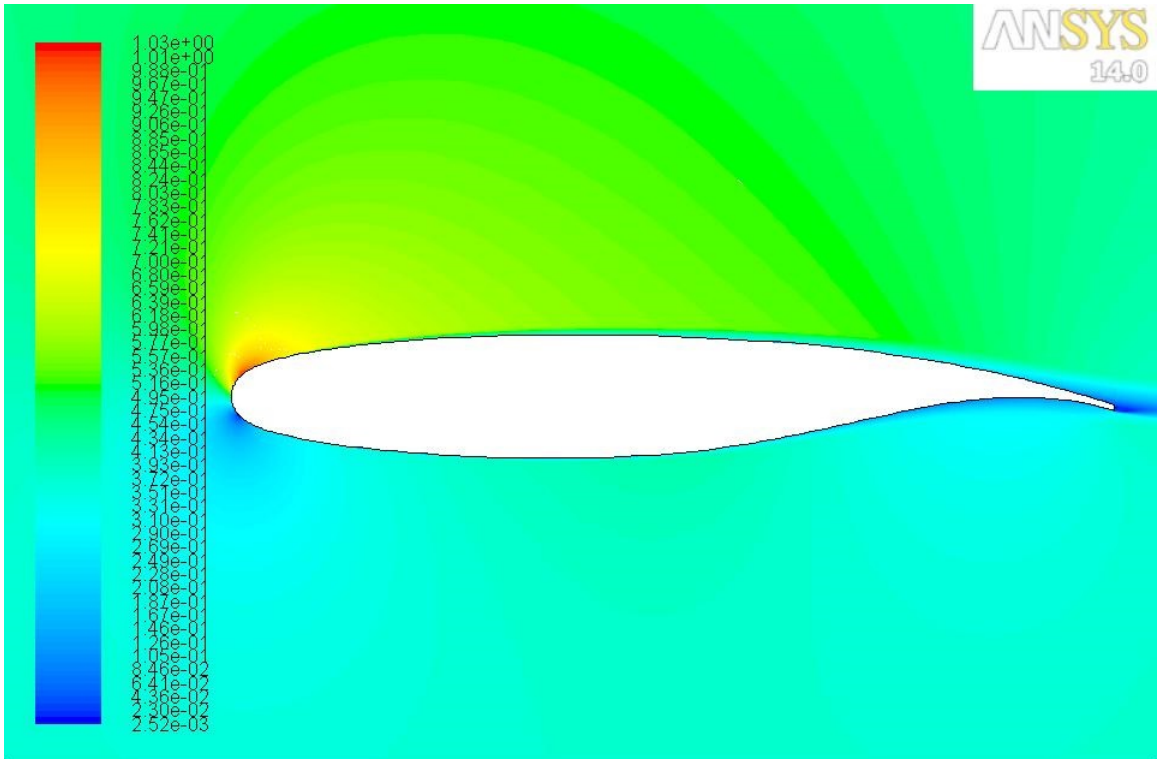

Figure 49: Mach field at $\alpha = 5°$, M=0.410

M_{Crit}	0.410
M_{DD}	0.466
M_{LD}	0.640

Table 6: $\alpha = 5°$ Mach numbers

The values of Cl are strange for the lowest Mach numbers. However, to verify if they are correct, besides the mesh sensitivity process, a transient calculation has been conducted, with same results. To consider is the fact that the higher the AoA is, the steeper the Mach-induced stall becomes.

12.6 Summary

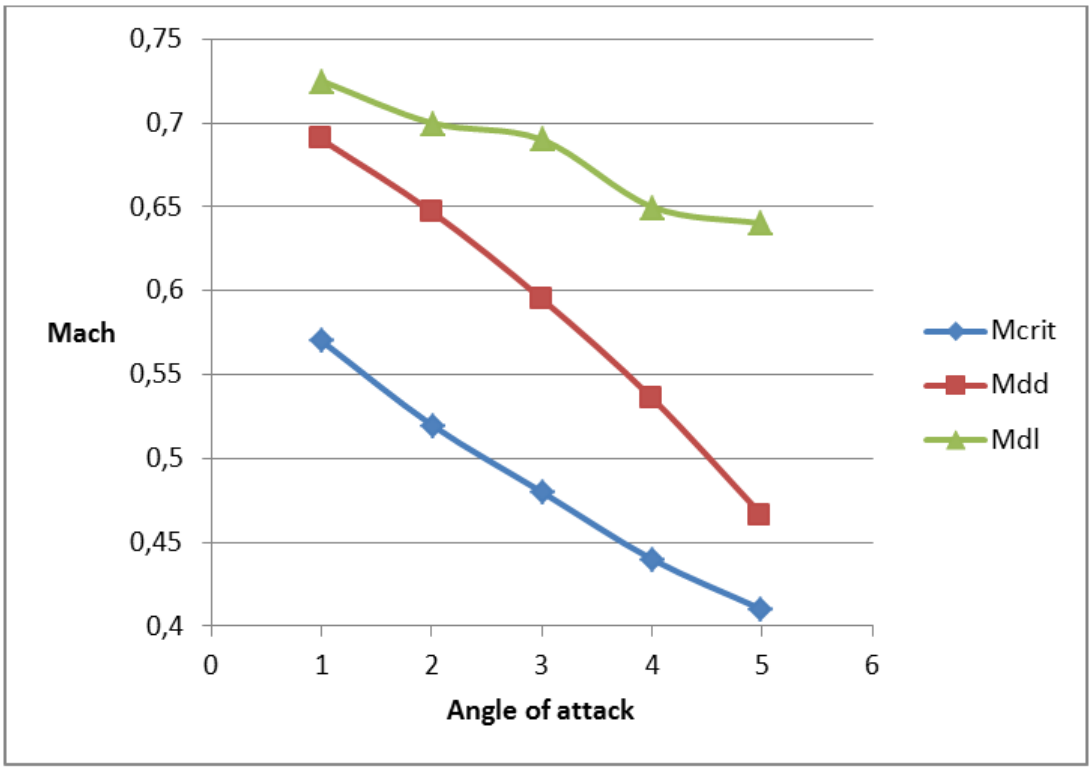

Figure 50: Mach numbers for different α

It can be checked in figure 50 that critical, drag and lift divergence Mach numbers reduce as the AoA is increased, due to the higher acceleration of the flow in the leading edge.

13 Phenomena in transonic regime

13.1 Pressure coefficient

13.1.1 Comparison of the supercritical airfoil with a normal airfoil

To have a clear idea of the difference between both types of airfoils, the wing´s root airfoil of the Boeing 737 has been considered, as it is not a SCA. The results are shown in figure 51.

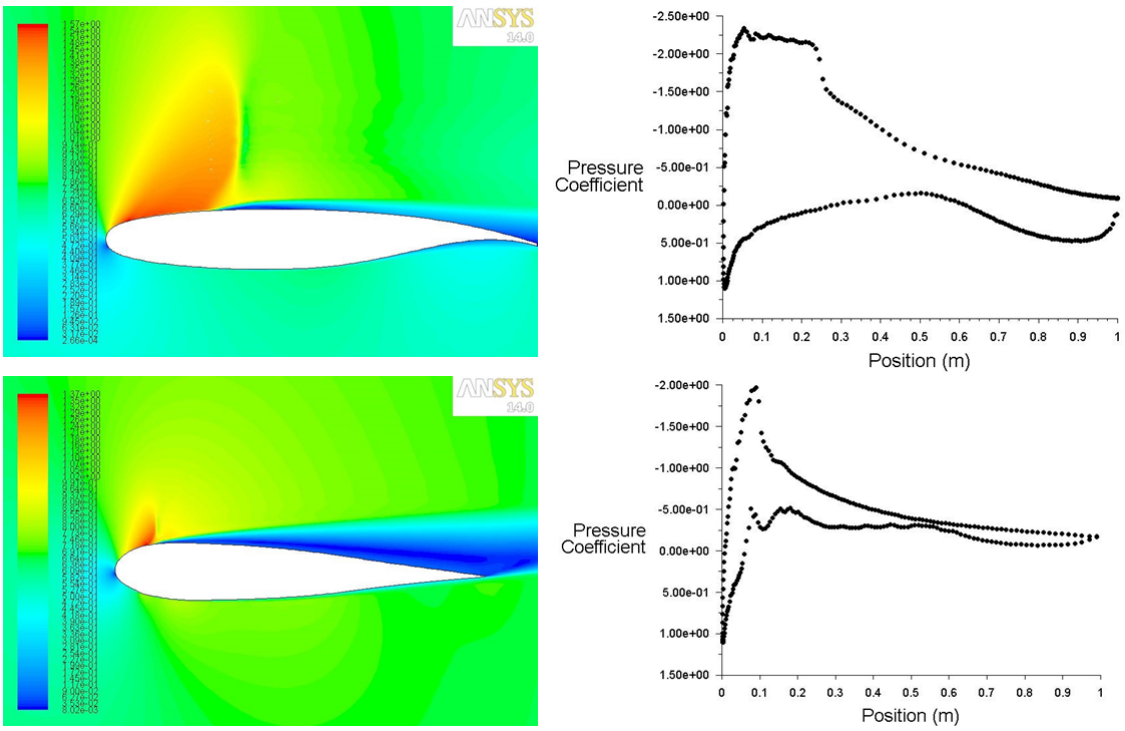

Figure 51: Comparison of supercritical airfoil vs. normal one at M=0.650 and $\alpha = 5°$

The SW in the normal airfoil is stronger, and as a strong adverse pressure gradient exists due to the curvature of the upper side, the BL after it is totally detached (the detachment is observed in the constant and low pressure coefficient), causing an increase in drag and reduction in the suction peak of the leading edge, so lift is also lower, as shown in table 7. The SW in the normal airfoil is located near the trailing edge, while in the SCA it is further downstream, consequently being the local Mach number in front of the SW higher. What is more, in the SCA the BL is not detached after the SW. The diving moment of the SCA is also much higher.

	Cl	Cd	Cm
Normal	0.3457	0.0649	0.0012
Supercritical	1.1440	0.0583	0.0990

Table 7: Comparison of normal and supercritical airfoil

13.1.2 Pressure coefficient greater than one?

Remember that Bernoulli equation it is not appliable, because the fluid is compressible and viscous, and also not adiabatic, so the following equation is NOT valid along a current line:

$$P_1 + \frac{1}{2}\rho v_1^2 = P_2 + \frac{1}{2}\rho v_2^2 \tag{10}$$

The pressure coefficient, $C_p = \frac{P-P_\infty}{\frac{1}{2}\rho v_\infty^2}$, is 1 in the leading edge stagnation point for incompressible and inviscid flows. But for compressible, viscous and non adiabatic flows the energy conservation equation must be considered, applied to a stream tube, equation 3. Viscosity and heat conduction with the rest of the fluid increase the pressure above the total pressure upstream ($P_\infty + \frac{1}{2}\rho v_\infty^2$), as the temperature also increases, due to the elevated viscous stresses.

13.2 Shockwave

In figures 52, 53, 54 and55 we can observe that the SW increases its strength and moves downstream to the trailing edge as the freestream Mach number increases. This movement could be also seen through the pressure coefficient plot.

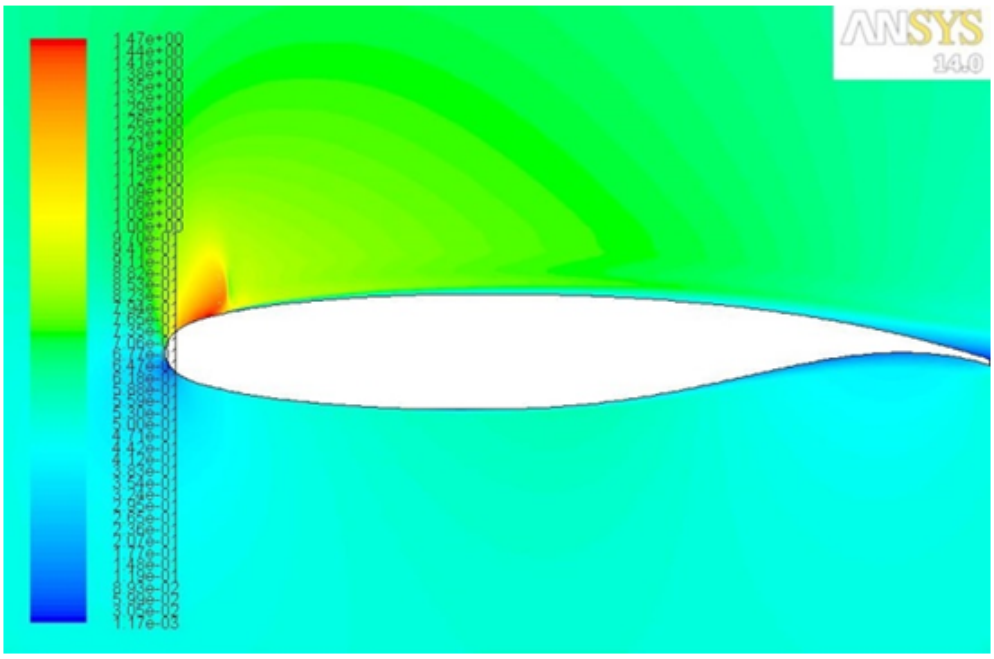

Figure 52: Mach field of M=0.550 for $\alpha = 4°$

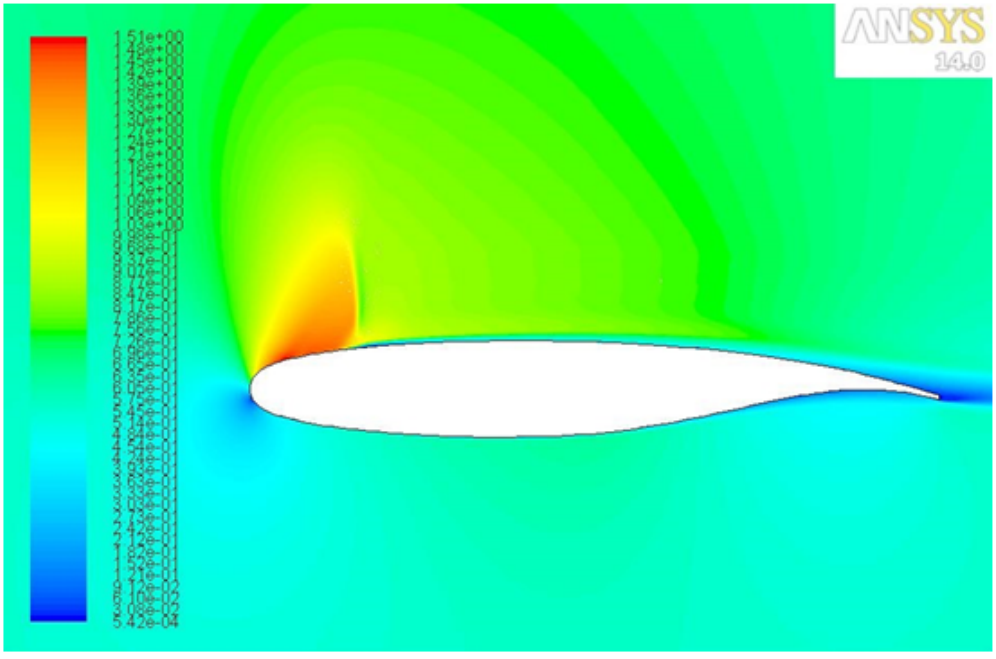

Figure 53: Mach field of M=0.600 for $\alpha = 4°$

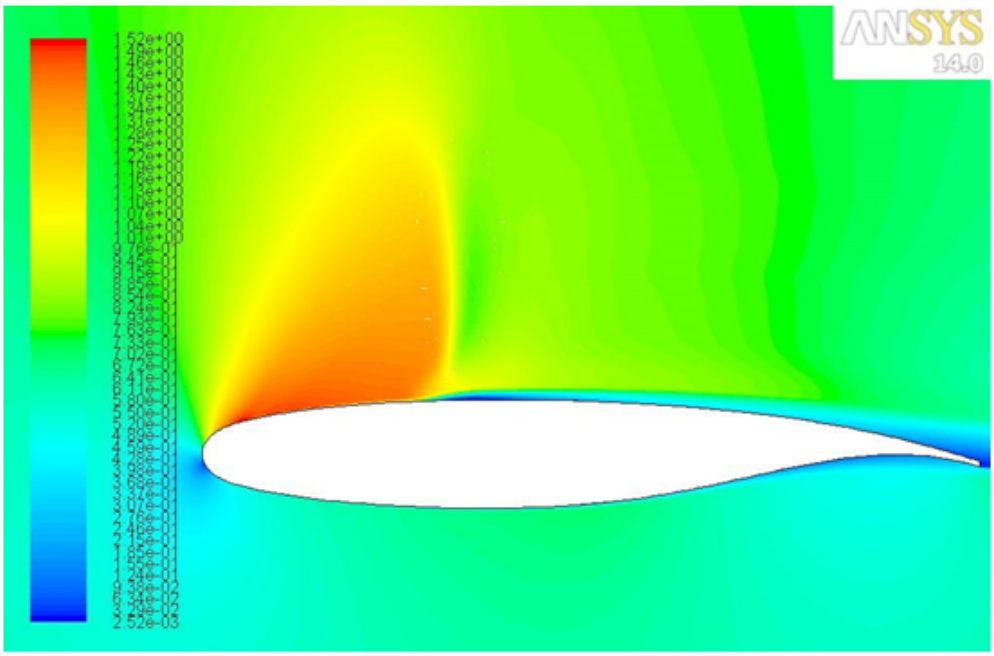

Figure 54: Mach field of M=0.650 for $\alpha = 4°$

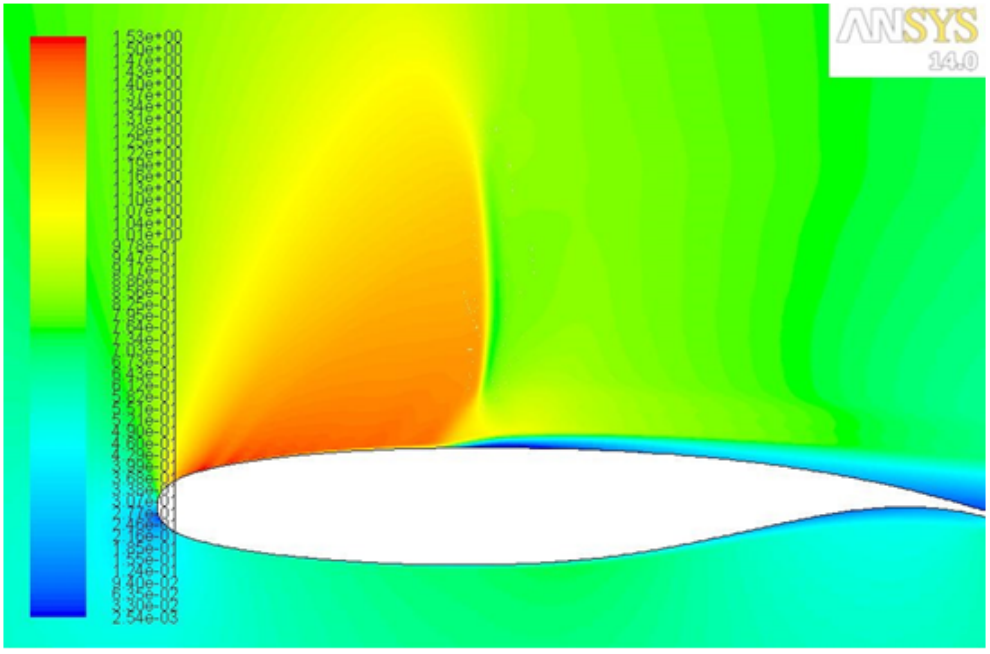

Figure 55: Mach field of M=0.670 for $\alpha = 4°$

It must also be noted the higher local number in front of the SW as the freestream Mach number increases, well above Mach 1. An important aspect is that, although the free stream velocity might be relatively low, a small SW exists near the leading edge, as seen in the first figure.

13.2.1 λ shape

This configuration on the foot of the SW occurs mainly when the BL after the SW is detached, and is clearly visible for the 737 wing root airfoil, figure 56.

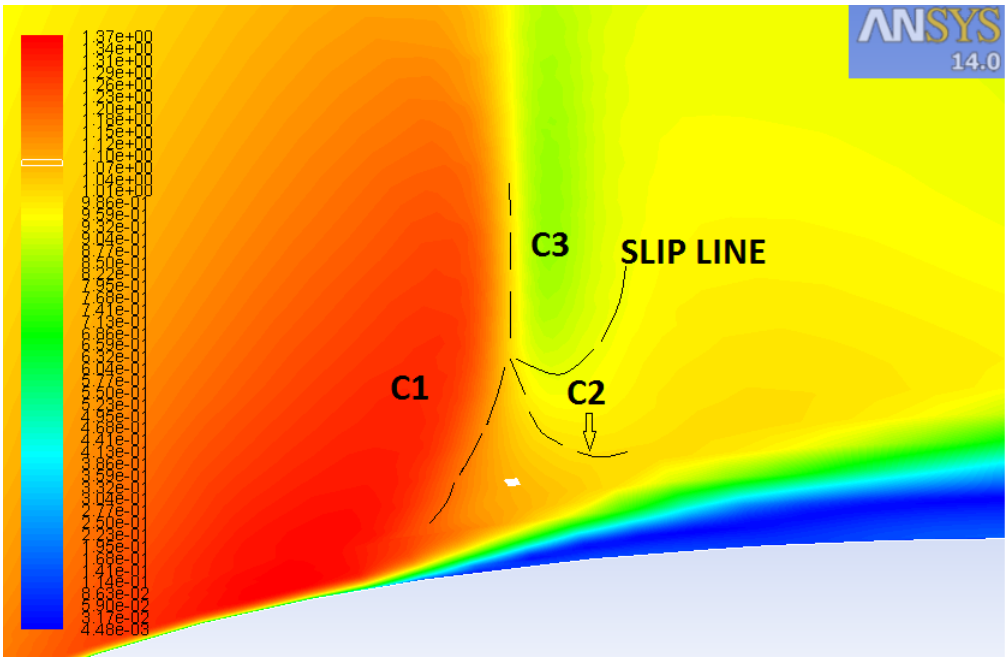

Figure 56: λ shape of the SW, 737 wing root airfoil at M=0.650 and $\alpha = 5°$

In fact, there are three different SW, C1, C2 and C3. C1 is an oblique weak SW, downstream which the fluid is still supersonic (a point is shown in white with its respective velocity in figure 56). C3 is an almost perpendicular SW, being the fluid downstream it subsonic. As there are two different states downstream C1 and C3, in order the flow to be continuous in direction, there must exist a third SW C2 after which the flow has the same pressure and velocity direction as downstream C3. The intensity of C2 decreases towards the BL, partly due to the compression waves generated by the growth of the BL. But as the speed value downstream C2[5] is higher than downstream C3 (this is a property of this kind of solution), a slip line (not a stream line) originates from the point where C1 and C2 join (called triple point) separating flow regions 2 and 3 (in the figure, this line is between the yellow and the green colors). The slip line is also called shear layer or vortex sheet, a thin layer across which the properties are continuous (Delery, J. [24]).

[5]The speed value downstream C2 could be locally supersonic, zone known as "supersonic tongue", if the local Mach number in front of the whole SW were 1.4.

13.3 Boundary layer

A characteristic of SCA is that due to the flatness of the upper side, after the SW the BL is thickened, but as the pressure coefficient is almost constant after the SW, the BL is reenergized with the external fluid, so it becomes thinner and it is not detached, as we can observe in figure 57. The zone colored in dark blue is the BL. After the SW, the flow may even detach with a subsequent reattachment caused by this reenergization, figure 58. It must be noted that the BL is not a fixed quantity of mass, but it is just the particles near the wall of the airfoil which velocity increase from zero to the external fluid speed. The BL is thickened or becomes thinner because it interacts with the external fluid (the one out of the BL), and if the external fluid is decelerated due to the BL (through the viscosity), the number of particles with lower velocity than the external flow will increase, thickening the BL. In other way, if the speed of the external fluid increases (because of the favorable pressure gradient), the BL might become thinner. In the BL there is a subsonic zone, the one closer to the wall, so the perturbations downstream the SW can be communicated in this subsonic zone, and this way all the fluid field, not only the part downstream the SW, is affected by the possible BL detachment.

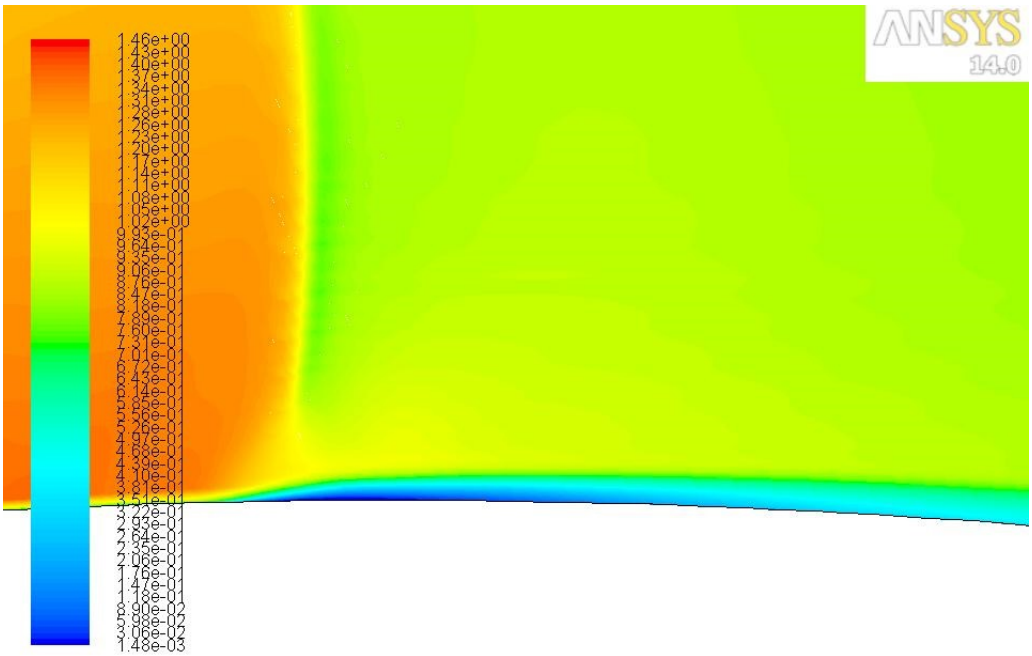

Figure 57: BL reenergization, M=0.670 at $\alpha = 3°$

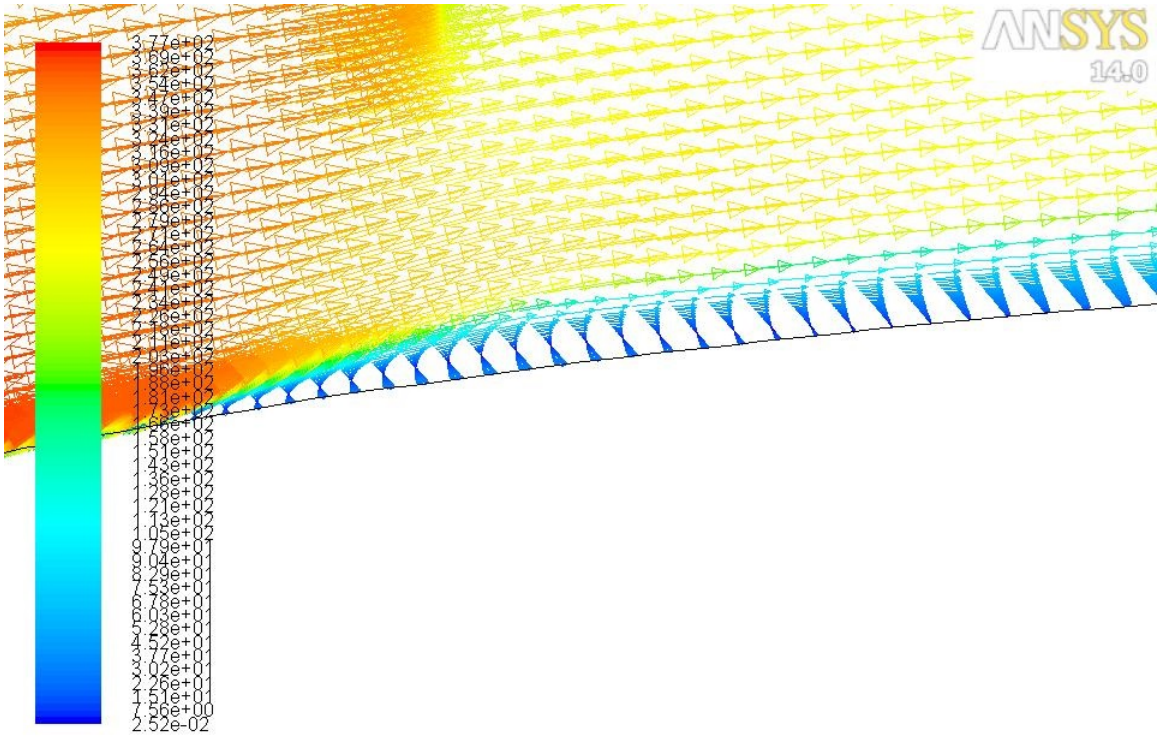

Figure 58: BL detachment and attachment just downstream the SW, M=0.570 at $\alpha = 5°$

Concerning the trailing edge, no BL detachment has been observed in the upper side, even at Mach numbers above the lift divergence Mach number. However, the thickness increases dramatically, figure 59. The point of detachment, if exists, is found where the local skin friction is zero, as the variation of the velocity in the normal direction of the airfoil is zero, figure 60.

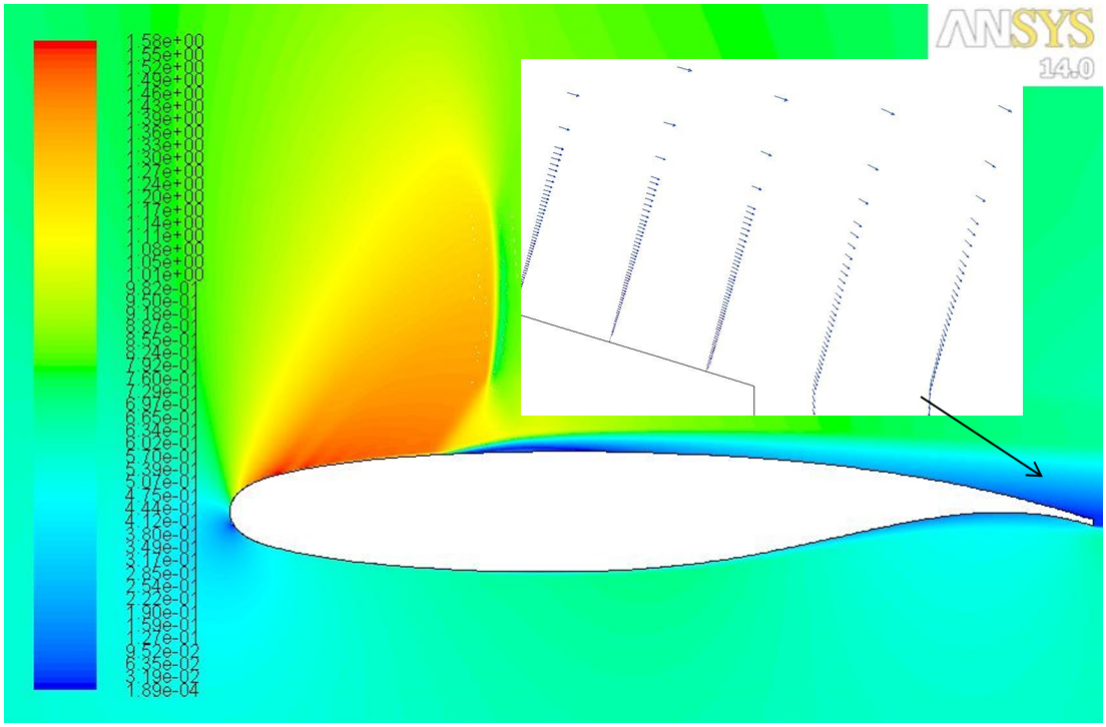

Figure 59: Trailing edge BL, M=0.650 at $\alpha = 5°$

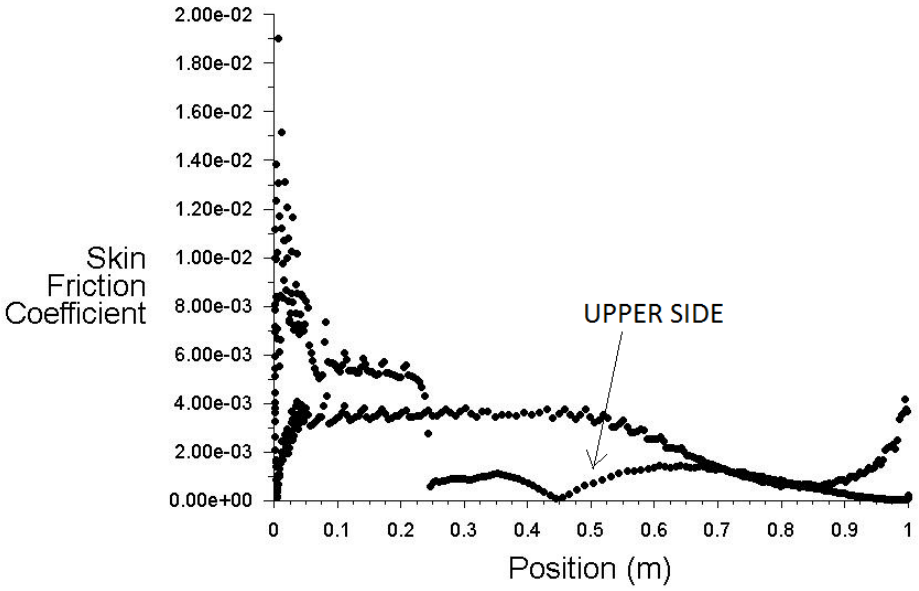

Figure 60: Skin friction, M=0.650 at $\alpha = 5°$

In the rearward part of the lower surface, although the BL is initially thickened, it is not detached (if the curvature in that part were increased, it could happen). The blunt trailing edge helps the BL of the lower surface to not detach (section 2.2.1). Due to the final beneficial pressure gradient, the BL becomes thinner again, figure 61. As no BL detachment is observed in the upper and lower surface of the rearward

section, a flight control such as the aileron would be still useful in this type of airfoil and these speeds, and no oscillation of the control surface would occur [25].

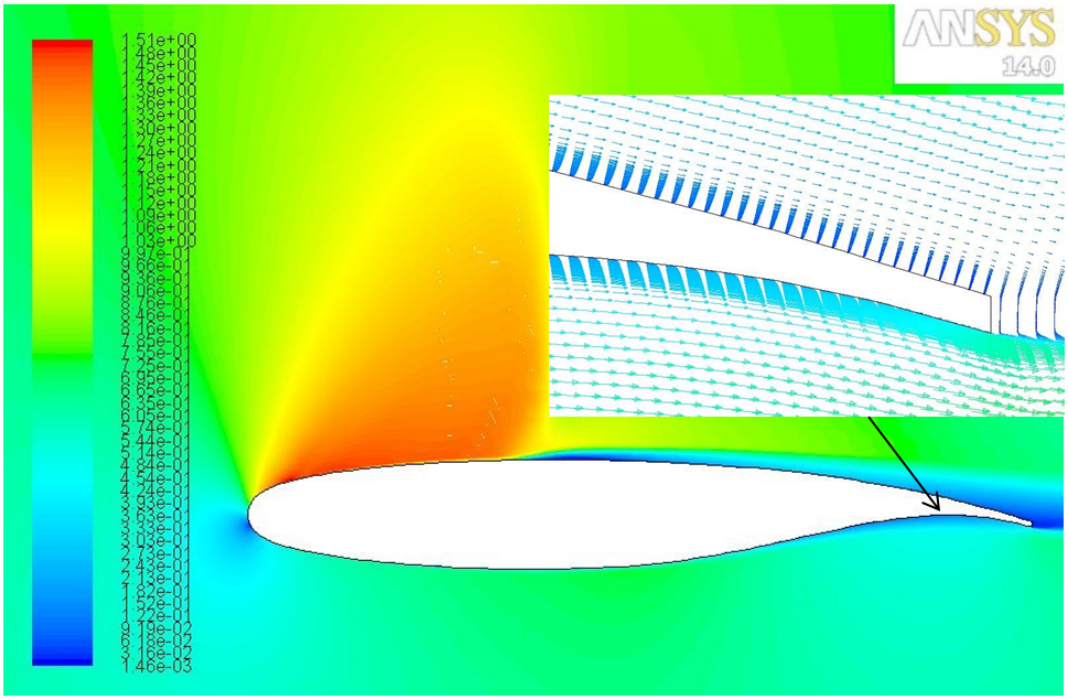

Figure 61: Lower side BL, M=0.670 at $\alpha = 4°$

13.4 Different working points

Different working points can be distinguished, and can be studied using the pressure coefficient distribution. With this, a first approach to the optimum Mach number for each AoA could be found. The theory related to the different working points is shown in section 2.2.2, and the figures there can be compared with those below.

In figure 62 we can observe the subsonic and slightly supercritical condition, in which a suction peak in the leading edge exists and the adverse pressure gradient is smooth just until the trailing edge, so the BL is not detached.

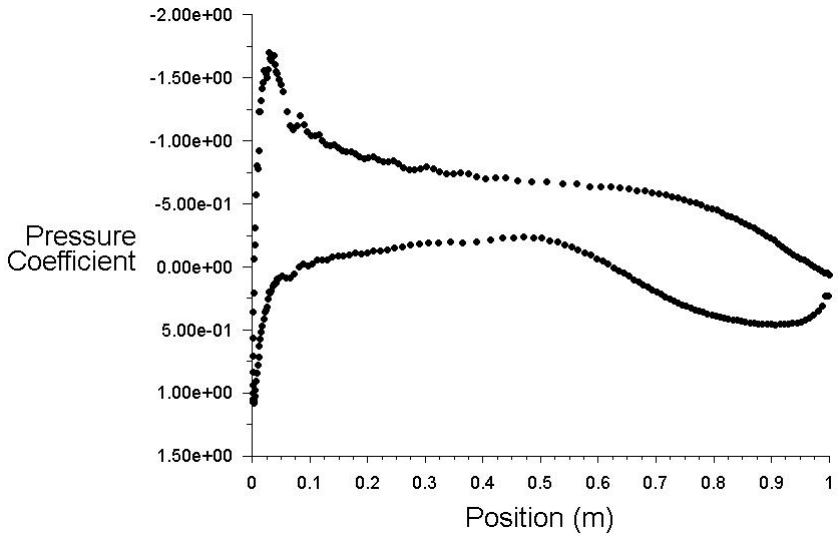

Figure 62: Cp distribution, M=0.570 at $\alpha = 1°$

Increasing the speed until just below the optimum value for this AoA, the SW is located upstream the optimum position, and as the flow is subsonic downstream it, it is reaccelerated, and a second SW might appear, or a high adverse pressure gradient exists near the trailing edge, and the BL might detach, figure 63.

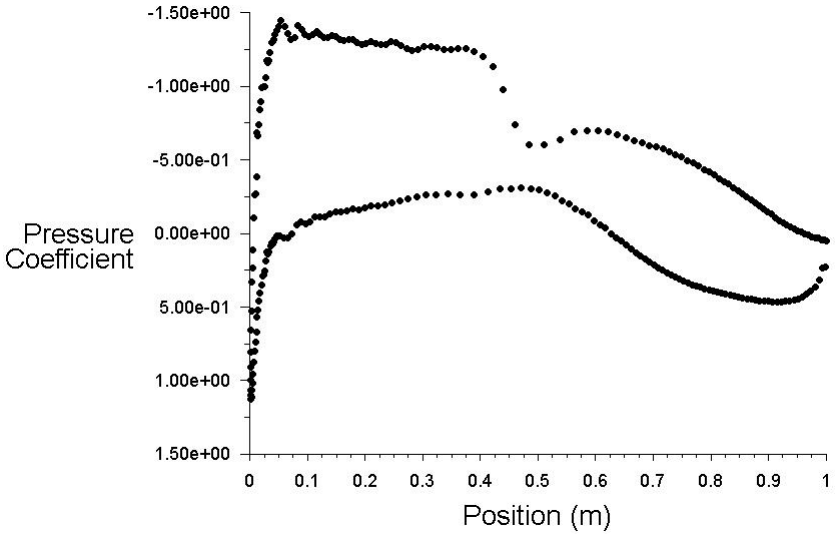

Figure 63: Cp distribution, M=0.710 at $\alpha = 1°$

Near the optimum Mach number for this AoA, a flat upper side pressure distribution can be observed up to the SW, after which the pressure is almost constant (and the external flow reenergizes the BL) until the zone near the trailing edge, where a pressure gradient exists, figure 64.

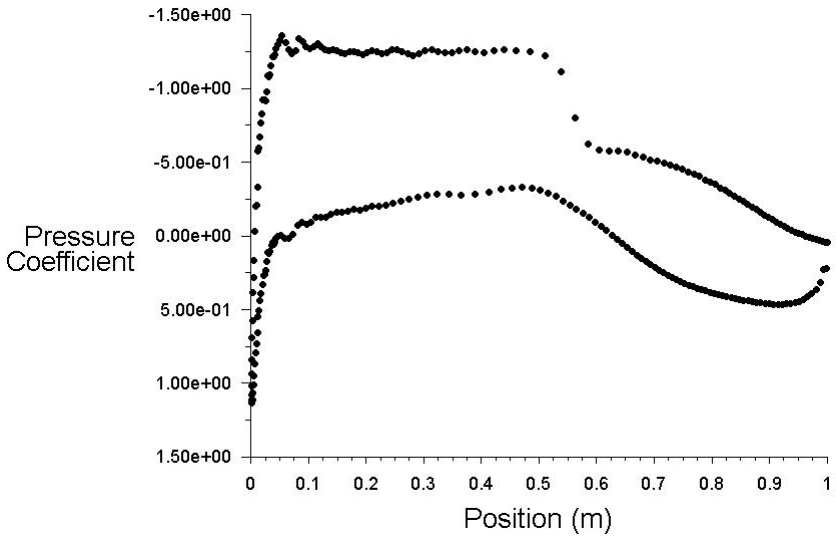

Figure 64: Cp distribution, M=0.725 at $\alpha = 1°$

When we refer to the optimum Mach value for each AoA, it is not the value with maximum aerodynamic efficiency, $E = \frac{C_L}{C_D}$, as this value starts to decrease when entering in the transonic regime, figure 65. It is a value that provides acceptable drag values over the Mach number and AoA range. It is usually a value that minimizes the strength of the shock, so in the design condition of the AoA, the Mach number is similar to the lift divergence Mach number [7].

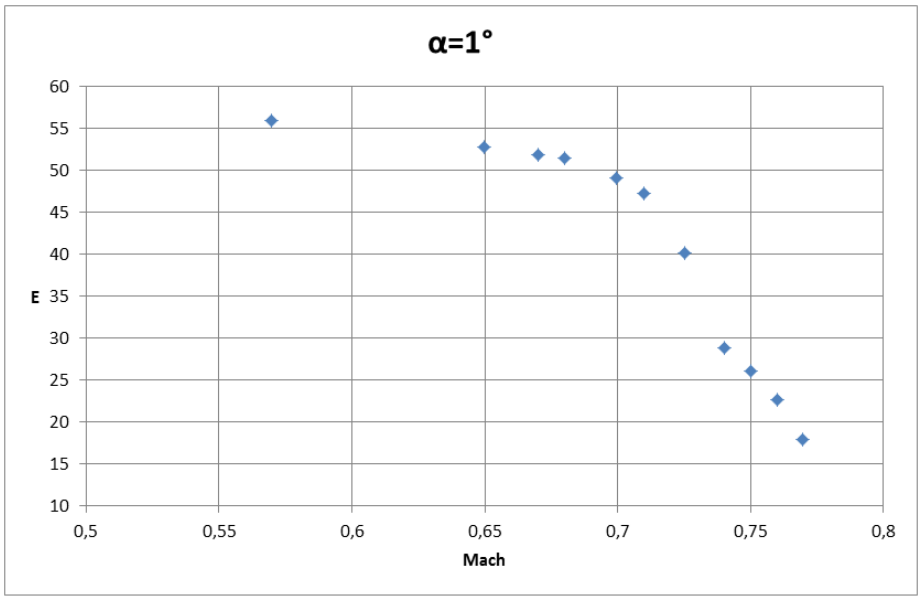

Figure 65: Aerodynamic efficiency at $\alpha = 1°$

Finally, when the Mach number is above the optimum one, the fluid still supersonic reaccelerates before the SW, as can be observed in the final decrease of pressure before the SW, figure 66.

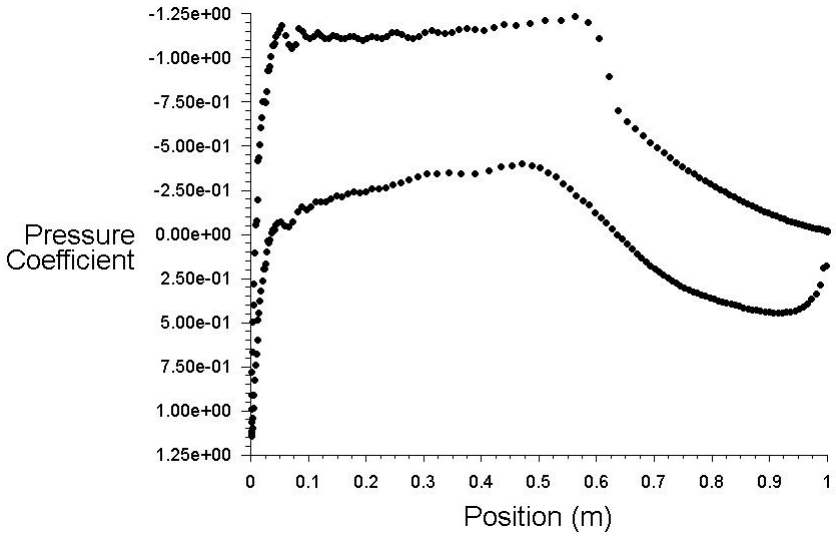

Figure 66: Cp distribution, M=0.750 at $\alpha = 1°$

It must be noted that, although with speeds above the lift divergence Mach number (in the case of $\alpha = 1°$, M_{dl}=0.725) the SW is developed further downstream, towards the trailing edge, the lift coefficient decreases as the value of the minimum pressure coefficient is lower (in absolute value), figures 64 and 66.

13.4.1 Low speed behavior

To study the low speed behavior of the airfoil, high AoA and a Mach number of 0.3 have been used, at a Reynolds number of $4{\cdot}10^6$. Due to the shape of the SCA, it is difficult to introduce flaps in a wing with such an airfoil. At elevated AoA strong adverse pressure gradients are likely to appear, caused by the elevated suction peak in the subsonic regime needed for a flatter Cp at transonic speeds, and the BL might dettach. Mesh sensitivity have also been done. As a large detached area appears, transient calculation have been performed.

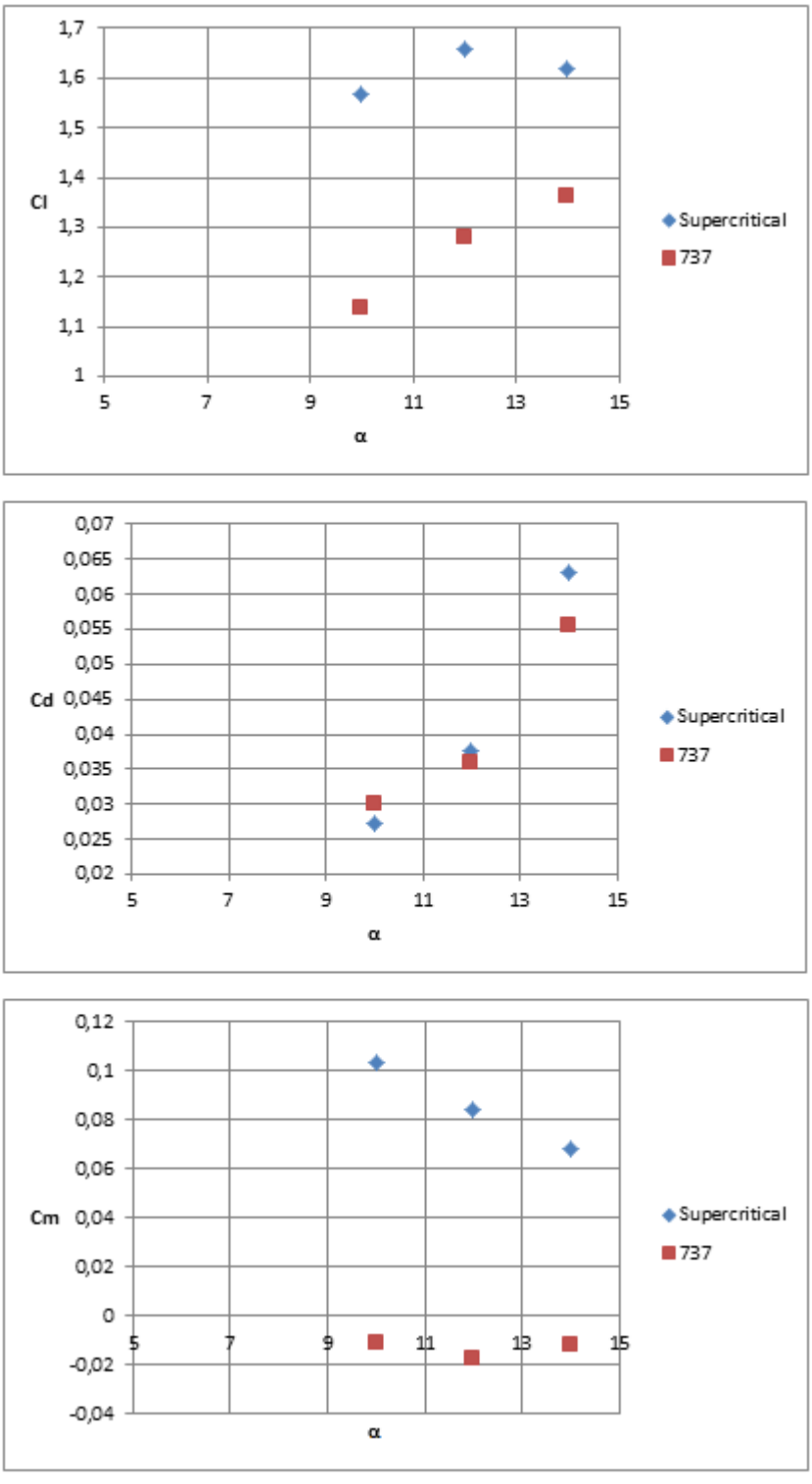

Figure 67: Coefficients for low speed behavior, at M=0.3

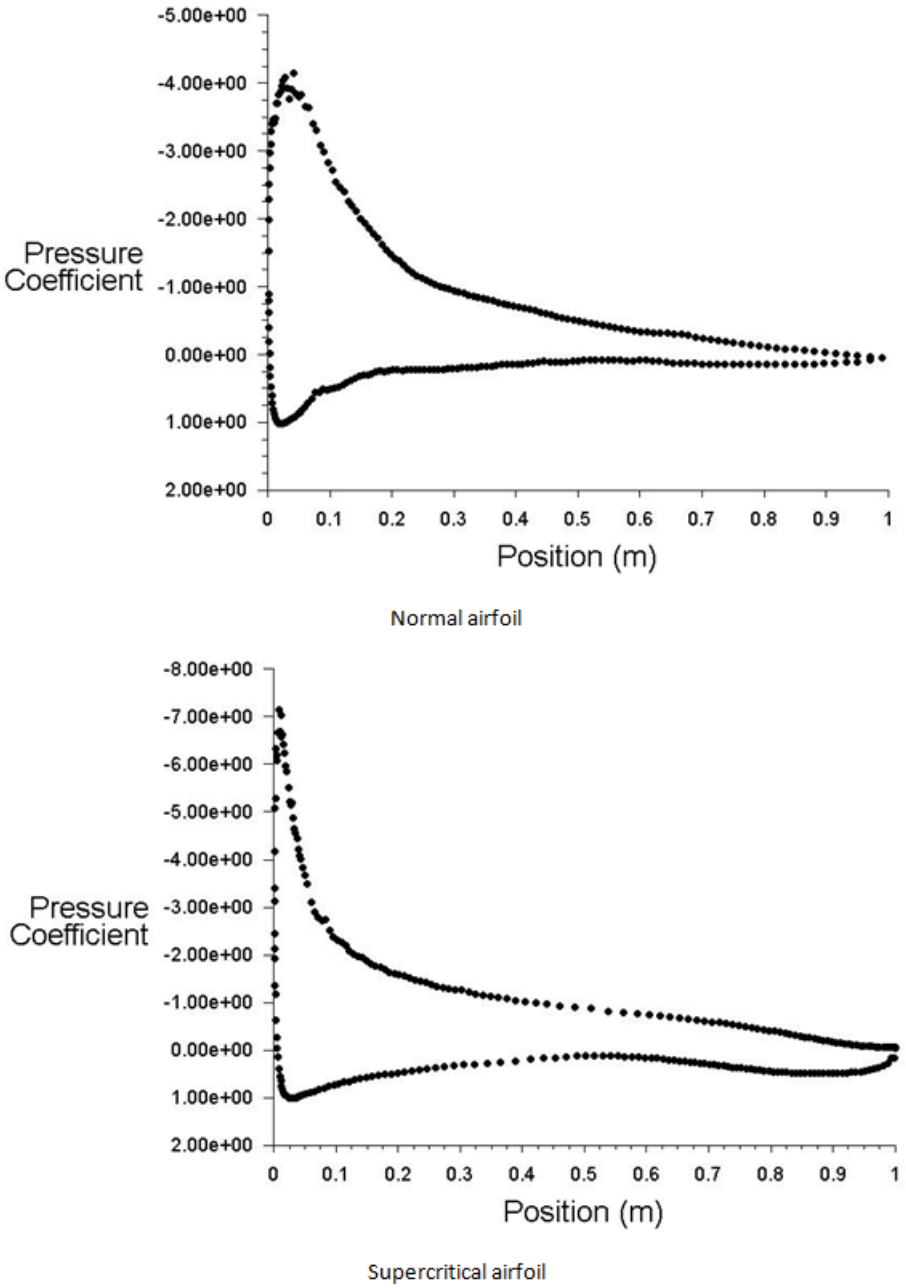

Figure 68: Cp distribution, M=0.300 at $\alpha = 10°$

As the gradient of pressure in the leading edge of the SCA is more pronounced, a larger detached BL develops. At the tested AoA, the lift coefficient of the SCA is greater, although the detached area is bigger, as shown in figure 69. The greater lift coefficient could be explained by the low curvature of the selected normal airfoil. However, the maximum AoA of the SCA is lower than that of the normal airfoil.

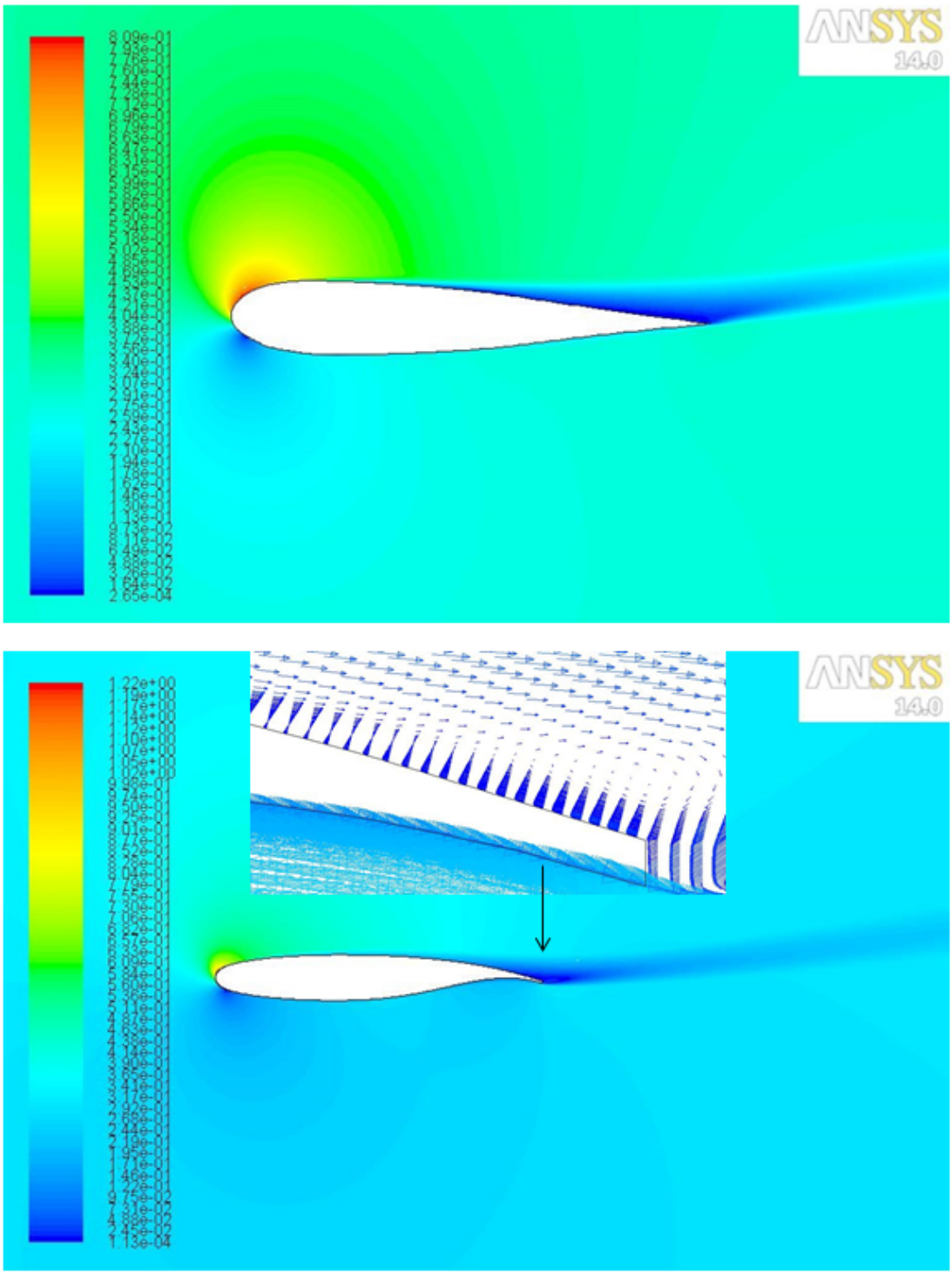

Figure 69: Mach field for normal and supercritical airfoil, M=0.300 at $\alpha = 12°$

Part VI

ENVIRONMENTAL CONCERNS

To estimate the energy used for the project, the main source of consumption has been the computer. As all the study, from numerical simulations to memory redaction has been made using the same computer, HP Pavilion P6-2416es, the power is 300 W [26]. The total time for the whole study (with redaction) has been 640 hours, so the energy consumed has been 691.20 MJ (equal to the electricity used by a family of four during two weeks). But, as the study has shown, the benefits overpass the investment. Concerning the CO_2 emissions, it has been calculated for Spain that 0.399 $KgCO_2/KWh$ are generated in a combination of all existing energy sources [27]. The conclusion is that 76 kg of CO_2 have been produced during the study, equivalent to a 0.64% of the CO_2 emissions in a flight from Madrid to Barcelona [28].

Long time ago, the main focus of aeronautical research was to fly faster, even at supersonic speeds. But as the oil price rose, the priority of the airlines (and consequently of the aircraft manufacturers) was to fly more efficient aircrafts, with a reduce fuel consumption. In this sense, the ACARE (Advisory council for aviation research and innovation in Europe) set a goal for 2020: the fuel consumption must decrease a 50 % relative to that of 2000. To achieve this, ACARE shows a more precise track: the drag must be reduced in the order of 15 to 20 % (mainly modifying wing and empennage), the efficiency of the engine has to improve 20 to 25 % and the weight has to be reduced about 5 %.

The higher the sweep angle is, the lower the maximum lift coefficient is due to the 3D effects. Using SCA, smaller flaps would be needed, reducing the weight of the wing and decreasing the fuel consumption, along with the required maintenance. Using SCA, the drag at transonic speeds is reduced, so the fuel consumption is reduced. In fact, most of the SCA research was done in the 70´s, when an oil crisis occurred. The next step is to design laminar flow SCA, which will reduce the viscous drag. In figure 70 the use of SCA and more efficient engines is shown throughout the drag coefficient of the Boeing 737: the -800 series is equipped with SCA (Obert, E. [29]).

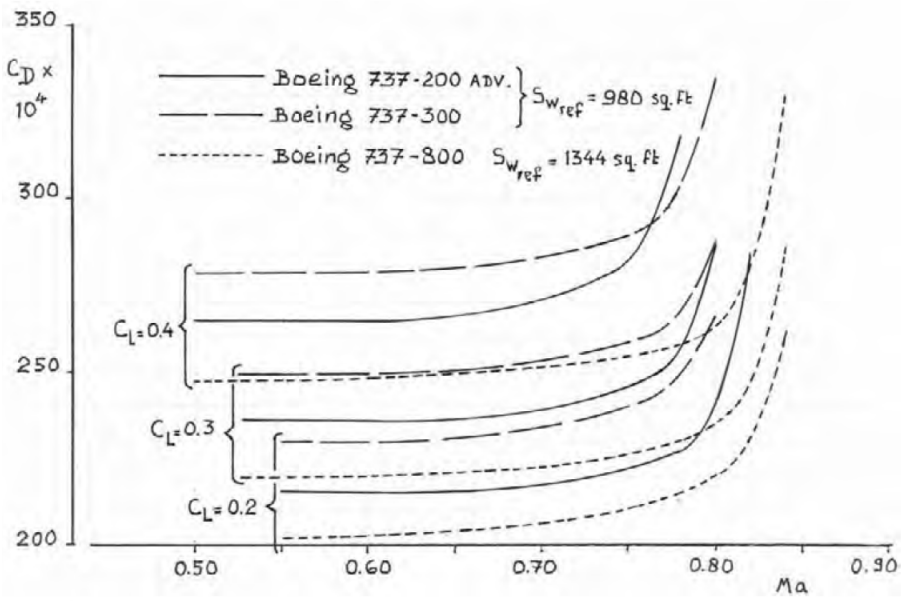

Figure 70: 737 drag coefficient; From Obert [29]

Part VII

BUDGET

For the budget, the time spent using the computer will be translated into money considering the amortization and the energy consumption. Also, the salary will be taken into account.

640 hours of computer usage have been spent, so with an energy price of 0.134 €/KWh (0.06 €/KWh during ten hours in the night) and 300 W, the cost of the energy is 19.81 €.

Three months using the computer are required, an it is expected that the lifetime of the computer is 4 years. As the computer cost 599 €, the cost of the use is 37.44 €.

With 8 €/hour, the salary is 5120 €.

The software used, the Academical Ansys, is free.

Concept	€
Electric consumption	19.81
Computer usage	37.44
Salary	5120
Total	5177.25

Table 8: Budget

Part VIII

CONCLUSIONS

14 General conclusions

In this project, the benefits and drawbacks of SCA have been demonstrated. First, the before unknown transonic regime, at which most of the commercial planes fly, has been described. Through the different explanations in the theory section, section 2, it is concluded that the analytical calculations of SCA are undeveloped to achieve accurate results so, apart from experimental tests, CFD is needed. At the first stage of the airfoil characterization or design, performing experimental tests in transonic wind tunnels would be a waste of money and resources, and CFD is the optimum alternative. The fact that some of the calculations have been done with transient calculation reinforces the idea that CFD is the optimum way to study the transonic regime.

Research over the BL control to control the stall behavior is being conducted, so in the state of the art section, section III, different ways to improve the low speed behavior of SCA are present, as well as drag reduction technologies.

The process of a numerical study, from meshing and its validation to grid sensitivity, has been done. ICEM has been shown to be an user friendly mesh generator, and it worth the time spent meshing the geometry manually, as basic principles of the meshing process, such as the cell height or the most efficient cell distribution have been practiced. In order the calculations to be stable and the results accurate, the available numerical schemes and turbulent models have been considered. For transonic flow, the selected turbulence model has been the SST $k-\omega$, commonly used in aerodynamics.

The most important phenomena in the transonic flow over SCA has been studied, so results interpretation skills have been acquired. In this context, the results (shown in section V) are more than reasonable, and they are in accordance with the theory.

Although the Mach numbers in the calculations might appear low (for example, the maximum drag divergence Mach number is 0.647), it must be noted that the aircraft is flying faster than these speeds. If the airfoil is at M=0.647, the aircraft is flying at:

$$M = \frac{0.647}{cos\Lambda} \tag{11}$$

being Λ the sweep angle of the wing. For a typical value of $30°$, it is M=0.747 the value at which the aircraft is flying when the drag divergence occurs.

15 Further developments (planification)

A relatively easy improvement on the study would be the use of a more standardized method to check the mesh sensitivity (instead of using percentages, section 10); it is the Grid Convergence Index, GCI. Some parameters of characteristic cells of each mesh must be found. The method compares the results of two consecutive meshes, one finer than the other, but the calculation of the index must be done iteratively. For more information about this method, see [30]. If this task is to be done, it is the first action to be taken, spending 15 hours.

The first compulsory action is increase the number of angles of attack. Although the AoA at which the aircraft will cruise and maneuver at these elevated speeds is relatively low, higher AoA should be tested to better characterize the airfoil. This way, the interaction between the possible detached flow in the rearward part upper side of the airfoil and the SW would be observed. However, one identified challenge is the wake meshing. For higher AoA, to accurately calculate the wake zone, this zone should be changed to follow the wake, but as C type of mesh has been selected (figure 24), it would not be easy to achieve a high quality mesh as it would be using an O type mesh. To complete this task, until the angle of attack is $10°$, 400 hours of calculation should be done, with 10 Mach numbers in each angle of attack (this increase in the number of hours is due to the use of transient calculation).

At higher Mach numbers, near M=1, a SW would appear in the lower surface of the airfoil, and the lift and drag coefficients, along with the momentum coefficient, would probably change drastically. The drawback is that transient calculation would be necessary. This study is not compulsory, as the aircraft is not intended to fly faster than the lift divergence Mach number, but it would take up to 72 hours of simulation to calculate three tests, using transient calculation.

All these tasks are interesting, but a problem arises: the buffet onset. This improvement of the study is critical to validate an airfoil, as buffet can cause not only flight instabilities, but also structural problems. This would be the second compulsory action. A transient study of the buffet would require a deeper study of the best transient numerical schemes, and this study would need more time: 20 hours to search the best parameters for the transient calculation and nearly ten tests at different Mach numbers, equal to 360 hours of simulation.

Finally, a state of the art development, the contour bumps (section 4), can be simulated by changing the geometry, and transient calculation is not required. Just to check the possible advantages and drawbacks of these contour bumps in terms of drag, 300 hours of simulation would be required.

Task	Hours
GCI	15
Increase number of AoA	400
SW in lower side	72
Buffet	360
Contour bumps	300
Total	1147

Table 9: Planification

References

[1] http://www.mp.haw-hamburg.de/pers/Scholz/paper/DGLR-2005-122Paper.pdf

[2] Meseguer, J. *Aerodinámica de altas velocidades*. 1^{st}ed. Madrid: Gaceta, 2011. ISBN 978-84-9281-246-2.

[3] Proctor, J. *Convair 880 & 990*. 1^{st}ed. Hong Kong: Great airliners series, 1996. ISBN 0-9626730-4-8.

[4] Bocci, A. J. NATO advisory group for aerospace research and development, airfoil design techniques. A: *Specialists´ meeting of the Fluid dynamics panel, 1989.* Loen, Norway, 1989.

[5] Sethunathan, P. Niventhran, M. Analysis of aerodynamic characteristics of a supercritical airfoil for low speed aircraft. *International journal of research in engineering and technology*. June 2015, Volume 3, issue 6. eISSN 2319-1163 pISSN 2321-7308.

[6] Harris, C. D. *NASA supercritical airfoils. A matrix of family-related airfoils*. Langley: NASA technical paper 2969, 1990.

[7] Whitcomb, R. T. *Review of NASA supercritical airfoils*. USA: NASA, 1974.

[8] Ansys Fluent theory guide, 2010.

[9] Xu, X. Investigation on improved correlation of CFD and EFD for supercritical airfoil. *Research Journal of Applied Sciences, Engineering and Technology*. 2014. ISSN 2040-7459.

[10] www.cfd-online.com

[11] Ansys Fluent user guide, 2010.

[12] Bakker, A. *Turbulence models, applied computational fluid dynamics*. 2002

[13] Xiao, Q., Tsai, H. M. Numerical study of transonic buffet on a supercritical airfoil. *American Institute of Aeronautics and Astronautics*. March 2006, Vol. 44, No. 3.

[14] Sommerer, A. Design of adaptive transonic airfoils by means of numerical optimisation. A: *European Congress on Computational Methods in Applied Sciences and engineering*. Barcelona, 2000.

[15] Owens, R. On the application of contour bumps for transonic drag reduction. *American Institute of Aeronautics and Astronautics*. 2005. ISSN 2005-0462.

[16] Zhao, K. Robust design of natural laminar flow supercritical airfoil by multi-objective evolution method. *Applied mathematics and mechanics English edition*. 2014, Vol. 35.

[17] Dandois, J. Buffet control by means of mechanical and fluidic vortex generators. A: *5th Flow Control Conference*. Chicago, 2010.

[18] Xiao, Z. Investigate of passive flow control methodologies using SST-IDDES. A: 28^{th} *International congress of the aeronautical sciences*. Brisbane, 2012.

[19] Little, J., Takashima, K. High lift airfoil leading edge separation control with nanosecond pulse driven DBD plasma actuators. A: *5th Flow Control Conference*. Chicago, 2010.

[20] Huang, X., Zhang, X. Streamwise and spanwise plasma actuators for flow-induced cavity noise control. *Physics of fluids.* 2008, 20.

[21] http://ocw.mit.edu/courses/aeronautics-and-astronautics/16-100-aerodynamics-fall-2005/lecture-notes/16100lectre48_cj.pdf

[22] http://geolab.larc.nasa.gov/APPS/YPlus/

[23] Jenkins, R. V. *Aerodynamic performance and pressure distributions for a NASA SC(2)-0714 airfoil tested in the Langley 0.3 meter transonic cryogenic tunnel*. USA: NASA, 1988.

[24] Delery, J. *Shock-wave BL interactions*. USA: NATO advisory group for aerospace research and development, 1986. ISBN 92-835-1519-6.

[25] http://www.langleyflyingschool.com/Pages/CPGS%204%20Aerodynamics%20and%20Theory%

[26] http://h10025.www1.hp.com/ewfrf/wc/document?docname=c03798995&tmp_track_link=ot_faqs

[27] http://www.minetur.gob.es/energia/desarrollo/EficienciaEnergetica/RITE/propuestas/Documents

[28] http://www.icao.int/environmental-protection/CarbonOffset/Pages/default.aspx

[29] Obert, E. *Aerodynamic design of transport aircraft*. Amsterdam: IOS Press, 2009. ISBN 978-1-58603-970-7.

[30] http://www.taoxing.net/web_documents/p4enew.pdf

[31] Patankar, S. V. *Numerical heat transfer and fluid flow*. USA: Hemisphere Publishing Corporation, 1980. ISBN 0-07-048740-5.

[32] Anderson, J. D. *Modern compressible flow with historical perspective*. Boston: McGraw Hill, 2004. ISBN 0-07-001673-9.